Development and Application of a Universal Distributed Data Acquisition System for Orbit Feedback Applications on Electron and Hadron Synchrotrons

Dissertation zur Erlangung des Grades
eines Doktors der Naturwissenschaften
der Fakultät Physik der Technischen Universität Dortmund

vorgelegt von
Gerrit Schünemann
aus Witten

January 24, 2017

Für Ina

1. Gutachter: Prof. Dr. Thomas Weis
2. Gutachter: Prof. Dr.-Ing. Harald Klingbeil

Abstract

To improve beam quality, the DELTA storage ring (TU Dortmund) conducted a number of orbit-feedback developments [32, 52, 110] in the past, including a successful fast local orbit feedback project [83,94]. To enable hadron accelerators to benefit from this knowledge, a collaboration was formed between DELTA, the storage ring COSY (Forschungszentrum Jülich) and the SIS18 accelerator (GSI Helmholtzzentrum für Schwerionenforschung GmbH, Darmstadt). The goals were the development of a global fast orbit feedback system for the DELTA storage ring, the development of a local feedback for the COSY electron beam cooler section and a global feedback for the SIS18 accelerator.

This thesis describes the development and application of a universal position measurement system, usable for electron and hadron accelerators and targeted to fast orbit feedback applications, in the framework of this collaboration.

The developed distributed system has input capabilities for electron or hadron beam position monitors and output options for feedback tasks and different control system connections. It is connected by a versatile communication structure [98]. The developed common hardware platform is reprogrammable and therefore usable as an input device as well as for feedback- or other measurement tasks. It delivers data at a constant data rate of 10 kHz, resulting in a target feedback-rate of up to 1 kHz. It was used to evaluate beam position data globally at DELTA, locally at SIS18 and locally at the COSY beam cooler section.

At DELTA, the system forms the basis for a future fast orbit feedback system, which is expected to significantly increase the beam quality for synchrotron radiation based research as well as ongoing electron-beam/laser interaction experiments(see [38]). The system can also be used as a high precision data source for the slow orbit feedback system in operation.

The COSY measurements show the possibility of a local fast orbit feedback system at the storage ring's electron cooler.

The data analysis of the SIS18 accelerator suggests the utilization of a feedback system to improve beam quality during ramping. The system's structure is expected to be utilized in a future SIS100 accelerator feedback.

Contents

Chapter 1

Introduction

Particle accelerators are nowadays an essential tool for physic's research. At present, a large number of accelerators, dedicated to storing atomic particles over a limited period of time, exist. These so called storage rings are circular accelerators. They have different objectives and store different particle types at various kinetic energies. Out of the large number of different "types", two are relevant to this work: On the one hand the so called synchrotron light sources, which accelerate and store electrons. They are used primarily for the generation of synchrotron radiation for experiments. Usually a synchrotron light source consists of an accelerator part, which is used to increase the electrons energy to the desired level, and a storage ring. This is used to "store" the electrons whilst their synchrotron radiation is emitted, in dedicated regions of the storage ring, to the experiments . The majority of the development during this dissertation was conducted at the storage ring of the synchrotron light source DELTA (see section 2.1).
The second type are hadron storage rings, which accelerate and store hadrons for particle experiments. In this case, due to the different objectives of each facility, these accelerators usually do not follow a common structure. In the course of this dissertation measurements were conducted at synchrotron accelerator SIS18 (see section 2.3) and the synchrotron accelerator COSY (see section 2.2). SIS18 is used to accelerate a wide variety of hadrons, to different energy levels, for experiments. The COSY synchrotron is used to accelerate only one type of particles, namely protons, for experiments.
Regardless of the particle type accelerated, the underlying physical principles are the same. A particle beam inside the accelerator's vacuum chamber is guided by magnetic fields and accelerated by electric fields. The ideal fields are designed in a way that the particles travel inside a zone of acceptance which is more or less tubular shaped. Each particle follows a path inside the acceptance.

The path of the center of mass of the particles is called the orbit. A defined ideal closed orbit is a path which is closed inside the acceptance after one revolution. In this context, the transverse deviation from this ideal orbit is called beam motion. The actual magnetic and electric fields, acting on the particles, underlie dynamic distortions. As the magnetic fields are, in most of the cases, created by electromagnets, they are are prone to electric- and also mechanical distortions. In case of faulty currents, unwanted magnetic fields are created. An unwanted mechanical vibration of the magnet also changes the magnetic field which influences the path of the particles. Even though these distortions are machine-specific, a generalization is possible. The frequency of the mechanical distortions is typically in the range of 0 Hz to 50 Hz. Usually these distortions are due to ground motion and other mechanical vibration, which couples directly or indirectly to the mechanical eigenfrequencies of the magnetic structures. In comparison the electric distortions frequency range is much larger and prone to a multitude of error sources. In combination, the typical frequencies acting on the orbit of the beam are usually in the range of 0 kHz to 1 kHz.
Beam motion plays an essential role in accelerator operation. In case of synchrotron light sources the paths of the accelerated particles are the synchrotron radiation source points. A most stable beam position results in a higher radiation flux intensity and increases the synchrotron radiation quality in terms of brilliance. During operation DELTA typically requires the transverse beam position to be stable in the range of micrometre whereas more recently built light sources have requirements close to the nanometer range beam stability. An example for this is the Soleil light source (France). In this case an integrated root mean square noise (without a fast orbit feedback) of below 5 µm for both transverse planes is achieved within regular operation [64]. A second aspect of a stable beam is the so called beam lifetime, which is the figure of merit for the loss of particles. It is defined as the time until the initial number of particles is reduced to a factor of $1/e$. In general a more stable beam results in a longer beam lifetime. This is due to a reduced amount of particle losses by particles falling outside of the accelerators acceptance. A long beam lifetime is essential for synchrotron radiation experiments. It has the benefit of having a higher radiation flux intensity over a fixed period of time.
In case of hadron accelerators, which are used for particle experiments, the key figure is the total luminosity supplied to the experiments. Beside other parameters it is primarily dependent on the rate of particles per time and beam width, secondarily on properties like repeatability of acceleration, maximum achievable intensity and beam lifetime. Due to the mass of hadrons, which is three orders of magnitude larger compared to electrons, the technical dimensions of hadron accelerators are also larger. This is also reflected in the allowed root

mean square beam motion, which is also larger on an absolute scale. The typical requirement for beam stability here is in the magnitude 100 µm to 1 mm.
As a result the closed orbit beam motion is subject to research at nearly all accelerator laboratories and facilities. The goal is to stabilize and control the beam motion to meet the requirements. For dynamic distortions this is achieved by a feedback control loop which, in case of circular accelerators, is called closed orbit feedback. The feedback is constantly measuring the beams position. This information is then used to calculate and apply a correction to the accelerators magnetic field, typically using dedicated corrector magnets. This principle of correction is primarily independent of the accelerated particle type.
By increasing the beam quality at electron as well as hadron accelerators, new experiments are rendered possible and the required time for existing experiments is decreased. This thesis describes the preparatory beam orbit studies for a universal fast orbit feedback system, based on the development of a universal data acquisition system for electron and hadron accelerators.

1.1 Aims of this work

The synchrotron light source DELTA (see section 2.1) is constantly taking actions to improve the quality of the synchrotron radiation produced by the storage ring. The first step was the evaluation and implementation of a closed orbit feedback for slow orbit deviations on the time-scale of seconds [110]. Following this process, a fast closed orbit feedback system was evaluated as a fast local orbit feedback (see [83, 94]) and the decision to implement a global fast orbit feedback was made. The superior goal in this case is the reduction of closed orbit beam motion in the range of 1 Hz to 1 kHz.
This improvement of the electron beam stability and the related synchrotron radiation quality, will positively affect all corresponding synchrotron radiation experiments as well as laser to electron-beam interaction for current Coherent Harmonic Generation Free Electron Laser (CHG-FEL) experiments (see [33, 38]).

In the framework of the future Facility for Antiproton and Ion Research (FAIR) project [16], research in the field of a fast orbit feedback system is also undertaken. This applies to the Schwer-Ionen-Synchrotron (SIS18) accelerator, which is operated by the GSI Helmholtzzentrum für Schwerionenforschung GmbH (GSI), as well as to the High Energy Storage Ring (HESR) [30], which is courtesy of the Forschungszentrum Jülich (FZJ). The SIS18 is going to be used as a booster for the larger FAIR storage rings. An intensity upgrade (from $3 \cdot 10^{10}$ to $3 \cdot 10^{11}$ for $U28^{+}$) is planned [85]. To ensure reliable and stable operation, the SIS18 requires a stabilized beam.
The HESR is going to utilize electron cooling to minimize the particle's transver-

sal energy distribution. This technique requires an overlap of an electron and the hadron beam. The quality of the overlap and hence the quality of the beam cooling is therefore directly dependent on a stable hadron beam position.

A collaboration between the DELTA, the GSI and the FZJ was formed in 2008 to develop the prototype of a universal Fast Orbit Feedback (FOFB) at DELTA which can then be transferred to the GSI and the FZJ accelerators in prospect of the FAIR project. The aim of this dissertation, in the framework of this collaboration, is the development of the data acquisition in preparation of this universal feedback system. This development requires dedicated beam orbit studies to determine the feasibility of the approach. The work is supported by the Bundesministerium für Bildung und Forschung (BMBF) (FKZ 06DO9055I) and the FZJ (contract no. COSY/FAIR-114).

1.2 Objectives

The task of this dissertation is the development of a universal data acquisition system and conduction of the associated beam-orbit studies, in preparation of an universal beam orbit feedback system.

The steps which have to be taken are closely related to the planned feedback systems. A total of three systems, based on the same underlying design, are planned by the participants of the collaboration:

- A global fast orbit feedback system for the DELTA storage ring.
- A local fast orbit feedback system for the COSY accelerator.
- A global fast orbit feedback system for the SIS18 accelerator.

In prospect of a global Fast Orbit Feedback a basic prototype of a data acquisition chain was developed [83], as well as the prototype of a fast local orbit feedback [94]. This thesis takes the data acquisition developments further towards a readily usable system for the storage ring of the Dortmunder Elektronen Speicherring Anlage (DELTA). The focus of the development was the Field Programmable Gate Array (FPGA) based hardware and software platform called BPM-Extender, which is a key component to all presented designs. This platform is used to build the data acquisition chain, including the fast data distribution network connecting different types of Beam Position Monitors, for the DELTA Fast Orbit Feedback. The system is designed to measure the global beam orbit of the DELTA storage ring at a constant data rate of 10 kHz and a nominal resolution of 16 Bits, equivalent to a 305 nm beam position resolution. The main criterion which has to be evaluated is the frequency distribution of

observable beam-orbit deviations. A second evaluation regards the suitability of averaged measurement data as data-source for the existing slow orbit feedback.

The planned COSY feedback system is based on the components and structure of the DELTA feedback. The task of this dissertation is the adaptation of the DELTA system to the planned HESR cooling section. This requires the adaptation of the data acquisition system for hadron beam position monitors. The objective is the evaluation of the Cooler Synchrotron (COSY) beam orbit and preparation of a fast local orbit feedback at the COSY accelerator cooling section.

The planned SIS18 feedback system is taking the development onto the scale of a global fast orbit feedback system for hadron accelerators. The task of this dissertation in this respect is to investigate the adaptability of the data acquisition system to the SIS18 storage ring and evaluation of the SIS18s beam orbit. The output rate of beam position data for this system, as it is based on the electron system, is fixed to 10 kHz. This is conducted in prospect of the planned high intensity booster operation. Evaluation criteria are the general stability of the beam's orbit, frequency components of the orbit motion, repeatability of the orbit and orbit deviations due to hysteresis effects.

1.3 Related Work

The techniques of fast orbit feedback, the FPGA based data acquisition and the fast data distribution are common technologies. Feedback systems are widely used in the synchrotron light source community (see list in [81]) to stabilize the beam and produce synchrotron radiation of required quality. Intense development work, in techniques utilized in this dissertation, has been conducted at the Paul Scherrer Institute (PSI) in Switzerland, the synchrotron light source Soleil in France and the Diamond light source in the United Kingdom, by the respective beam diagnostic groups (exemplary [1,11,37,79,82]). The fundamental work for feedbacks at DELTA was the development of a fast orbit feedback for the DELTAs booster synchrotron named Booster Dortmund (BoDo) (see section 2.1) in 2003 [52]. The basis for a slow orbit feedback at the DELTA storage ring was created in 2002 [110]. This system was extended to the current system in 2005 [32].

Orbit feedback at hadron machines on the other hand is not as common because the margin for orbit errors is usually larger in absolute terms. Nevertheless nowadays requirements to beam stability, as well as reproducibility, lead to orbit feedback development and deployment at hadron machines. The most prominent example being the Large Hadron Collider (LHC) [88, 99] where a beam loss would be critical to structural integrity. An example for an upgrade is the

Relativistic Heavy Ion Collider (RHIC) in the United States, where improvement of energy ramp commissioning and tuning efficiency is the main goal [75]. The COSY accelerator is currently operated without an automated orbit feedback program for the hadron beam, various research is being conducted in the field of beam stability and oscillation feedback [50].
The same applies to the SIS18 accelerator, which is currently completely operated without an automated orbit feedback system. Current research in beam orbit diagnostics include response matrix studies [70], an upgrade to the beam pickups [55] and a data acquisition (DAQ) system [47].

1.4 Structure of the Thesis

Chapter 2 introduces the three different accelerator facilities, including the technical aspects and procedures, as far as relevant for this work. A short introduction to closed orbit feedback, with respect to the different accelerators and resulting designs of the orbit feedbacks, is given. The physical properties of emittance and acceptance at accelerators are introduced as figures for accelerator beam lifetime. The chapter closes with a structural overview on FPGAs, showing the advantages of the design for fast DAQ.
The design of a feedback DAQ system is part of the feedback system design. Chapter 3 introduces the general design and classification of FOFB systems. The accelerator specific designs, with focus on the DAQ, are then derived from this general design.
The technical implementation, installation and testing of these designs and the systems developed for measurements, is described in chapter 4. The conducted measurements and results are described in chapter 5. A summary and discussion of the findings in given in chapter 6.

Chapter 2

Accelerators and principal physics

After briefly presenting the utilized accelerators and each specific requirement for a stable orbit, this chapter gives an introduction to orbit measurement and correction. As the SIS18 accelerator is a so called booster, the technique of ramping, the effect of magnetic hysteresis and its connection to the beam orbit is presented. Beam lifetime is closely connected to the physical size of the particle beam and its transversal position in the vacuum chamber. The underlying properties of emittance and acceptance are introduced. The chapter closes with an introduction to FPGAs and the resulting software design techniques.

2.1 The synchrotron radiation source DELTA

Situated at the Center for Synchrotron Radiation and being part of the Technische Universität (TU) Dortmund University, the electron accelerator facility Dortmunder Elektronen Speicherring Anlage (DELTA) is used for the production of synchrotron radiation for a wide variety of experiments. It also serves as an university accelerator with dedicated beam time for research and development by accelerator physicists.
This combination, including the previous research on feedback systems done at DELTA, qualifies the DELTA storage ring as an ideal test facility for feedback systems.
The following subsections contain an overview of the accelerator compound relevant to this work. This includes an introduction to the DELTA control system structure and data management. The DELTA control system is a typical example for an accelerator control system. The integration of a feedback system

into this control system is exemplary to other control systems.

2.1.1 Layout and general data

DELTA consists of three accelerator structures, two transfer structures and one electron source (gun). The accelerating structures are the linear accelerator Linear Accelerator of DELTA (LINAC), the booster synchrotron Booster Dortmund (BoDo) and the synchrotron storage ring. The LINAC and BoDo are connected via the Transferkanal 1 (T1), BoDo and the storage ring are connected via Transferkanal 2 (T2) (see fig. 2.1).
The electrons exit the gun and enter the LINAC with a kinetic energy of 90 keV. This energy is increased to 80 MeV at the end of the LINAC. After transfer, the final energy is reached after 8 seconds of ramping with the BoDo synchrotron. The highest final energy possible, which is also the most common mode of operation, is 1.5 GeV. The electrons are then extracted to the storage ring. Typically the accumulated current is 130 mA at a mean lifetime of ten hours and more.
The magnet structure of DELTA consists of dipole, quadrupole and sextupole magnets. Slow horizontal and vertical dipole field correction is achieved by dipole corrector coils which are, for technical reasons, attached to the quadrupole magnets.
The emitted synchrotron radiation is supplied to the experiments via numerous beam lines. One superconducting wiggler (SAW), one permanent magnet undulator (U55) and one electromagnetic undulator (U250) is utilized. Three user beam lines are using the synchrotron radiation emitted by the DELTA dipole magnets, while additional dipole beamlines are available for diagnostic purposes.
DELTA uses Beam Position Monitor pickup buttons (BPM knobs), integrated into the vacuum chamber, for beam position measurements. 14 of these button-type BPM knobs are part of BoDo, 54 BPM knobs are part of the storage ring. Details of the storage ring's magnetic lattice are found in [80]. The design of the BPMs of BoDo and the DELTA storage ring is described in great detail in [52].

2.1.2 The DELTA control system

The DELTA control system is divided into three hardware layers and three corresponding software layers. These layers are interconnected by two transport layers [110, Ch. 5]. Figure 2.2 shows the layout of the control system structure.

The lowest layer consists of the accelerator hardware (e.g. magnet power supplies, vacuum probes etc.) itself. Due to the variety of devices, the format of input- and output information varies considerably. To unify the process of control, a field bus system has been selected as interconnection layer. Each

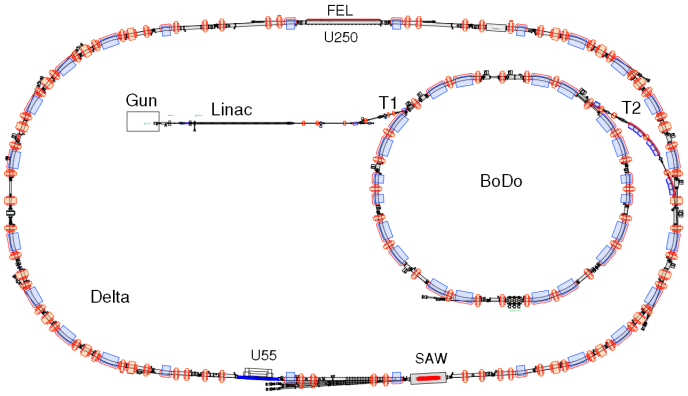

Figure 2.1: DELTA accelerator layout, showing the electron source (Gun), linear accelerator (Linac), transfer structures (T1, T2), the accelerator synchrotron (BoDo) and the storage synchrotron (Delta), including undulators (U55, FEL) and the wiggler (SAW).

device either has a native bus support or is connected to a converter device with a bus support. The buses used for this purpose are mainly Controller Area Network (CAN) and General Purpose Interface Bus (GPIB).
The middle layer consists of so called Input Output Computers (IOCs). At DELTA these are industrial grade computers based on VxWorks. The IOCs form the connecting layer between the accelerator hardware and the control system. Therefore, the middle layer contains the necessary driver information for the accelerator hardware. The input and output format for the data is unified by this layer. The connection layer between the middle layer and the operational layer consists of a standard ethernet connection.
The actual operation of the accelerator is done on the operational layer only, which provides interfaces for the accelerator-operating personal. This layer mainly consists of different standard Personal Computers (PCs) and laptops running a centralised distribution of the operating system Linux.
The actual software side of the control system is based on the distributed object database system Experimental Physics and Industrial Controls System (EPICS). The information is stored in so called records, which represent the database objects with values and properties. In case of DELTA, these records are stored on the IOCs. The operational layer contains the graphical user interface to these records. At DELTA user interfaces based on the scripting language named Tool Command Language (Tcl), generated with the so called “tk toolbox”, are used, alongside with interfaces and programs written in the Matlab environment.
Further information about the hardware is found in [53, Ch. 6.6], a detailed description of EPICS is found in [110, Ch. 5.1].

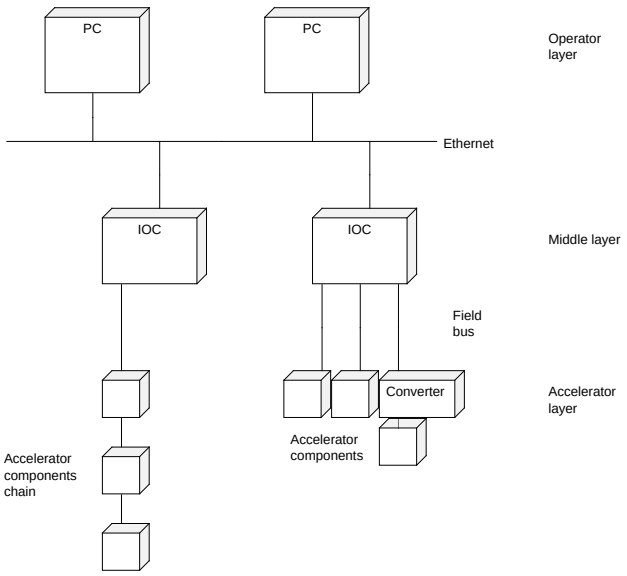

Figure 2.2: The DELTA control system, divided into layers for clarity. The bottom layer (accelerator layer) contains the components which are connected directly or by means of a converter with a field bus system to the middle layer. This layer uses dedicated Input Output Computers to create a database which can be accessed via ethernet from the top layer (operator layer).

2.2 COSY

This section introduces the COSY accelerator facility, a basic layout is shown in fig. 2.3. This includes the technical parameters, as well as an introduction to electron cooling, a technique widely used at hadron accelerators for emittance control, with respect to feedback systems.

Within the framework of the upcoming FAIR project (see [16]), COSY is utilized as a test facility for the upcoming HESR (see [30]). This also makes COSY an excellent test facility for future proton/deuteron accelerator feedback systems.

2.2.1 Layout and general data

COSY is a so called cooling storage synchrotron for protons situated at the Forschungszentrum Jülich at the Institute for Nuclear Physics. The stored protons are used for experiments with the proton beam, but can be extracted as well for external experiments [48]. COSY has a circumference of 183.5 m and a momentum range of 600 to 3700 MeV/c. The acceleration cycle length is adjusted between ten seconds and several hours, depending on the experimental

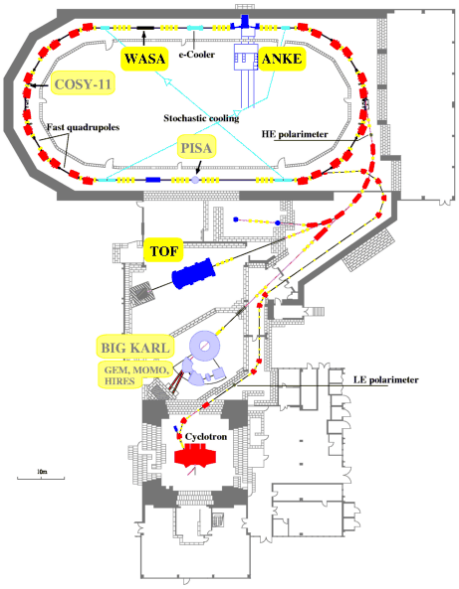

Figure 2.3: COSY accelerator, beamline and experiments layout [49]

requirements. Thirty horizontal and vertical BPMs are utilized for closed orbit measurement [31, 59].
The COSY facility houses a number of different experiments [29]. The figure of merit for the majority of experiments is the integrated beam luminosity I, given by [108, Ch. 7]

$$I = \int L \cdot dt = \frac{N_p}{\sigma_p}$$

where L is the beam luminosity, the figure of merit for single events, given by

$$L = \frac{\dot{N}_p}{\sigma_p}.$$

N_p are the number of particles, σ_p is the particle interaction cross section. A second type of experiments at COSY requires a maximum beam lifetime [51]. In both cases the best results are achieved in a stabilized orbit environment.

2.2.2 Electron cooling at COSY

A temperature can be assigned to a particle beam when using a kinetic gas theory approach. The internal temperature of small particles is expressed as their average velocity. The temperature T is given by

$$T = \frac{m\bar{v}^2}{3k_B}.$$

m is the particle mass, $\bar{v}$ the average velocity in the system and k_B the Boltzmann constant.
The "cooling" in COSY, that is the reduction of the beam's emittance (see section 2.6.1), is achieved by so called electron cooling. At COSY the emittance is reduced from about 60π mm mrad to 0.3π mm mrad (horizontal) and from 15π mm mrad to 0.4π mm mrad(vertical) [58]. During this process an electron beam of a low temperature, but equal mean velocity, is inserted into the path of the revolving, higher temperature, proton beam (For technical details of the original cooler see [61]). A cross section of the interaction region at COSY is shown in fig. 2.4. Due to small angle Coulomb scattering between electron and protons, temperature energy is transferred between the two. By always supplying a newly created cold electron beam, which is extracted after the process, the protons are cooled until the thermal equilibrium is achieved. In accelerator terms, the transverse emittance and energy spread of the protons is reduced by the low emittance and low energy spread, electron beam.
The time required to reach the equilibrium is called the damping time. It is directly proportional to the quality of the positional overlap of proton and electron beam [8, Eqn. 1-4]. Hence a feedback-stabilized proton-beam orbit is expected to reduce the damping time.

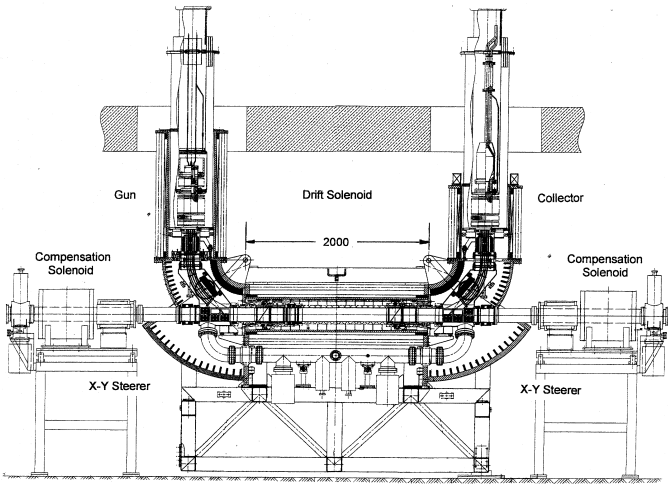

Figure 2.4: Cross-sectional view of the current COSY electron cooler [51]. Electrons are inserted on the left side (Gun) to the revolving proton beam also coming from the left. After interaction inside the cooling solenoid channel they are extracted on the right side to the collector. Due to their higher mass, the protons continue to the right. The electron beam is guided by a solenoidal magnetic field, therefore additional compensation solenoids are required.

2.3 GSI/SIS18/FAIR

In the framework of the FAIR project, the prospect of a beam-orbit feedback application is the overall increase of the beam intensity. The following is an introduction to the GSI facility. In this case the focus lies on the main accelerator synchrotron, called the SIS18, as it was utilized as a test-bed for the feedback design. The SIS18 accelerator will also be an integral part of upcoming FAIR facility. Hence a broad overview of the FAIR project is given subsequently.

2.3.1 GSI/SIS18

The GSI Helmholtzzentrum für Schwerionenforschung GmbH (GSI) is situated in Darmstadt, Germany. The GSI is running an ion accelerator, capable of accelerating ions of all stable elements up to uranium, as well radioactive and cooled high charge states (up to $\mathbf{U}^{92+}$) stable beams [26]. It consists of a linear accelerator (LINAC), the booster synchrotron SIS18, the Experimentierspeicherring (ESR) storage ring and various experimental and diagnostic beam lines [21]. The SIS18 is the main synchrotron of the existing GSI facility. It has a circumference of 216 m and a magnetic rigidity of 18 T m. The maximum ramping rate of the main electromagnetic dipoles is $10\,\mathrm{T\,s^{-1}}$. Two cavities with a frequency span of 0.8 to 5.6 MHz are installed [23]. The typical ramping duration is 3 s. The typical kinetic energy after ramping is 4.5 GeV for protons. The beam can be extracted in different modes with durations from 1 µs to 8 s [24]. 12 BPMs are utilized for beam position monitoring [24]. For each of these BPMs, the analog position signal is converted to the digital domain by a I-Tech Libera Hadron electronic [57].

2.3.2 FAIR

The Facility for Antiproton and Ion Research (FAIR) project is an internationally funded upgrade and extension to the existing GSI Helmholtzzentrum für Schwerionenforschung GmbH (GSI) accelerator elements. The FAIR accelerator compound will be built in the coming years [16]. The largest new ring accelerator is the Schwer-Ionen-Synchrotron (SIS100), a heavy ion synchrotron with a circumference of about 1100 meters. To improve the beam properties, beam cooler facilities are used. The facility will also be able to produce and provide secondary beams, consisting of antiprotons and exotic nuclei, to experiments [15]. The SIS18 accelerator is going to be used as a booster for the upcoming FAIR project (see also fig. 2.5). To reach the required intensity an upgrade program for the accelerator was initiated [85]. In the context of this upgrade, a feedback system is seen as one of the components to reach the planned

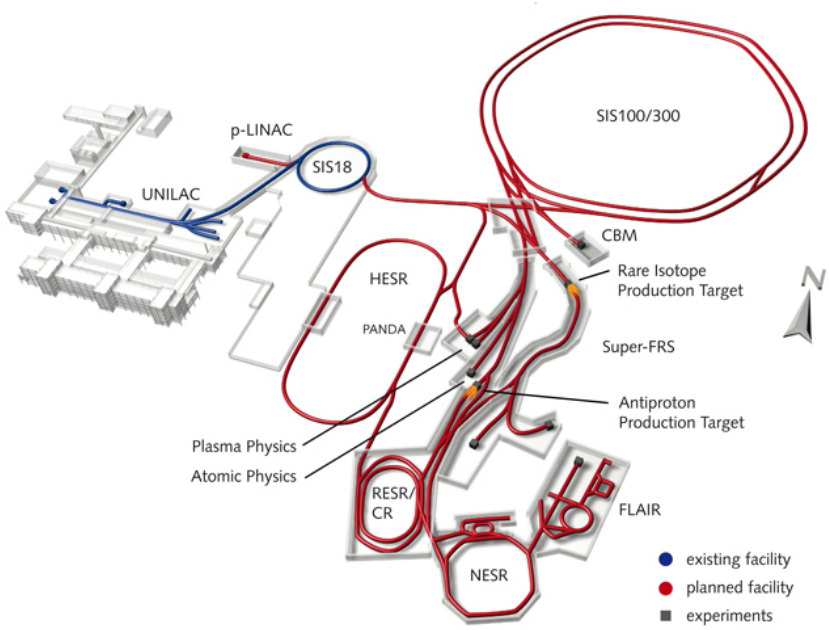

Figure 2.5: Layout of Facility for Antiproton and Ion Research (FAIR) accelerator facility and GSI compound [22]. Part of the existing GSI accelerator facility, namely the UNILAC linear accelerator and the SIS18, will be seamlessly integrated into the planned accelerator. The main accelerator elements of the planned facility are the SIS100/300 synchrotron, the connected storage rings (HESR, RESR/CR, NESR) and the corresponding experiments.

intensity.

2.4 Orbit measurement and correction

The main task of an orbit feedback system is to stabilize the beam orbit. A central element of such a system is the data acquisition and correction calculation. This section provides an overview of the physical basics of orbit measurement and techniques and terms of position calculation as well as a short introduction to the calculation of the corrective magnetic field. Differences between hadron and electron machines are exemplified.

2.4.1 General principle

The measurement of the orbit is achieved by so called Beam Position Monitors (BPMs). Regardless of the type of particles (e.g. electrons or hadrons), all BPM systems convert the position of the particle beam into an electrical signal which is then processed further. Usually BPMs are isolated metal plates (also

called pick up buttons) which couple to the electric and magnetic fields of the charged beam. For a bunched beam the electric fields are time dependent and thus the signal induced is an alternating current. Depending on the type of accelerator and the corresponding beam properties, different designs are used. An exemplary electron and hadron BPM is illustrated in figs. 2.6 and 2.7. Typ-

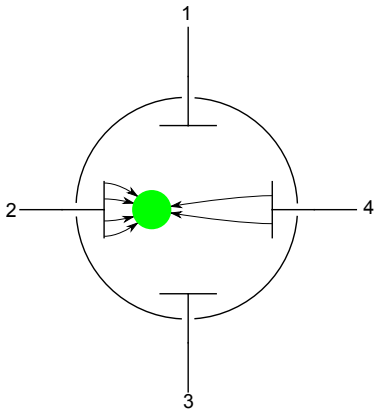

Figure 2.6: Depicted view of a four-pickup-button style BPM for both transverse directions. The electric field is shown for an electron beam and the horizontal direction. Due to the properties of the beam and the corresponding field, this design, which uses small pick-up buttons, is typically used at electron machines.

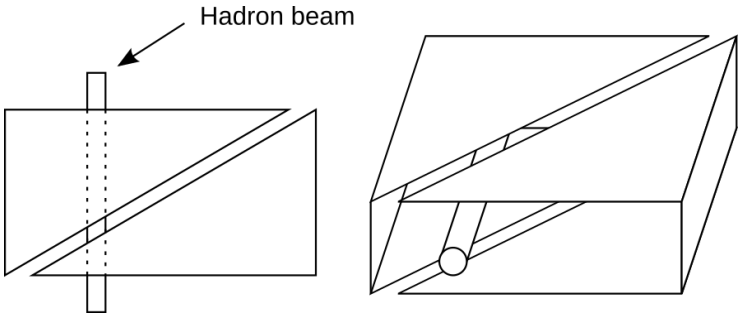

Figure 2.7: Illustration of a linear-cut style BPM (left: top view, right: 3-D view) with triangular BPM plates for one transverse direction. This design, due to the beam's and corresponding fields properties, is typically used for hadron machines. To obtain the position data for the other transverse direction, the BPM is rotated by 90 degrees.

ically four pick up buttons, spread around the vacuum chamber circumference, are utilized differentially to obtain one position readout. The induced voltage depends on beam position, beam current and longitudinal charge distribution.

The transverse position (x, y) is calculated by [18]:

$$x = \frac{1}{S_x} \cdot \frac{U_{right} - U_{left}}{U_{right} + U_{left}} + \delta_x \equiv \frac{1}{S_x} \cdot \frac{\Delta U_x}{\Sigma U_x} + \delta_x \tag{2.1}$$

$$y = \frac{1}{S_y} \cdot \frac{U_{up} - U_{down}}{U_{up} + U_{down}} + \delta_y \equiv \frac{1}{S_y} \cdot \frac{\Delta U_y}{\Sigma U_y} + \delta_y \tag{2.2}$$

where U are the respective button voltages, δ is the offset and S is the monitor coefficient of the BPM. In case of DELTA the geometry is different (see fig. 2.8) with two buttons on top and bottom of the vacuum chamber. In this case the parameters change to [45]:

$$\Delta U_x = U_2 - U_1 + U_4 - U_3 \tag{2.3}$$

$$\Sigma U_x = U_1 + U_2 + U_3 + U_4 \tag{2.4}$$

$$\Delta U_y = U_1 - U_3 + U_2 - U_4 \tag{2.5}$$

$$\Sigma U_y = U_1 + U_2 + U_3 + U_4 \tag{2.6}$$

The beam position is measured at the positions of the BPMs, orbit data of

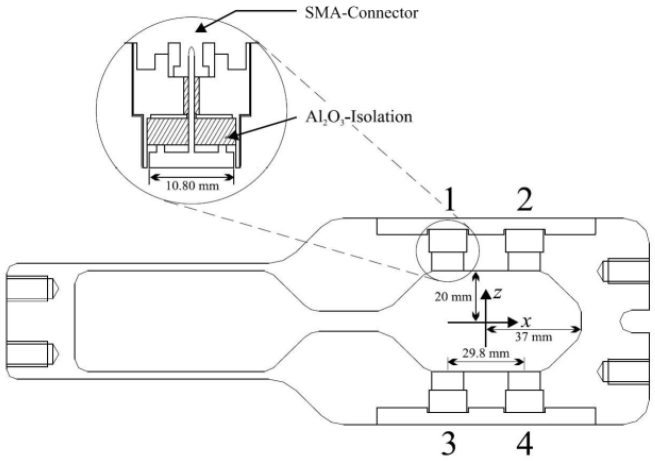

Figure 2.8: Cutting plane view of the DELTA vacuum chamber including four BPM knobs.

intermediate positions can only be obtained by using beam optic calculations. The beam position is always relative to the position of the BPM. A detailed overview of different BPM systems is given in [18].
A second type of BPMs utilized at electron accelerators and light source facilities are so called Photon Beam Position Monitor (PBPM). These measure (direction and intensity of) synchrotron radiation photons which allows for the calculation of the point of origin and thus indirectly the electron beam position. Examples

of design are described in [77, 84].

The change of an actual orbit towards a so called golden orbit is called orbit correction. The transverse beam position is changed by altering the accelerator's magnetic lattice. Magnetic dipole fields for each transverse direction are used. Depending on the technical details of the accelerator either dedicated corrector magnets or so called combined function magnets, these are lattice magnets which are equipped with additional corrector coils, are used. The achievable correction in terms of maximum amplitude and frequency depends on the maximum attainable magnetic field frequency and distribution. Due to the nature of recirculating accelerators, a magnetic field change at one point changes the orbit globally. The most common method to obtain the numeric values for the correction is to invert the so called beam response matrix. This matrix links the influence of each corrector magnet's magnetic field change to the resulting global orbit. By inverting this matrix, a corrector setting for a given orbit change is received. In most cases this matrix is not a square matrix as the number of corrector magnets is not equal to the number number of BPMs). Hence the mathematical operation of Singular Value Decomposition (SVD) is used for the inversion. An additional advantage of this method is the minimized integral corrector strength for a given orbit change, which is a result of the mathematical properties of the method. The SVD method is only one way to calculate a correction, in-depth information about this topics can be found in [94, Ch. 2.3.2] and [110].
The coefficients of the matrix can either be calculated theoretically from the accelerator optic's model or practically from the accelerator itself. The theoretical approach is valuable when planning a feedback design or when planning the installation of corrector magnets, as it allows the evaluation of multiple options. During operation the practical approach is usually taken, as it takes the practical uncertainties and deviations of the theoretical model directly into account. The procedure to find the matrix coefficients is usually the following, assuming the accelerator's lattice contains n correctors and m BPMs. As a first step the influence of every one correctors on the beam orbit at each BPM has to be measured. Each corrector strength is sequentially varied and the according orbit change of the particle beam is measured. This results in a vector with m rows, one for each corrector magnet. When combining all these vectors, a matrix with m rows times n columns is obtained, this matrix is called the orbit response matrix. Multiplying a vector of correction settings with this matrix results in the corresponding beam orbit change at the BPM positions. After inversion using the SVD method, the multiplication of the inverted matrix with a vector of (desired) orbit changes results in a vector containing the required values for the corrector magnets, see fig. 2.9.

During normal accelerator operation the beam position is measured and the orbit vector is created. By subtracting the ideal orbit vector from this orbit vector an orbit change vector is generated i.e. the vector containing the necessary orbit changes. These vectors are then multiplied with the inverted orbit response matrix and the obtained correction to the magnetic fields can then be transferred to the corrector-magnets power-supplies.
Due to the properties of the calculation, the matrix can also be split into single columns or group of columns. This allows a local calculation of a single corrector value, as long as the complete orbit data is available. Therefore a feedback can be split into multiple corrector-calculation locations, which are connected by data distribution network.
As the orbit should be corrected continuously, the calculation is done repeatedly

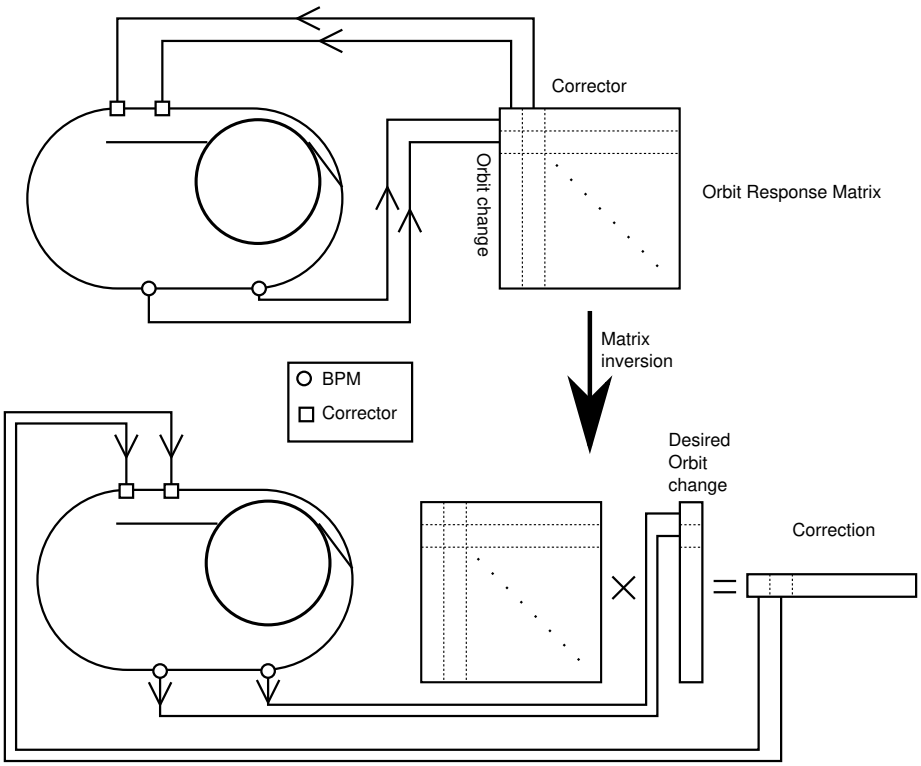

Figure 2.9: Orbit response matrix calculation and application. The response matrix is created by measuring the influence of every corrector on the BPM-positions. After inversion, a desired orbit change is multiplied with the matrix, thus yielding the necessary corrector strength.

with the frequency of correction. Hence a major requirement for the application of this method is the availability of the synchronized orbit data with the desired frequency. As a result, this places hard synchronized real-time constraints on

the feedback's data acquisition and distribution.

2.4.2 Aims and limits of closed orbit feedbacks

The purpose of a closed orbit feedback is the stabilization of the beam's two transversal components (orbit) with respect to the requirements. The focus of the feedback is the correction of unpredictable (non-periodic) influences on the beam. The maximum frequency of beam motion which can be stabilized is called the cut-off frequency (or 0dB-point) of the feedback system. It is the main figure of merit for any orbit feedback. To understand the basic concept of an orbit feedback, looking at the system as a control loop is beneficial. In case of an orbit feedback, the control loops output can be approximated as a low-pass filtering of the input. Figure 2.10 shows the frequency response (Bode plot) of a first-order lowpass filter. At the cutoff frequency, the phase shift of the output is 45° in comparison to the input. In case of an orbit feedback this output is fed-back onto the input, it is clear that the input is not canceled out completely for these frequencies. Therefore a suitable frequency range and a corresponding underlying filter has to be found when designing a feedback system. Figures 2.11 and 2.12 show an idealized view of the effect of a digital feedback loop on the Power Spectral Density (PSD) of the beam motion as described in [94]. In this case also, due to the filter characteristic, the phase shift between the current beam position and the actual output (the change of the accelerator's magnetic fields), is also frequency dependent. This results in a good attenuation for low frequencies, declining up the cut-off frequency. For higher frequencies, due to the phase error, the distortion is attenuated. Due to the lower gain of the feedback loop at high frequencies, this effect is reduced when nearing the maximum frequency of the system. The actual effect is very much depending on the utilized hardware as well as on the correction algorithm and filters used. Usually the filter is implemented as a digital filter. This allows to easily change the filter coefficients to adapt the filter to the requirements. Examples with different parameters can be found in [94]. In general it is always desirable to establish an orbit feedback with a cut-off frequency as high as possible. The final limitation in this respect for every feedback is the technical boundary of the involved components, e.g. at DELTA the stainless steel vacuum chambers hysteresis does not allow high frequency magnetic fields to effectively act on the beam. In practice the required performance of a feedback is the direct result from the design-budget of the beam motion.

Often an accelerator is designed and built without an orbit feedback. In this case, a detailed analysis of measured PSDs provides the information for the development of a corresponding feedback.

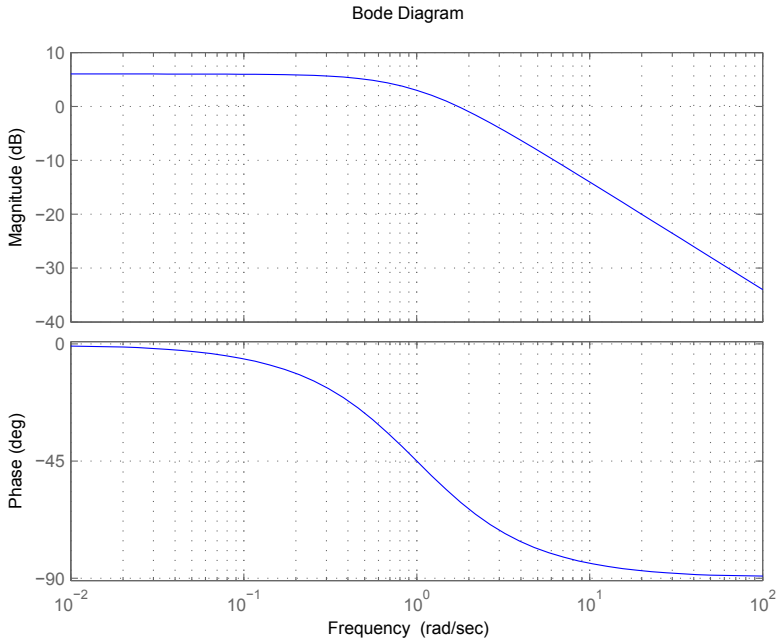

Figure 2.10: Bode plot of a typical low-pass filter (first order). On top the amplitude-response of the resulting signal is plotted, below the phase-response of the signal. At the cutoff-frequency the phase shift is 45°. A feedback is typically based on a filter like this, therefore the characteristics of the feedback loop are very similar. (From: [107])

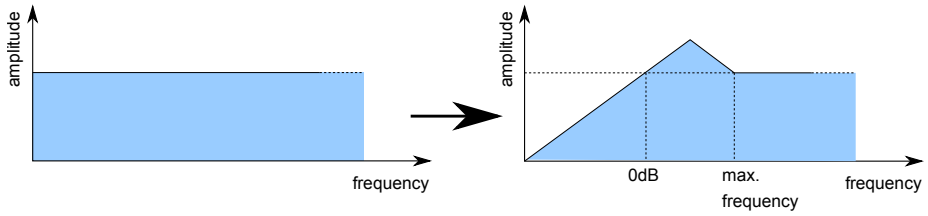

Figure 2.11: Influence of an typical orbit correction on power spectral density of white noise beam motion (left to right). The lower frequency components are damped up to the 0dB point, due to delays higher frequency components are amplified.

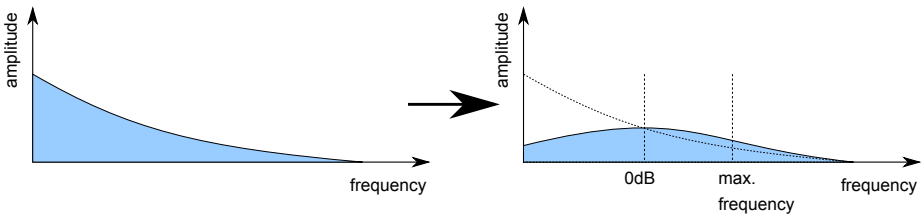

Figure 2.12: Influence of a typical orbit correction on the basis of fig. 2.11, assuming a more realistic pink noise spectrum beam motion. Proportionally more energy is stored in well correctable frequencies below the 0dB-point, hence an overall gain is achieved.

The beam motion sources (and thereby corresponding counter measures) can be broadly categorized due to their frequency. The following list is a summary of [4, 36], applicable to all accelerators and by no means exhaustive:

- Shortterm(<1hour)
  - Mechanical vibrations: ground vibration, mechanical devices, girder resonances, insertion device variation, cooling water circuits, power-supplies, booster operation
  - Electrical noise: power-supply noise, electrical stray fields, booster operation
- Mediumterm(<1week):
  - Variation of external conditions (mostly temperature related): vacuum chamber or magnet movement, watercooling, temperature, day/night variations
- Longterm(>1week):
  - Ground settlement
  - Seasonal effects(temperature,rainfall), sun/moon tide cycle

In respect to the aims of orbit feedbacks, existing accelerators and storage rings can be divided into the category of electron or hadron storage rings. In case of electron storage rings, electron light sources are relevant to this work. The difference itself is due to the different mass-to-charge ratio ($\frac{m}{Q}$ with $m_{\text{proton}}/m_{\text{electron}} \approx 1836$ [74]). Assuming the same kinetic energy, the associated technical dimensions and synchrotron radiation emission differ as a result. The total emitted power P of the synchrotron radiation scales with the fourth power of the mass. In this case [100, p. 767,21.38]

$$\frac{P_{electron}}{P_{proton}} \approx 1836.1526^4 = 1.367 \cdot 10^{13}.$$

The energy loss due to the emission of photons in all three dimensions is compensated for only longitudinally by the RF-system. As a result the transverse beam motion is greatly reduced, which in turn allows for tighter constraints on beam movement. This effect is called synchrotron radiation damping. In case of hadron accelerators the damping effect is very weak and is usually neglected (with exception of the LHC [109]).
With respect to the integral magnetic fields, the required physical length of the accelerator's magnets scales linear to the mass-to-charge ratio (Lorentz force in combination with Newtons law).

Position stability requirements at synchrotron light sources

The aim of beam stabilization at synchrotron light sources is the stabilization of the synchrotron light flux at the beam line experiments. This applies to all possible degrees-of-freedom of beam stability and flux stability. Today fast orbit feedbacks are major components of transversal beam stabilization measures. This is a demanding task and the main goal of ongoing beam stability research [4].
The exact beam stability requirements (including the transversal beam stability) result from the synchrotron light flux stability requirements of each beam line experiment. Even though the exact numbers strongly depend on the accelerator, a general accepted rule of thumb for modern synchrotron light sources is to have an accuracy for positioning and pointing below a few percent of beam size and divergence. The dependency between beam position offset and flux transmission change is essentially quadratic [36].

Stability requirements at hadron storage rings

Hadron storage rings are aimed differently as most hadron machines are utilized as particle colliders. The qualitative factor for those experiments is often the (integral) beam luminosity (see section 2.2.1). In case of orbit feedbacks the missing synchrotron radiation damping results in different spectra of transversal beam movement. The higher particle mass results in a generally lower correction frequency for feedback systems. This is due to the physically larger magnets required (as direct result of the mass-to-charge ratio and indirect due to the larger aperture required due to the higher emittance, see section 2.6.1). In terms of an equivalent electric circuit of an electromagnet, in this case it is dominated by the series of the main coils resistance (R) and especially the inductance (L). The physically larger the electromagnet is, the higher the resistance and

inductance becomes. This in turn means the natural time constant

$$\tau = \frac{L}{R}$$

of the system increases. Therefore a comparably higher voltage is required to drive an electric current to produce an equivalent magnetic field. As such the maximum technically achievable frequency is limited for larger electromagnets.

As a consequence hadron machines are usually utilizing closed orbit feedbacks with cut-off frequencies of below 10 Hz, reducing the opposable noise sources. The general objective in this case is "to keep the beam in the pipe!" [88]. Many hadron accelerators do not feature a closed orbit correction loop because of corresponding low orbit stability requirements. The accelerator's global parameters (including the magnetic lattice) are optimized in those cases by offline computation or trial-and-error.

Nevertheless experimental demands rise and therefore the demand for a stable orbit, good reproducibility and increased luminosity. Even though positional stability is only part of the parameter space, a closed orbit feedback is a necessary mean to reach maximum possible results.

2.4.3 Orbit measurement and correction at DELTA

Orbit measurement at the DELTA storage ring is accomplished by an orbit measurement system, which contains 54 BPMs. One BPM consists of four BPM knobs, integrated into the vacuum chamber (see fig. 2.8) and one readout electronic, calculating the beam position. These electronics are manufactured by Bergoz Instrumentation [43] called the Bergoz MX-BPMs. The electronics are of analog type. This means the analog BPM knobs signals are fed to an analog position calculation circuit, which supplies an analog signal representing the beam position.
The Bergoz electronics are installed, (usually) in bunches of four in one special Bergoz cradle, distributed at the girders of the DELTA accelerator. 14 of these BPMs are installed in BoDo for orbit measurement. The LINAC utilizes no BPM knobs, the T1 transfer structure uses no BPMs, the T2 transfer structure makes use of 3 single shot BPMs by Bergoz Instrumentation. The system is described in detail in [83, Ch. 2], the BPMs themselves are described in [83, Ch. 3.1.1]. Connected in parallel to the Bergoz MX-BPMs, a total of seven I-Tech Libera are installed around two of the insertion devices (for details see [35]).

Orbit correction at DELTA is currently implemented as a global Slow Orbit Feedback (SOFB) as part of the control system (see section 3.1.2). Figure 2.13 shows the data path for this system. The actual correction calculation is a

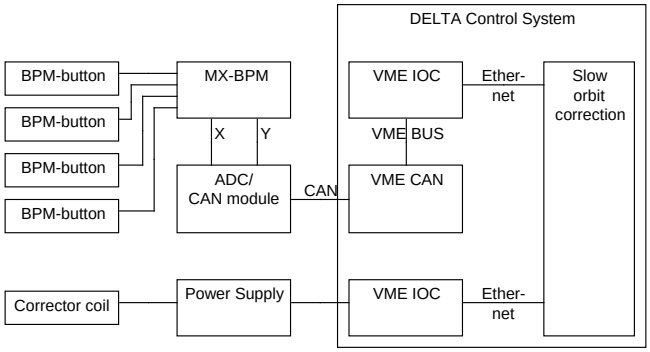

Figure 2.13: Data path of BPM position data to control system at DELTA. The analog beam position signal is digitized after position computation by the Bergoz MX-BPMs. By utilizing a CAN interface for the IOCs, the digital position data is supplied to the control net, and thereby to the slow orbit correction. After correction calculation the corrector coil current is set to the required value, utilizing the control system data path.

program which runs on one of the control system terminals. The typical cut-off frequency of this is below 10 Hz. The limiting factor in this case is the control systems maximum data update rate as well as the interface for the corrector power supplies [110, Ch. 8.2]. For details of this system see [32].

Aims and limits of the DELTA closed orbit feedback is the reduction of the transverse beam motion. Utilization of the storage ring as a light source sets the aim for the allowable range of beam motion to 10 percent of the beam size [34]. Because of the technical limitations, the SOFB is aimed only at low frequency distortions. The goal is to increase orbit reproducibility and eliminate the need to manually correct the beam position in case of long term drifts.
The FOFB is aimed at further reducing the remaining high frequency beam motion. For this reason the technical components have been selected or designed to meet this demand. The final limitation for DELTA is set by the storage rings stainless steel vacuum chamber. Due to its technical properties it acts like a low-pass filter to the applied magnetic field. Prior measurements have determined the 3 dB point of the transmission to be at a frequency of 1.3 kHz for the horizontal direction [94].

2.4.4 Orbit measurement and correction at COSY

COSY utilizes 29 shoebox (electrode pairs) BPMs, about 5 per betatron oscillation, to measure the beam position using sum and difference signal. 16 of these have a round cross section, whereas 11 which are used in bending sections have

a rectangular cross section. Details of the mechanical construction are described in [62]. Figure 2.14 shows the side view of a round cross section BPM. The natively used readout electronics are presented in detail in [6].
COSY is not equipped with an on-line orbit correction. In case of a misaligned orbit, the measured position is transferred to the ORBIT system, a dedicated software tool which was created for COSY lattice calculations (see [14]). The software then calculates the required corrector values which are then applied to the accelerator's magnetic lattice.

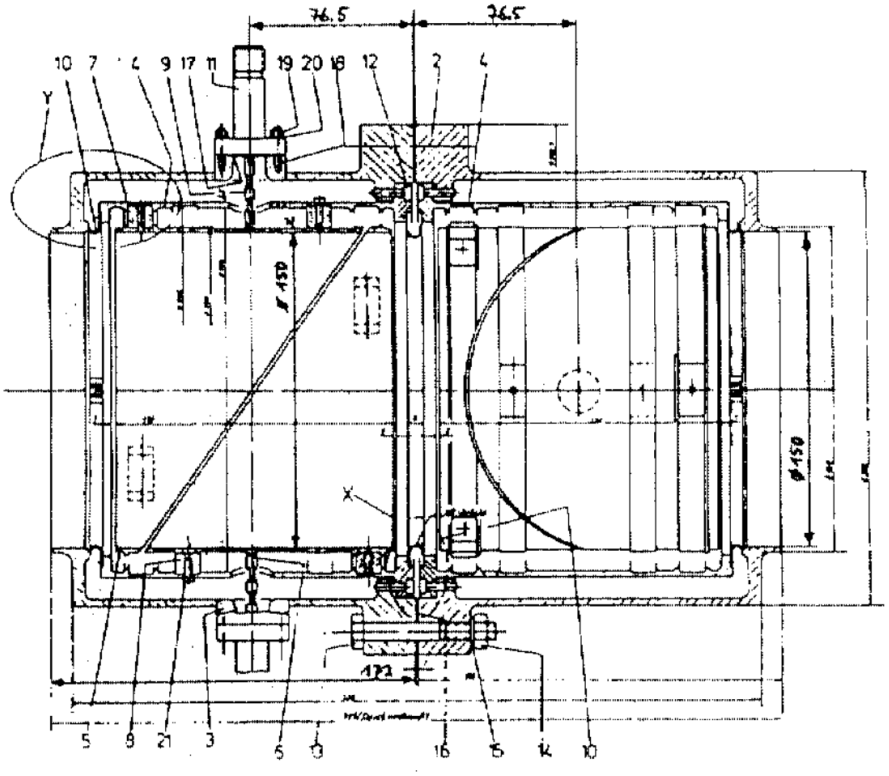

Figure 2.14: Mechanical design view of a round cross-section COSY-BPM. For the two transverse directions, the two sets of slit BPM plates, are combined in one space-saving housing. The plates are directly connected to electrical connectors leading to the outside of the vacuum chamber. From: [62]

Aims of the COSY closed orbit feedback is the improvement of the beam control and as such the improvement of beam cooling time. In case of the HESR a closed orbit feedback system is also aimed at higher intensity as well as improved beam control. In case of COSY an electron cooler is being used, in case of the HESR it is going to be used, for beam cooling. A stable orbit is required for the best achievable electron/hadron overlap. The highest possible intensity

and beam lifetime for experiments on the other hand, a situation similar to SIS18, is again achieved by an optimized and feedback controlled orbit.

2.4.5 Orbit measurement and correction at SIS18

The SIS18 is structured into 12 symmetric sections (magnetic periods) containing 2 bending dipoles, 3 quadrupoles, BPMs, vertical correctors and (not symetric) horizontal correctors [68]. The straight vacuum chamber sections are utilized for different devices (e.g. insertion, extraction devices). The 12 BPMs

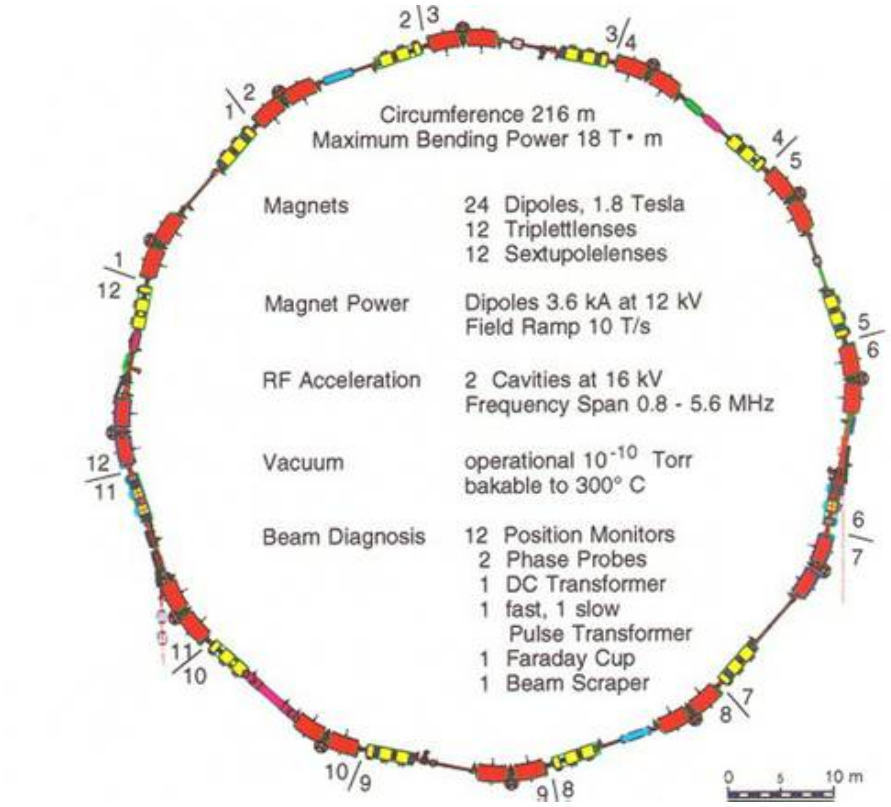

Figure 2.15: Schematic overview of the SIS18 structure and sections, figure from [23]

utilized are, due to their appearance, known as "shoebox" BPMs. A scheme is presented in fig. 2.7, the construction itself is discussed in detail in [55]. The analog signal coming from the BPMs is amplified and feed to I-Tech Libera Hadron type position calculation. After processing the digital data is transferred to data-servers which also implement the connection to the control system. The design is presented in detail in [47].

The orbit is corrected by 6 horizontal and 12 vertical steering magnets (steerers). The horizontal steerers are built-in correction coils inside the bending

dipoles. The vertical steerers are dedicated dipole coils [71].

Aims of the SIS18 closed orbit feedback are set with respect to the planned FAIR facility. As no closed loop feedback currently exists, the aims of a feedback are an easier and faster control of the beam's centre of mass during ramping, as well as a correction of unwanted low frequency disturbances to assist reaching the set intensity goal. The positive effect of a corrected orbit on the SIS18 beam lifetime and thus on the maximum possible intensity has been shown by [70].

2.5 Synchrotron energy ramping

Circular accelerators are designed for a given trajectory of the charged particles. The primarily involved equipment in this process are dipole magnets, which bend the path of the charged particles, and cavities, which supply the particle's energy. The path of the particle is received after solving the equations of the forces acting on it. A particle with charge q and velocity $\vec{v}$ receives the Lorentz force $\vec{F}$, inside an electromagnetic field

$$\frac{d}{dt}\vec{p} = \vec{F} = \vec{F_E} + \vec{F_B} = q\left(\vec{E} + (\vec{v} \times \vec{B})\right).$$

In case of an idealized homogeneous magnetic field inside the dipole magnets, setting $\vec{E} = 0$ and $\vec{v} \perp \vec{B}$, this transforms to

$$\frac{d}{dt}p = q\,|\vec{v}|\left|\vec{B}\right| = qvB.$$

As a result the particle trajectory is describing a segment of a circle. For the relativistic momentum

$$p = mv = \gamma m_0 v$$

where γ is the relativistic factor, after combination

$$\frac{d}{dt}\gamma m_0 v = qvB$$

is received. The centripetal force for a trajectory on a circle with radius r is

$$a = \frac{d}{dt}v = \frac{v^2}{r},$$

for a stable closed loop it has to be equal to the Lorentz force

$$\frac{v^2}{r} = \frac{qvB}{\gamma m_0}$$

Solving this equation for B yields

$$B = \frac{\gamma m_o v}{qr}.$$

As the trajectory is given, r has to be constant. q is assumed to be constant. Therefore a change of the magnetic field B requires a change of velocity v and vice versa.

Synchrotron accelerators fulfil this requirement by increasing or decreasing the bending magnetic field synchronously with the particles' momentum. The momentum itself is changed, when the particle passes through the directed electromagnetic field inside the accelerator's cavity. A common way to display the progression of the acceleration process is a plot of the particles' energy, and therefore the bending magnets magnetic field, versus time . Figure 2.16 shows a typical ramping process, the acceleration of particles from a start-momentum to different (typically higher) kinetic energy. It is usually divided into three phases. First the injection of particles into the synchrotron. The electromagnetic configuration of the accelerator is held constant and set to accept the injected particles, e.g. it is matched to the kinetic energy of the injected particles. Depending on the accelerator, the beam is bunched directly by the means of the cavity. After the injection the particles' momentum is increased by the use of cavities, synchronously the bending magnets magnetic field is increased. This process is called the actual ramp. When the desired particles kinetic energy is reached, the magnetic field is held constant again to extract the particles. This phase, due to its appearance, is called flat top. After this, the configuration is ramped down again for the next ramping phase to start.

For electron acceleration, due to their small mass, the cavity's frequency can be kept constant during this process as the actual velocity is relativistic already at injection energy. This also results in a synchronicity of cavity frequency and beam bunches.

In case of hadrons, due to their larger mass, the change of particle momentum results in a change of particle velocity. In this case the frequency of the cavity is increased during the ramping process. This makes the particles non-synchronous to the cavity frequency and in case of beam diagnostic bunch recognition, advanced techniques have to be utilized. Also the γ-transition energy is sometimes crossed during this ramping, requiring a phase adjustment of the cavities (see [100, ch.5.4.6].

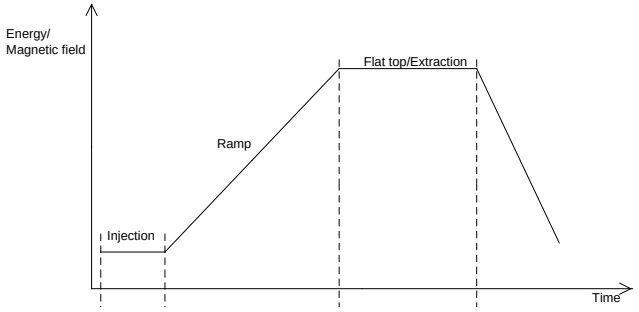

Figure 2.16: Typical three-phase progress of a single synchrotron ramping. Particles are injected and bunched during injection phase at injection energy configuration. During ramping the kinetic energy and the bending magnetic field is increased until the desired energy level is reached. During the extraction phase, called the flat top, the configuration is held steady until all particles are extracted. The ramping is followed by down-ramping for the next cycle.

2.5.1 Ramping and Magnetic Hysteresis

Hysteresis characterizes a system, whose current output state is not only dependent on the current input, but also on the past state of the output. As a result, depending on the past state, the system is able to reach different output states by the same input [104] [105].

Bending magnets are typically electromagnets consisting of an electric coil and a ferromagnetic yoke. Ferromagnetic materials in general underlie magnetic hysteresis as a material property. As a consequence the magnetic field is not directly proportional to the applied current, but also to the magnetization of the material. Figure 2.17 shows an idealized ferromagnetic hysteresis curve. When increasing the coil current and thereby the external magnetic field H influencing the yoke material, the magnetic field B inside the yoke changes depending on its pre-magnetization. Also the material is subject to saturation, limiting the maximum possible internal field.

A well defined magnetic gradient during each ramping is essential for operation. This is degraded by the effect of the hysteresis. To countermeasure the standard procedure [69] is an additional conditioning phase after each each ramp (see fig. 2.18). During this phase the material is driven into saturation, creating common start point for the next magnetic cycle.

A second effect in case of steep current gradients are occurring eddy currents which degenerate the magnetic field.
To countermeasure the combination of both effects, a magnetic field feedback is proposed [69].

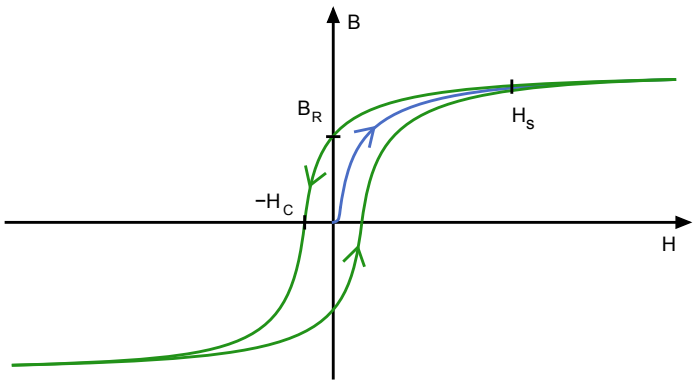

Figure 2.17: Sketched magnetic hysteresis curve. Magnetic field H versus magnetic field B, saturation level H_S and coercivity H_C (input field required to zero internal field). Zero point magnetization is shown in blue. Figure amended from [103]

.

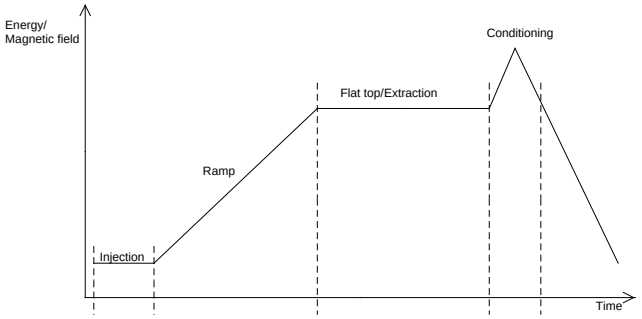

Figure 2.18: Typical synchrotron ramping with additional conditioning phase after extraction. By driving the magnetic ferrite into saturation a well defined starting point for the next ramping cycle is set.

2.6 Transverse beam emittance and acceptance

2.6.1 Emittance

Following the common definition of properties in [5], each particle in an accelerator is characterized by the six-tuple

$$(x, p_x, y, p_y, \sigma, E)$$

where x, y are the particle's transversal coordinates in relation to the ideal beam-particle path. The transversal impulse components are $p_x \approx x' \cdot p_0$ and $p_y \approx y' \cdot p_0$, with p_0 being the ideal beam particles impulse. σ (or often referred

to as s) is the longitudinal coordinate on the ideal beam path from a defined zero reference point (often also expressed as longitudinal phase deviation from the synchronous phase $\varphi = \psi - \psi_s$ [100, ch. 8.2.1]). The particles energy E is usually given either as the total impulse or as deviation from the ideal beam particle's energy (ΔE).
To describe a particle beam, containing many particles with similar values in the six-tuple, an ensemble six-tuple can be formed. This tuple can represent the beam as a whole or in well defined fractions (e.g. bunches).

Making the assumption of linear beam dynamics and no coupling between the horizontal and vertical transverse planes, it is sufficient to consider the two dimensional phase space of x, x' (and y, y' respectively). The beam is then characterized by the statistic parameters of the phase space.
The phase space is obtained by following the steps in [108, Ch. 3.8ff] and [86] with [63], generally solving the equation of motion for one transverse dimension of a particle in an accelerator. The result is

$$x(s) = \sqrt{\epsilon}\sqrt{\beta_x(s)}\cos(\Phi(s) + \phi) \tag{2.7}$$

$$x'(s) = -\frac{\sqrt{\epsilon}}{\sqrt{\beta_x(s)}}[\alpha_x(s)\cos(\Phi(s) + \phi) + \sin(\Phi(s) + \phi)]. \tag{2.8}$$

Where $\beta(s)$ is the amplitude function , Φ and ϕ the phase function of motion and the emittance ϵ. After substitution and introduction of γ the resulting equation

$$\gamma(s)x^2(s) + 2\alpha(s)x(s)x'(s) + \beta(s)x'^2(s) = \epsilon.$$

shows the relation between x and x', for a beam with so called Twiss Parameters α, β, γ. This is the general equation of an ellipse in the x-x' plane, having the area

$$\epsilon = \frac{F}{\pi}. \tag{2.9}$$

This ellipse is called the particle phase space ellipse. At this point the assumption is made, that Liouville's theorem is satisfied in this model of accelerators. As a result, the area of the ellipse and thus ϵ becomes a constant of motion of each particle.

To define a practical emittance of a particle beam, consisting of many particles, the transverse charge density distribution can be assumed to be Gaussian in the form of

$$p(x, z) = \frac{Ne}{2\pi\sigma_x\sigma_z}\exp\left(-\frac{x^2}{2\sigma_x^2} - \frac{z^2}{2\sigma_z^2}\right),$$

for a beam consisting of N particles of charge e, z being the vertical beam axis

and σ_x, σ_y the gaussian standard deviation for the transverse directions. By setting $z = 0$ the horizontal distribution

$$p(x) = p_0 \exp\left(-\frac{x^2}{2\sigma_x^2}\right)$$

with $p_0 = \frac{Ne}{2\pi\sigma_x\sigma_z}$ is obtained. Different definitions of emittance are used throughout the accelerator community [78, p. 348].The most common approach for electron machines is to define the beam emittance ϵ_{STD} as beam emittance. This is the emittance defined by the particles which are inside the 1-sigma environment of the density distribution via

$$\epsilon_{STD} = \frac{\sigma^2(s)}{\beta(s)}$$

The corresponding phase space ellipse area (see eq. (2.9)) contains 39% of the assumably two-dimensional-gaussian distributed particles [63].

Hadron machines usually use the $\epsilon_{95\%}$ beam emittance, which contains 95% of all beam particles. This is due to the fact that hadron beams are not necessarily gaussian distributed. If assuming a gaussian distribution, roughly 95% of the particles are contained in an emittance phase space ellipse corresponding to the 2.5σ environment of the beam distribution.

$$\epsilon_{95\%} = \frac{(2.5\sigma(s))^2}{\beta(s)}.$$

The physical emittance of modern 3rd generation light sources is in the range of nm rad [3, p.17] (e.g. Diamond Light Source: 2.74 nm rad horizontal, 0.0274 nm rad vertical), while hadron accelerators are in the range of µm rad (normalized SIS18 at injection: 0.78π µm rad horizontal, 2.49π µm rad vertical [25]; normalized LHC: 3.75 µm [9]).

2.6.2 Acceptance

Sufficient physical space for the passing beam is a critical criterion for accelerator operation. The space required for one beam particle in the transversal direction is defined by the corresponding emittance and β function of the accelerator. The maximum possible position amplitude for a particle at a given position s is

$$x_{max}(s) = \sqrt{\epsilon\beta_x(s)}.$$

In analogy to this, an accelerators acceptance is defined as the minimum of the local acceptance

$$A = min\left(A(s)\right) = min\left(\frac{d(s)^2}{\beta(s)}\right)$$

where $A(s)$ is the local acceptance, and $d(s)$ the corresponding vacuum chamber dimension. The acceptance can be regarded as an emittance, which makes direct comparison possible if a particle is able to pass through the accelerator structure.
In practice the accelerator's acceptance has to be larger than the beam emittance. With electron machines a factor of seven is suggested as a minimum, $A > 50\epsilon_{STD}$ is regarded as well operational. This is due to the fact, that the emittance is only conserved for conservative systems. The internal energy loss due to synchrotron radiation causes a stochastic change in the betatron amplitude which also allows for possibly large amplitudes of motion. In addition to this the ϵ_{STD} contains only a fraction of the beam, with particles in noteworthy percentage being around a 4σ environment.

Hadron machines, which in general produce negligible synchrotron radiation due to the higher mass of the particles, are operational with a much lower acceptance to emittance ratio. [20, Ch.2.3.1.3.1] states a value of $A > 2\epsilon$ for a high energy transport line. One of the limiting factors here is the beam particle momentum spread which, depending on the optical structure of the accelerator, causes particles to travel on dispersion orbits, hence needing more physical size for the beam. The emittance assigned to such a beam is called the dispersion emittance [89, Sl. 21]).

2.7 FPGAs

Whenever complex digital data has to be processed in parallel or with deterministic timing, the "classic" approach is to built a dedicated integrated circuit. To design such application specific integrated circuits (ASICs) is a time consuming task and uneconomic for small circuit quantities. Hence reprogrammable chips have been developed to close this gap. These allow to directly implement and test a circuit design. During time the internal complexity of these chips is rising steadily, with different internal structures being used. At first very basic Programmable Logic Arrays (PLAs) were used, then more advanced Generic Array Logics (GALs) and Complex Programmable Logic Devices (CPLDs) and nowadays Field Programmable Gate Arrays (FPGAs) are available in a range of complexities. The latter are being utilized for this work.
As a number of different internal architectures are available, the basic process of development including the software structure, is common to all of them. The

following subsections present an introduction to this process. The subsequent subsection describes the so called Intellectual Property Cores (IP cores), a common software design practice for FPGA programming.

2.7.1 FPGA logic

FPGAs are integrated circuits, capable of being reprogrammed after manufacturing. The FPGA itself contains programmable logic components and interconnections [101] which are wired to correspond to the configuration. FPGAs, by design, are capable of true parallel data processing. Due to these properties, they are typically used when a small number of versatile circuits for large amounts of complex parallel data processing is required. Typical clock frequencies are in the 100 MHz range, depending on the design.

The FPGA design flow follows multiple steps, the complete process it called design "synthesis". At first a valid configuration is typically specified using a Hardware Description Language (HDL). The programming code is then transformed into a Register Transfer Level (RTL) description and afterwards into a setting for the internal logic gates. The result is then used to program the actual FPGA chip.

FPGAs in general differ in three properties: The number of logic gates, which define how much logic can be stored. The internal structure, which determines how the information is represented internally. The additional internal hardware, like a micro-processor which enhances the functionality of the device.
A more in depth view of the FPGA used during this thesis, as well as further information about the design process, is found in [83, ch. 3.1.2].

2.7.2 IP core

An IP core is a piece of reusable software which represents a functional logic block for an FPGA with well defined interfaces. This functional block can be of any size, a single logical AND-gate can be regarded as an IP core as well as a complete processor design. The ability to reuse these blocks in different designs rapidly saves development time. Figure 2.19 shows a basic example of reusing one IP core in two different designs. Therefore combining different cores to compose a bigger system is very common. The equivalent of a compiler based programming language would be the usage of libraries. Even though these exist in HDLs as well, the difference is usually a self contained functionality. This means, not only single operations on specified data are performed by library functions, but a complete functional block, e.g. an internal memory, is represented by the IP core.

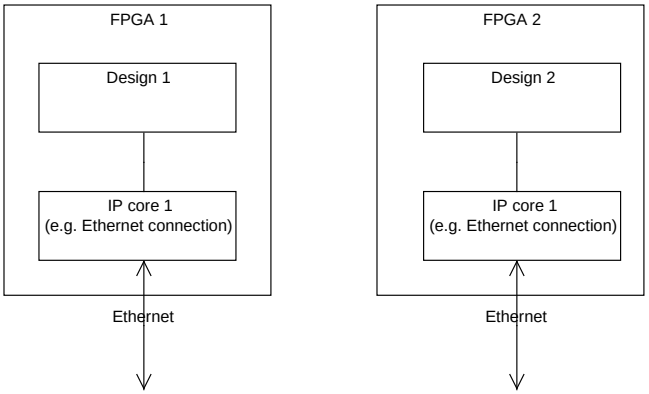

Figure 2.19: Example of universal IP-core usage. Instead of completely reimplementing the required functionality, the ethernet IP core is instantiated in both designs.

IP cores are available in different formats, representing the different levels of synthesis. Most common are three types: HDL based, netlist type, and hard-IP-Core. The first type is a representation of the functionality in form of a HDL. This enables every option of adoption and synthesis. The second type, the so called "netlist" version, is a further synthesized version of a design. It contains the description of the design's logical blocks and interconnections. This enables a better synthesis of the complete design as the internal routing of signals can still be optimized. On the other hand the designs are not easily modified, which protects the intellectual property contained in the core. The third type, Hard-IP-Cores, are cores which contain a hardware representing format. These cores can only be integrated as a whole into the design, often only on specific FPGA models. This offers good protection of the contained intellectual property at the cost of flexibility.

Chapter 3

Fast Orbit Feedback system design

This chapter gives an overview of the design-process of a fast orbit feedback. A general introduction to feedbacks as control loops is given and a more detailed categorization of orbit feedbacks, including possible advantages and disadvantages of different designs, is presented. The chapter closes with the conceptual development of the DELTA, COSY and SIS18 orbit feedbacks and the resulting required data acquisition structure for each feedback.

3.1 General design

3.1.1 Orbit feedback as a control loop - requisites

Control theory defines a feedback as a system which tries to minimize the deviation between an actual level and the reference level of a specified system parameter. An orbit feedback is a system, which is designed to optimise the orbit of a particle beam by means of magnetic fields to a reference level, which is called the reference orbit. Because the goal is to reduce the deviation, it can be classified as a so called "negative feedback" system [102]. An orbit feedback is usually realized as a closed loop controller, where the effect of the applied correction is measured (in contrast to an open loop controller which has no feedback over the effect of the correction). The beam orbit is constantly measured in a loop and a correction is then calculated and applied. Figure 3.1 shows an abstract overview of an accelerator orbit control loop. In contrast to Single Input and Single Output systems, a typical storage ring orbit feedback is a Multiple Input and Multiple Output system, with the beam orbit being measured as well as corrected at multiple locations. Under the assumption of linear accelerator

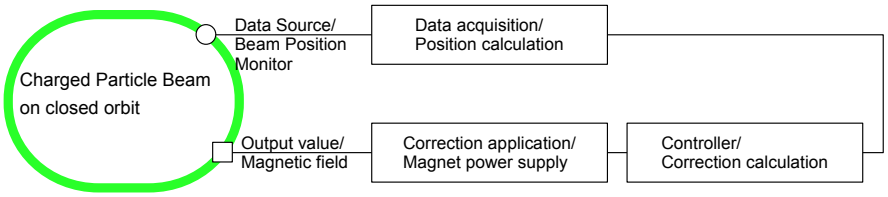

Figure 3.1: A basic closed orbit control loop for accelerators. The data source are the beam position monitors which couple to the particle beams electromagnetic field. A transverse position is then calculated from this data, which is used as input for the actual correction calculation. The result is a change in the magnetic configuration of the accelerator, which is applied to the accelerator's electromagnets by corresponding power supplies.

optics, an idealized orbit feedback is a Linear Time Invariant (LTI) system. It is linear because the superposition of beam offsets cause a superposition of corrective magnetic fields. It is time invariant because identical input parameters at any time produce identical output parameters with a set delay.
To reduce complexity, a real orbit feedback design should meet both properties. The linearity is achieved by the correction algorithms utilized. The time invariance has to be guaranteed by the use of corresponding time deterministic hardware like FPGAs or fixed delay circuits.
A real accelerator has additional parameters which are non-linear, vary over time and are not regarded by a LTI feedback. The design should keep the effects of these parameters to an acceptable minimum. A second approach is to measure the effect and adopt the feedback loop, increasing the complexity of the feedback system.

3.1.2 Classification of orbit feedback systems

Even though there is no fixed convention which is used throughout, orbit control systems can be broadly classified by the following criteria:

Orbit influence: Generally a feedback is called local, if only a part of the existing BPMs and correctors are utilized by the feedback. On the other hand a global feedback is usually utilizing all of the existing BPMs and correctors. In terms of optical functions a local orbit feedback should only influence the orbit inside a closed orbit bump, leaving the rest of the beam's orbit undisturbed. A feedback can be called global, if corrector magnets and BPMs cover the entire accelerator lattice. A sufficient distance between each station is 90 degrees betatron phase advance [2, ch. 6.3.1].

Speed of correction: A figure of merit for an orbit feedback is the maximum rate of correction. Depending on the accelerator, a feedback is typically called a Slow Orbit Feedback (SOFB) if the maximum correction rate is below 10 Hz. Feedbacks working within a typical range of 10 Hz to 10 kHz are usually called Fast Orbit Feedbacks (FOFBs).

Beam position data source: The main data source for the position data are the BPMs which directly couple to the electric field of the accelerated particles (see section 2.4.1). To improve beam stability most third generation light sources also use Photon Beam Position Monitors (PBPMs) as part of beam position monitoring [73]. These PBPMs are usually situated inside a photon beamline, indirectly measuring the beam position by detecting the beam emitted synchrotron radiation heading and position. An integration of the PBPMs as data source into the feedback control loop is also possible.

Control loop implementation: As the correction algorithm can be split to a desired number of separate matrix multiplications, the calculation of a correction can be split to different physical locations. This means, a feedback can be implemented in a centralized or distributed manner. Figure 3.2 shows

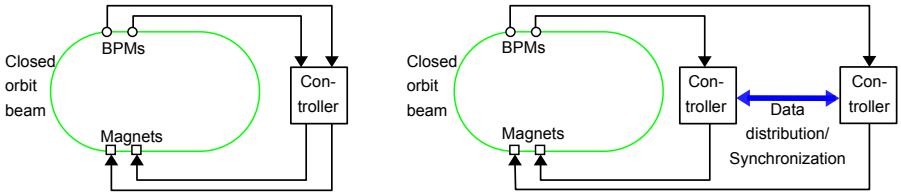

Figure 3.2: Global centralized feedback (left). The data is collected in a central point, where also the correction is calculated. Global distributed feedback (right). The data is collected by different stations which interchange their position data and calculate the corresponding corrections.

a structural view of both systems. The advantages and disadvantages of each approach is summarized in the following list, adopted from [87]:

- Centralized feedbacks feature a central point. All incoming BPM data are transferred to this location, the corrections are calculated and send out to the corrector power supplies and correctors.
  This allows multiple options of data processing, filtering etc. Additional features, like a feed forward system, can easily be integrated into the control loop. Also the configuration and adaptation is easier than with multiple, possibly different, feedback stations.

Critical to operation is the total network delay. Depending on the accelerator layout a central point also results in long cable length and therefore high signal runtime from BPM to the central point as well as back to the correctors and corrector power supplies. Also the amount of network connections to the central point is quite high. This also results in high incoming and outgoing data rates. Depending on the filtering and correction calculations made, a centralized approach may also result in a high computational workload. Today's standard PCs are easily capable of these computations, but it does become an issue when dealing with smaller - e.g. embedded systems. The scalability of such systems is limited, the ability to reduce or enlarge the number of BPMs and correctors has to be taken into account at system design time.

- Distributed systems partition the feedback loop. Each station has an arbitrary number of BPMs and correctors attached. The required BPM information for correction calculation is transferred between the stations using a data network.
  This reduces the number of incoming and outgoing connections of each station. As a result the internal data rates and the computational power needed is proportionally reduced. Depending on the design and the structure, failure of one or more stations does not necessarily lead to a breakdown of the entire system. Distributed systems are easier to maintain in respect to exchangeability of single stations.
  The disadvantage is a lower flexibility on the software side. A change of the feedback algorithm or other software has to be updated on every station. To ensure a timed correction, a synchronization structure is required as well as a data transfer structure which is capable of the deterministic data distribution. The separation of each corrector station results in independent orbit changes. The correction algorithm has to be designed not to create local orbit feedbacks which interfere with each other. The worst case would be a system which creates a non-closed orbit. In addition to the structural differences, the cost of the additional hardware for the stations as well as the data-distributing and synchronization structures required has to be taken into account.

3.2 Design for DELTA

The FOFB system for DELTA is required to be a modular, upgradeable research orientated global feedback. As a first step, a distributed feedback as general structure was chosen. This decision is the result of a number of practi-

cal constraints that were taken into account:

- As described in section 2.4.3, the orbit is measured by a mixture of Bergoz BPMs and I-Tech Libera Electron/Brilliance BPMs. To keep a homogeneous environment and save development time, this system had to be extended to support the additional feedback stations. In general the quality of the correction rises with the number of BPMs, therefore both BPM types had to be integrated into the feedback system as data sources.

- The actual correction calculation, that is the implementation of the SVD-algorithm and finding of suitable feedback parameters, for DELTA had to be developed.

- The possible installation positions and thereby the number of correctors and their strength was not set at design stage. The design had to be kept open in that respect.

- A centralized feedback implementation requires a deterministic and fast network structure from the BPMs to the central point and back to the correctors. The existing DELTA control net, due to the internal timing constraints, is not directly suitable for such a purpose. Therefore a new network structure would have to be built up, attaching to both types of BPM electronics. At design time, there was no commercially available network hardware which directly fulfilled these constraints. On the other hand, the Diamond Communication Controller (DCC) for distributed systems was already available to DELTA as an pre-implemented IP core(see section 2.7.2). In any case the Bergoz BPMs would require additional front-end hardware, therefore choosing a FPGA based design enabled the integration of the Bergoz BPMs and I-Tech Libera Electron/Brilliance electronics into one system. Also the clocking and synchronization hardware required for the I-Tech Libera electronics was already developed and installed (at the I-Tech Libera electronics installation points).

- The design of the Bergoz interface electronics (or station) was also underlying practical constraints. The existing Bergoz MX-BPMs are installed in sets of four (or less) inside Bergoz BPM-chassis around the DELTA storage ring. In order to keep cable length to a minimum, each station had to be able to connect to one of these chassis with an arbitrary number of connections.

- Apart from these physical constraints, operational constraints were also an issue. During the development the accelerator had to remain operational on hardware and on software (control system) level. A suitable on the

shelf test-bed had to be created. A possible integration into the control net, down-sampling and as thus utilizing the fast feedback orbit data for the slow feedback application had to be prepared. This has the advantage of higher orbit precision [83, Ch. 6.2.3].

- A good maintainability and easy operation was key to the design. This had to result in the usage of standard user interfaces software and, in case of the developed distributed feedback, the use of equally built stations which are interchangeable with each other.

- The feedback system was set out to be economically reasonable. This had to be achieved by utilizing as much pre-made as well as in-house built components in combination with existing hardware.

All of these requirements were best satisfied by a global distributed feedback, based on FPGA controller stations utilizing the DCC as communication interface. These stations were then called "BPM-Extender" for the Bergoz BPMs. Figure 3.3 shows a schematic view of the resulting layout. The promising results

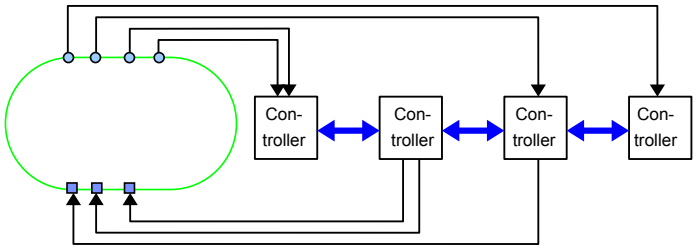

Figure 3.3: Structure of a global distributed orbit feedback for the DELTA storage ring. A mixed number of BPMs and correctors are connected to each controller. Correction calculation is distributed, the orbit data is transferred over a fast data structure

of the experimental local FOFB developed during previous works [83, 94] were part of this process.

Figure 3.4 shows the layout of the FOFB integrated with the SOFB. Auxiliary connections for synchronization (common clock), trigger signals (rising edge trigger) as well as control system connections (ethernet) were omitted.

The design is evolved from the design in [83, Ch. 4.1]. The prototype FPGA-board as well as the corrector station is replaced by the BPM-Extender device as a hardware platform.

The analog position data is transferred from the BPM knobs to the BPMs electronics, where the actual beam position is calculated. In case of the Bergoz MX-BPMs utilized, this is an analog calculation, resulting in an analog position value. This analog value is split between the SOFB data path and the FOFB

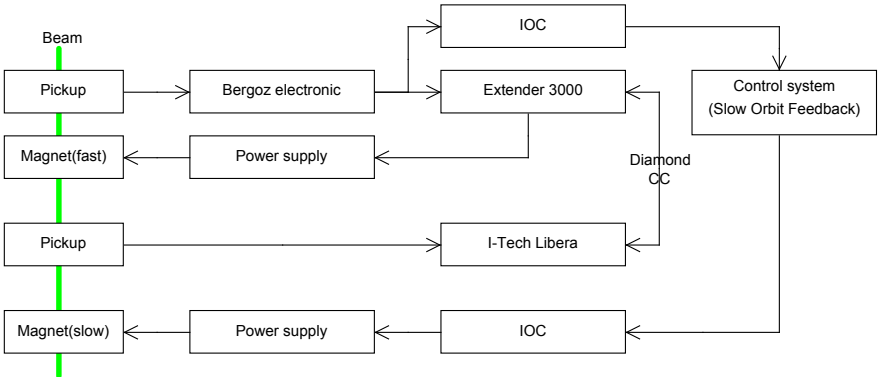

Figure 3.4: BPM data path for slow and fast orbit correction system. The fast orbit data is exchanged between Libera and Extender devices via DCC.

data path. For the already existing SOFB it is converted by Analog-Digital-Converters (ADCs) after an analog low pass filter (see [32, 110]). The ADCs data is then made available to the control system by IOCs. The control systems orbit control calculates a slow correction, which is applied through IOCs to the corresponding power supplies.

The analog FOFB position data from the Bergoz MX-BPM is converted to the digital domain by the BPM-Extender stations, utilizing the on-board ADCs. The orbit data is exchanged using the fast data network (Diamond CC), which features BPM-Extenders as well as I-Tech Libera devices. The latter are directly connected to the BPM knobs and digitally sample the analog button values to compute the beam's position. The BPM-Extender corrector stations calculate the correction and apply it to the beam using power supplies and corrector magnets.

The system is integrated into the DELTA control net (see section 2.1.2) by running EPICS servers. These supply the orbit and status data as well as receive control data.

3.3 Design for COSY/HESR

COSY itself is utilised as a testbed for the upcoming HESR(see [30]), especially for the upcoming HESR electron cooler (see [93]). Therefore the design had to take the requirement of a local feedback for an electron cooler into account. In preparation of the global SIS18 feedback, the decision was taken to design a local feedback at the existing COSY electron cooler with the prospect of to be adopted later to the HESR electron cooler section. The main design strategy from the DELTA system, including the distributed control loop, was kept. The

formerly utilized hardware was reused where possible. The BPM system was exchanged to fit to the COSY-BPMs requirements. Figure 3.5 shows a structural

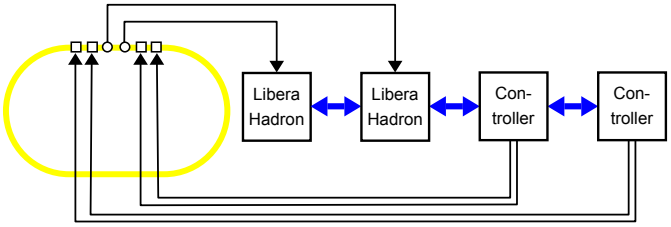

Figure 3.5: Planned local orbit feedback for the COSY accelerator electron cooler section. Two Hadron BPMs are used for the beam position calculation. The position data is sent to two DELTA, BPM-Extender type, corrector stations. These calculate the required correction and drive the corrector magnets power supplies.

overview of the COSY orbit feedback system.

The specific requirements and the resulting impact on the design were:

- COSY is a proton/deuteron accelerator using corresponding type BPMs (see section 2.2.1).
- Hadron BPMs require suitable position calculation electronics. In this case the I-Tech Libera Hadron (see appendix B.1.4) was chosen. These electronics feature the same FPGA as used in the other designs. A software package for bunch recognition and position calculation, developed at the GSI facility, is available [27].
- The DCC had to be integrated into the GSI I-Tech Libera Hadron FPGA design to integrate the I-Tech Libera Hadron electronics into the feedback control loop.
- As triggered measurements are planned, a suitable way for trigger inputs had to be found.
- COSY is run by the COSY-control system (see [65, 66]). A way to to integrate the feedback into the control system had to be found.

The main task was the integration of the DCC on the I-Tech Libera Hadron (details in section 4.2). Figure 3.5 shows the resulting fast local feedback structure for a proton accelerator, featuring a distributed control loop.

The analog data from the shoebox type BPMs is converted to the digital domain using the I-Tech Libera Hadron BPMs. The calculated position is then transferred via the communication structure (DCC) to the BPM-Extender type

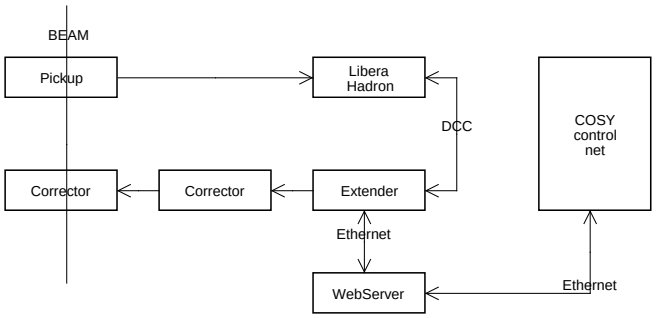

Figure 3.6: COSY feedback control loop. Data is sampled by I-Tech Libera Hadron, transferred using the DCC, correction is calculated and applied using the BPM-Extender. The control system is integrated via Webserver displaying the orbit and SSH connection for control.

corrector stations, where the correction is calculated and forwarded to the corrector power supplies. Integration into the control system is achieved by a webserver which is connected to the corrector stations (see fig. 3.6). This server acts as a front-end to the system, displaying the position data as graphics on a website as well as offering the ability to control the BPM-Extender and I-Tech Libera Hadron behaviour via Secure Shell, see also [106] (SSH). Trigger signals, generated by the control system, are applied to the system's internal trigger distribution.

3.4 Design for GSI/FAIR

The feedback design for the SIS18 accelerator follows the same design principles compared with the DELTA and COSY feedback designs, allowing the reuse of the developed system components. In prospect of the FAIR project, it is a testbed for the upcoming SIS100 and Schwer-Ionen-Synchrotron (SIS300) accelerator feedbacks. The design for the SIS18 feedback had to follow certain general requirements:

- The SIS18 is designed to accelerate hadrons and a range of ions (see section 2.3.2), possibly resulting in different feedback parameters.
- The BPM electronics already utilized at the GSI are I-Tech Libera Hadrons (see section 2.3.2).
- The feedback had to be designed to work at variable beam energies, specifically during the ramping period. At the SIS100 the accelerator optics, and

therefore the response matrix for the correction, changes during ramping (see section 2.3.2).

- Due to the upcoming FAIR upgrade, the control net is going to be restructured to a Front End Software Architecture (FESA) based system [72]. A possible integration of the feedback into the FESA system had to be taken into account by assuring technical compability.

Different particle types and bunch structures are supported by the FPGA software on the I-Tech Libera Hadron, developed by the GSI [27]. The feedback parameter set is not fixed, hence adoption of the feedback to different particle beams is possible. The main task is the response matrix change during ramping. As this is a matter of software implementation, the software design takes this alteration into account. The hardware and distributed control loop design is not affected by this requirement. A possible integration of FESA software components is achieved by using Linux as the operating system.

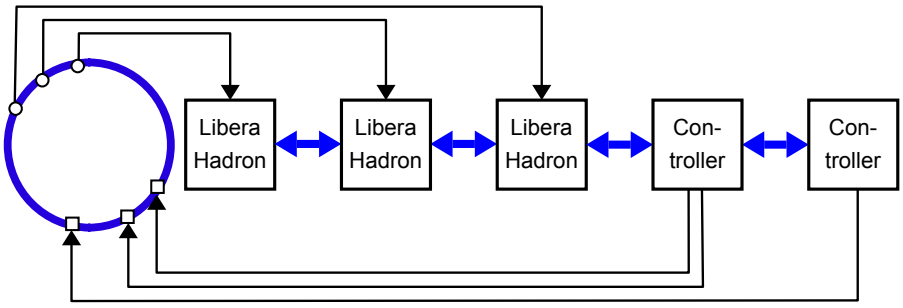

Figure 3.7: Overview of the planned orbit feedback for the SIS18 accelerator, for comparison see fig. 3.3. The beam position data is sampled by I-Tech Libera Hadron type BPMs. The data is transferred via DCC to the BPM-Extender type corrector stations, which calculate the correction and apply it to the beam using corrector magnets.

Figures 3.7 and 3.8 illustrate the resulting distributed system. It features the same structure as the COSY system, with I-Tech Libera Hadron data acquisition, BPM-Extender based corrector stations and ethernet server connectivity. Connection to the control system is achieved via FESA.

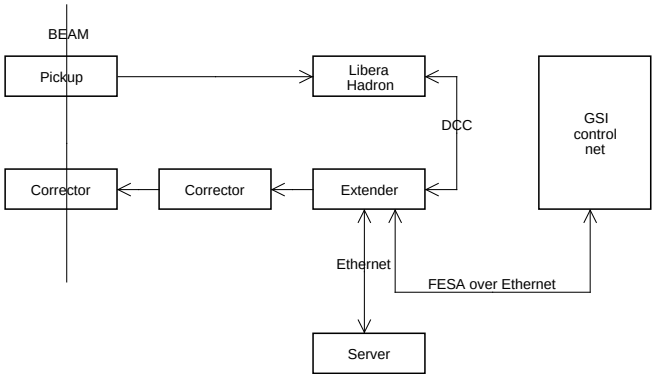

Figure 3.8: Planned SIS18 feedback control loop. Data is sampled by I-Tech Libera Hadron, transferred using the DCC, correction is calculated and applied using the BPM-Extender. The control system is integrated via FESA.

Chapter 4

Implementation

This chapter describes the implementation of the feedback system components. At first, a central element of the design, the BPM-Extender system, is described in detail. It is followed by the implementation details of I-Tech Libera Hadron, especially the Diamond Communication Controller. The chapter closes with a description of the measurement system built and the installation at the different accelerators.

4.1 The BPM-Extender 3000 system

The BPM-Extender system is a central component of the data acquisition and thereby of the feedback design. Developing the hardware and software was the most time consuming task during the course of this thesis.
The BPM-Extender system serves multiple purposes in the feedback systems. The distributed control loop is composed of BPM-Extender type stations in all presented feedback designs. The DELTA design also utilizes it as a Bergoz BPM to DCC converter, utilizing the analog measuring capabilities and integrating the Bergoz BPMs into the control loop. By software adaptations it is designed to act as a corrector station doing the required correction calculations. Additional connection options to different control system are possible by utilizing the on-board processor.

The following subsections describe the design process. The result of this process are the hardware structure and the software system structure, both are described in the later subsections. The software structure is divided into the different levels of the design. From the low-level FPGA structure, through the mid-layers, up to the top-level Linux operating system.

4.1.1 System design process

The design process of the BPM-Extender was grouped into three stages: Gathering of the requirements, hardware design and software design. Both design stages underwent a coarse to fine approach. After identifying the required components a general system layout was created. Each component of this layout was then elaborated step by step up to the required level of detail.

Technical requirements

The technical requirements which had to be met by the design are summarized below:

- Connectivity for four Bergox MX-BPMs in one Bergoz RFC chassis. This enables a mounting of the BPM-Extender near or next to the cradles, such keeping the cable length for the analog signals to a minimum.
- Inputs for external system clock, machine clock and trigger as well as a trigger enabled. These are the standard signals distributed around the DELTA storage ring.
- FPGA based system. It is a requirement for the DCC connectivity and ensures deterministic properties of the system.
- Fast Data output connection. This is a direct connection to the FPGAs pins, keeping versatility to a maximum, e.g. to connect corrector power supplies.
- Small form-factor pluggable (SFP)-slots. These are required for connectivity to the fast orbit data communication structure.
- RS232 connection, which is the standard input and output method of the in-built PowerPC. It is required for controlling and debugging.
- Remote access over Ethernet. The standard physical network technology at DELTA is ethernet.
- Easy maintainability and connectivity.

Due to the system's qualities, resulting from the requirements, the BPM-Extender system can also be seen as a feedback system hardware platform which is utilized differently by programming it with different software.

4.1.2 Hardware components

The BPM-Extender device is a combination of commercially available components as well as custom designed electronics. The choice of components and combination into the system is described in the following.

The electronic circuit design, Printed Circuit Board (PCB)-layout, fabrication and assembly as well as simple hardware tests of the BPM-Extender devices were conducted by the electronics development department of TU-Dortmunds physics department.

FPGA as hardware base

An FPGA as underlying hardware architecture for the system was chosen for multiple reasons. Apart from the requirement of an FPGA for the DCC, the advantage is the deterministic behaviour of FPGAs based systems. It allows synchronization and timekeeping of the feedback system whilst offering re-programmability. The actual FPGA being used, including the board it is soldered to, were already selected and evaluated beforehand (see [83]). This also includes the basic layout for the input, clocking and trigger reception.

The BPM-Extender device hardware structure

Figure 4.1 shows the hardware structure of the BPM-Extender device. The functional elements are combined into hardware blocks. Inside the casing they share the same PCB for partitioning and flexibility. The logical partition enhances error finding capabilities and exchange of single components. A flexible adoption of the design to specific needs if required is thereby possible. The main component of the BPM-Extender is the FPGA carrier circuit board. The secondary component is the so called ADC-board which houses the ADCs and logic for Bergoz connectivity as well as the physical inputs of the clocking and trigger signals. SFP connectors for the fast data network are carried by the SFP-board, a high-speed output adapter board transforms the high speed FPGA connection, the ethernet connector is guided to the outside. A RS232 display, four switches and status Light Emitting Diodes (LEDs) were added to the design for maintainability and status indication. Figure 4.2 shows the actual component layout inside the casing.

XUP-board

The Xilinx University Program (XUP) Virtex-II Pro Development System (in short called XUP-board) is a commercially available FPGA prototyping board available from Xilinx [42]. It carries the FPGA and auxiliary electronics and

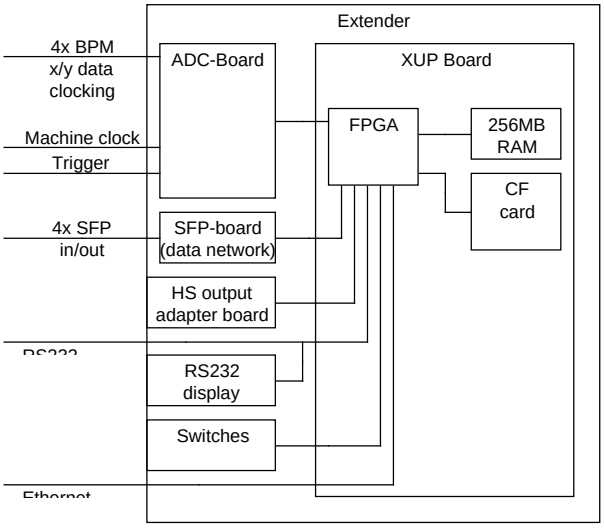

Figure 4.1: Extender depicted hardware structure with interconnecting buses. Dedicated PCBs are used for functional blocks and external connections as ADC, SFP, etc. These are connected via general purpose I/O connections to the FPGA board which houses the FPGA, the RAM and the compact flash card.

connectors. For reference see [39]. Figure 4.3 depicts the layout of the utilized XUP-board components. The following hardware alterations were made before installation in the BPM-Extender casing, the mentioned references (e.g. “ref. Y3”) are to the manufactures on-board identifiers:

- Exchange of the on board 75MHz quartz with a 106.25MHz quartz (see [12]) for RocketIO clocking (ref. U10). The frequency of the RocketIO communication is determined by this dedicated quartz, the new quartz matches the frequency of the I-Tech Libera RocketIO communication, which is not interchangeable.

- Installation of the machine clock feed to the on-board quartz connector (ref. Y3). This connection allows clocking the FPGA from the outside for clock-synchronous operation of all BPM-Extender devices.

- Installation of connectors for the fourth RocketIO port (ref. J19-J24). The FPGA features eight on-die RocketIO ports, four are directed to the PCB. Three of these are routed to the existing connectors and one to soldering connectors. These were equipped with Sub-Miniature-A (SMA) connectors.

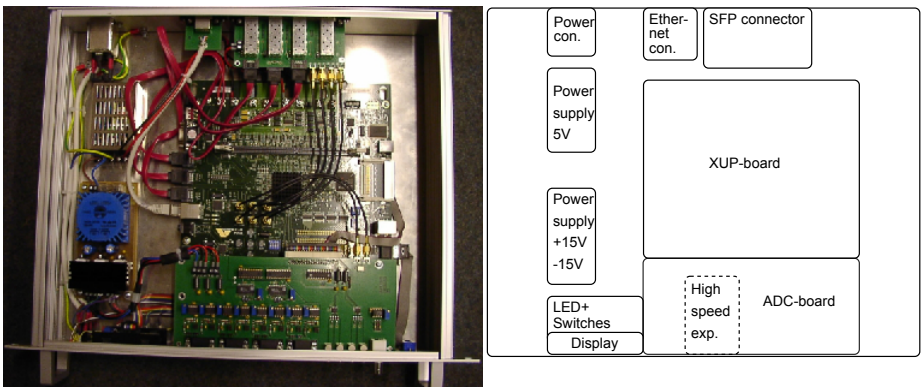

Figure 4.2: Extender device internal layout in detail. The front-side is to the bottom, it contains the main display, LEDs and switches for control, the connectors for the Bergoz MX-BPMs as well as a general purpose I/O high speed connector. The back-side contains the power connector and connectors for the fast data network (SFP). The design features one 5 V general power supply and a dedicated ±15 V power supply for the ADC reference voltage.

- Installation of a passive heat sink on the FPGA and an additional fan. As high thermal stress of the FPGA was observed during testing the hardware was installed for thermal safety.
- Installation of 256 MB Random Access Memory (RAM) module to the standard Dual In-line Memory Module (DIMM) slot.
- Installation of a Compact Flash (CF) card, which is required for the planned operation, to the standard CF card slot.

Analog-Digital-Converter board

The ADC board is the main component when utilizing the BPM-Extender system for Bergoz connectivity, housing all necessary hardware. Apart from the ADCs (and including filtering), a number of status signals is level converted and transmitted. A second part of the board is used for clock and trigger reception, with level shifting being the only conditioning of the signals. The chosen Analog Devices AD974 ADC was already evaluated and tested during the design for the ADC board (see [83, Ch. 5.2.1] which contains all technical information). Two minor modifications were made, an additional clock input connector was installed and the 106.25 MHz quartz was transferred to the XUP board.

Small form-factor pluggable board

Mounted on the back chassis panel are the connectors for the SFP modules. Internally they are mounted on one small PCB containing adapters for the

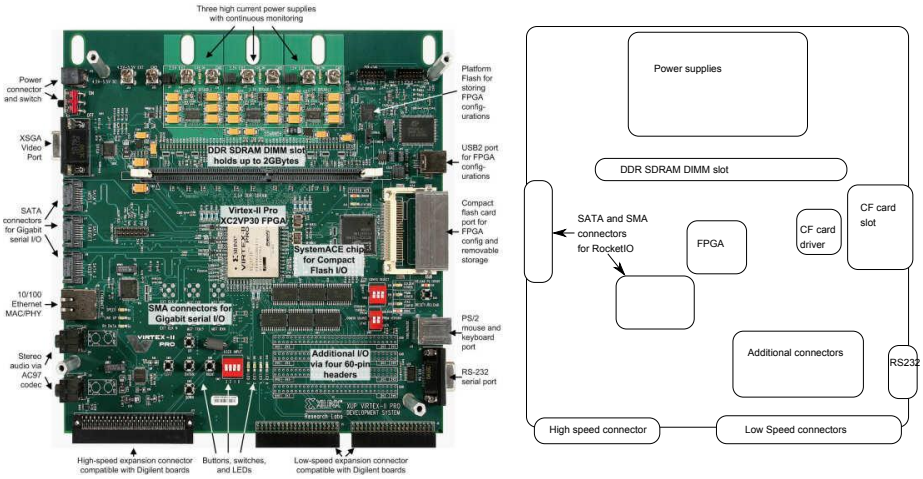

Figure 4.3: The XUP board in detail. The most relevant components are highlighted. These include the connections to the various PCBs inside the casing. The connectors for the fast data network are directly attached to the XUP board using the RocketIO connectors.

XUP board connectors. Three Serial Advanced Technology Attachment (SATA) type connectors and one 4xSMA connectors as well as power connectors are present. Figure 4.5 is an overview of the PCB layout. The SFP modules can be individually power supplied for different module types via jumper selection. The utilized Avago AFBR-57R5APZ (see [90]) SFP to glas-fibre modules require this power supply.

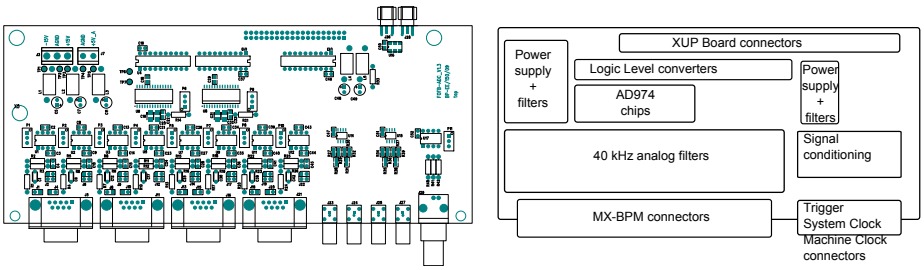

Figure 4.4: The ADC board in detail. The ADCs are centered on the board. On top are the connectors to the XUP board. The connectors to the BPMs are at the bottom, accessible from outside of the casing when build in. The board features a selectable analog low-pass filter for the ADC inputs to reduce aliasing. Also placed on the PCB are signal converters for different clock and trigger signals.

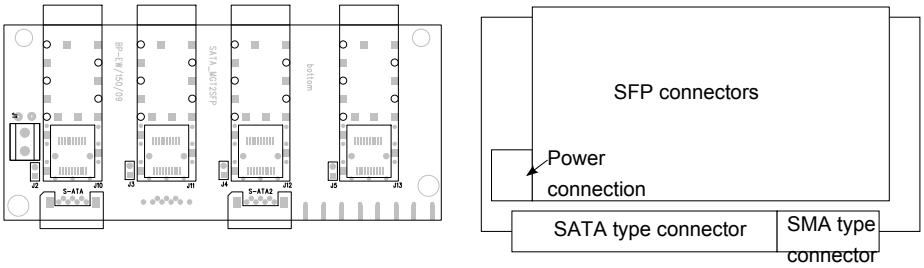

Figure 4.5: The SFP board in detail. The board is a physical adapter from XUP boards SATA- and SMA type connectors to powered SFP connectors.

Highspeed port adapter

The XUP-board features a so called high-speed-expansion connector (on-board ref. J37), which is directly connected to the FPGA. These connections are fed to the outside of the casing as versatile connection. The connection was used for debugging status signals, a possible future use are feedback applications. A direct connection was chosen for maximum flexibility, the connector is changed to a standard 40-pin ribbon cable connector. It is expected to support the expected data rate of well below 100 kHz and cable length lower than 1 m.

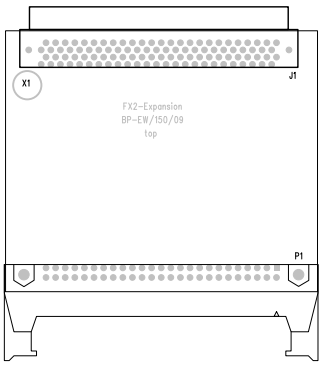

Figure 4.6: The high speed connector board in detail.

Additional connectors

A number of additional connectors were fitted:

- RS232 connector. The XUP-board features a RS232 connector directly wired to the FPGA. This connector is extended to the front chassis panel. The actual RS232 protocol is generated by the FPGA.

- Serial Display. An RS232 compliant Liquid Crystal Display (LCD) type EA SER204-92HNLEK (see [28]) was fitted to the front chassis panel. It is also directly connected to one of the FPGAs pins. This enables the option to drive the panel as a single output, or if wired in parallel to the RS232 output, as a mirror of the external communication.

- Ethernet connector. The XUP-board features a standard Ethernet connector, it is extended to the back chassis panel utilizing a small PCB. The required Ethernet protocol is generated by the FPGA.

- Clocking and trigger signals. Five connectors for clocking and trigger signals are installed. Four differential inputs capable of up to 125 MHz. One Bayonet Neill–Concelman (BNC) trigger input for trigger signals up to 800 kHz.

Switches and LEDs board

A set of four switches for future application is installed on the front chassis panel below the display. Additionally every input and output of the BPM-Extender is equipped with an LED for visualizing the internal status, a shared PCB houses the required resistors for the LEDs and de-bouncing logic for the switches. Figure 4.7 shows the board's layout.

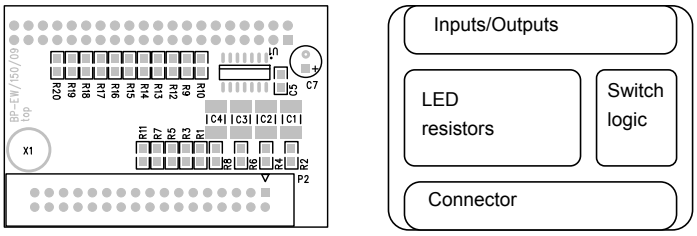

Figure 4.7: Layout of the LED and front-switch connector board. To provide some signaling to the user a number of LEDs are available. For user input four switches are attached to front of the housing. The board contains analog de-bouncing filters for these switches and resistors to drive the LEDs.

Internal power supplies

The FPGA as well as the ADCs require specific Directed Current (DC) voltages. Two separate, standard switching power supplies, are featured in the BPM-Extender.
One supply delivers all voltages required for the FPGA and surrounding logic, including power to the ADC chip. The second supply is used only for the ADCs reference voltage. This increases stability and precision of the reference voltage and hence of the ADC readout. The bipolar ADCs are supplied with $+-15\,\mathrm{V}$.

LED-board

An external PCB was created (not shown) to debug single signal states for signals below 1 Hz. It attaches to the high-speed-expansion port of the BPM-Extender, containing 40 LEDs and corresponding resistors, each representing a respectively routed signal. Usually this feature is used during development to monitor internal status signals.

4.1.3 Software system structure

The BPM-Extender software structure is a result of the hardware and functional requirements as well as general system design. Two general, interleaving, design strategies were applied.

Layered design

A typical FPGA system is divided into different layers, mostly (as chosen for the design of the BPM-Extender) into three layers with different objectives (shown in fig. 4.8).

The bottom layer is connected to the external signals. It contains all the logic required for the input and output of these signals. This layer is implemented as logic in the FPGA, yielding the advantage of deterministic and fast parallel data processing. The disadvantage is the lacking flexibility in case of an design change (as the whole system has to be time-consumingly resynthesised). An example for a bottom layer component would be an ethernet driver, receiving and sending ethernet packets and extracting/inserting the actual data out of/into these packets and managing the required hardware communication protocol.

The middle layer is the so called transport layer. It is the connecting layer between the bottom and the top layer. It contains a bus structure and nodes to this bus. These nodes are connected to the top- and bottom layer on the one hand and the bus structure on the other. The bottom layer data flows through

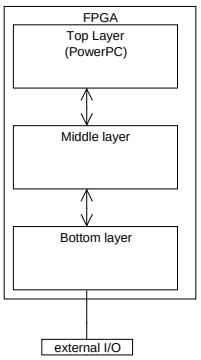

Figure 4.8: General System Design. By splitting the system into 3 layers which are interconnected by well defined interfaces, the overall complexity of the system is reduced. This reduces development time and allows for an easier maintenance. The bottom layer contains the connection to external signals while the middle layer transports this information to the top layer where the actual data processing takes place. The two lower layers are implemented as FPGA logic while the top layer consists of a PowerPC micro-controller.

the bottom layer nodes over the bus to the top layer nodes and the top layer and vice versa. In case of the BPM-Extender design these connections, as well the nodes, are implemented as FPGA logic. A design with external buses is possible as well. The integration of the bus structure is advantageous, as it can be adapted to the required task. The downside is the increased design-size and limited debugging options.

The top layer contains the system's processor. Usually it takes over the task of controlling and managing hard- and software of the underlying bottom and middle layer. In case of data processing this means receiving data from the bottom layers external connection over the middle layer, processing it and sending the results over middle layer to the bottom layers external connection again. A processor is used for the flexibility it offers, as changes are quickly implemented in source code which can be installed and executed at runtime of the system. Often an operating system is implemented to support the system, in case of the BPM-Extender Linux is utilized.

Component based design

The software design follows the same design principles as the hardware design. Both designs are strongly component based. Hence each hardware component in the design corresponds to at least one FPGA software component (which again may consist of many subcomponents) in the source code. The bottom layer of the software design is a result of the external structural condition. Due to this,

the flexibility of the design is increased. In case a component is (ex-)changed only the corresponding software component has to be altered. The system is then designed from the bottom layer towards to the top layer. After analysis of the bottom layer for the information it requires as input/output and their timings, the communication and thereby the middle layer is defined. The use of a microprocessor as top layer resulted directly from the requirements in case of the BPM-Extender device. It includes an operation system and the integration of the interface to the bottom layer.

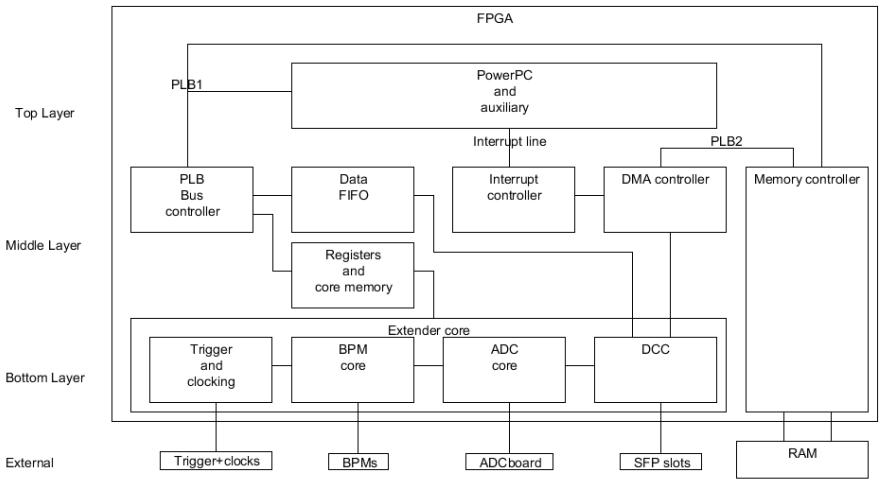

Figure 4.9: Extender Internal layered FPGA structure and RAM. The bottom layer was developed from scratch (apart from the memory controller) whereas the middle and top layer used predefined components which were adopted to the required needs.

As described in section 2.7 the FPGA design is composed of IP cores and interconnecting logic. Figure 4.9 shows the structure of the BPM-Extender FPGA design.

The bottom layer contains all the BPM-Extender input and output specific IP cores contained in the BPM-Extender IP core.

The middle (communication) layer contains different communication components which are connected to the PowerPC processor (top layer). The bus used is the Processor Local Bus, it was chosen because of its availability and integration in the Xilinx development tools. Most of the bottom layer components are memory mapped, which means each component has a memory region which is mapped to its in/outputs. The functionality for this is provided by the memory component. A data First In First Out (FIFO) component (connected to the DCC) has been added as an alternative way of orbit data transfer to the

top layer, the advantage being a longer availability of the data before readout. For Direct Memory Access a DMA- and an interrupt component has been added together with a second Processor Local Bus connection. Details of the PowerPC connection are given in section 4.1.5.

The PowerPC itself as top layer is available as a configurable IP core which also makes use of dedicated micro-controller components on the FPGA fabric. Therefore it is able to deliver a good computing power while still being adaptable to different requirements. In this case the the external RAM is utilized over the Processor Local Bus and the corresponding memory controller component. The component attaches directly to the PLB on the one hand and to the RAM on the other hand. It supports multiple bus connections, in this case it contains two Processor Local Bus connections. One for the PowerPC and auxiliary data, one exclusive line from the BPM-Extender Direct Memory Access (DMA) component for fast orbit data transfer.

IP cores

This subsection gives an overview of the functionality of each IP core.

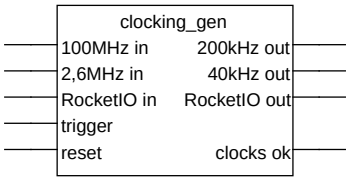

Figure 4.10: Example of a small IP core: The BPM-Extender clocking generator IP core

Clocking IP core The different parts of the design require different clocking (or clocks). The clocking core contains all the necessary logic for this task. A detailed view of the clocks is given in section 4.1.4. Figure 4.10 shows the clocking generator core with its inputs and outputs. The IP core also contains the logic to suitably convert the clocking signals (e.g. the RocketIO clock is converted from differential to single signal), as well as triggered clock synchronization (and synchronization signals to sub-components like the DCC), and drivers for the clock status LEDs.

BPM and ADC core The BPM-core includes the logic to distribute the clock signals required for the Bergoz BPM clocking as well as finding a measurement optimal Bergoz SYNC configuration. The ADC core contains the logic

to drive and readout the ADCs on the ADC-board. The functionally of both cores is described in great detail in [83, Ch. 5.3.1]. After being enabled, the core configures the Bergoz electronics and starts the sequential readout. The converted data is then supplied at the outputs. Validity of the data is indicated by a dedicated signal.

DCC The task of distributing the position data between the feedback stations is taken over by the DCC. It is a time-frame based, deterministic communication protocol, for details see [98].

Access to the DCC data is established by utilizing the DCCs inbuilt 2-port RAM. One port is used by the DCC for internal reading and writing of the position data, the other one is fed to the outside. It is connected to the DMA controller for orbit data transfer to the system memory. The configuration and data transfer of this core in the BPM-Extender context is described in detail [83, ch. 5.3.2-5.3.3].

PLB Bus controller Transfer of non time-critical data as well as settings for the cores is exchanged between the PowerPC and the cores over the Processor Local Bus (PLB). The PLB controller used is a Xilinx supplied PLB IP core from Xilinx which is PLB architecture compatible and provides the complete PLB bus structure [40].

Registers and Memory Operation of the cores is controlled through values set in the in-built registers and memory. By connecting these to the cores on the one side and the PLB controller on the other side, an access to those values via PLB and thereby via PowerPC is possible. As this integrates the cores into the memory space of the PLB and thereby the memory space of the PowerPC processor, this technique is called memory mapping.

DMA controller To enhance the data throughput to the system's RAM as well as keeping the option to access the system's memory without a PowerPC open, a DMA was integrated. It connects directly to a second PLB in the design, writing it's data, that is the DCC position data, to a register preset location. By connecting it to a second port on the system's memory controller, the highest possible data throughput is achieved. An interrupt is raised via the interrupt controller when data writing is finished and readout from the PowerPC can begin. The DMA core also supplies the required information for an interrupt driven scatter gather Direct Memory Access implemented on the top level.

Interrupt controller The interrupt handler core collects possible interrupts in the BPM-Extender core and reports them as a collective interrupt to the PowerPC. In this case the Xilinx LogiCORE IP Interrupt Control core was configured and used (see [41]). In case of the BPM-Extender system, the BPM-Extender core writes the orbit data via DMA to the system's RAM. After finishing this write, the interrupt is raised, signalling the processor to start the readout of the orbit data.

Data FIFO A secondary option of data transfer is giving by the utilization of an IP core based FIFO, also connected to the PLB. It is mainly used for the transfer of the ADC data to the processor for debugging purposes.

PowerPC A single PowerPC was added to the FPGA design, it was clocked to 300 MHz and 16 kB of cache was added for performance. Part of this core is available in hardware on the FPGA fabric, the required surrounding logic and configuration options are created during core generation.

4.1.4 Clocking Domains and Clock Domain Crossing

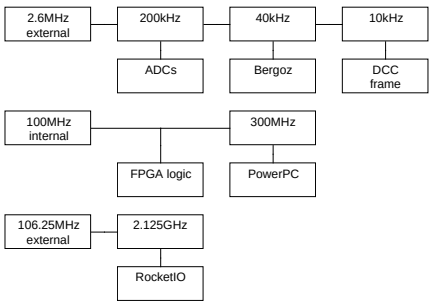

Figure 4.11: Distribution of clocks inside the design.

As a result from the requirements, the design contains multiple clock domains derived from two clock sources. The RocketIO ports are driven with 106.25 MHz base frequency multiplied by 20 for operation, the ADCs are clocked with 200 kHz readout frequency, the Bergoz BPMs are driven by a derived 40 kHz clock which also generates a 10 kHz signal for the DCC frames. All other logic is driven by the internal 100 MHz clock including the PowerPC, after multiplication to 300 MHz.

Where data is transferred from one clock region to the other, a clock-domain-crossing was established. In case of single signals a register transfer circuit was used, in case of multiple signals buffer logic was used.

4.1.5 Software components

Utilizing a microprocessor to control the BPM-Extender device requires the design of a software structure. Its design requirements were already set by the hardware design and by the functionality analysis:

- FPGA connectivity
- Ethernet connectivity/remote access
- EPICS connectivity
- Preferably Open source and/or low cost software

The FPGA connectivity, that is the connection between PowerPC and the FPGAs components (or cores), is already given by the hardware design (see section 4.1.3).

Linux was chosen for ethernet connectivity and EPICS functionality, a custom implementation would not have been beneficial.

Linux as operating system

The choice of Linux reduced the cost of implementation. On the hardware side, drivers for nearly all FPGA components, as well as the on-board components like the compact flash adapter, are already available from Xilinx. On the software side, Linux as operating system takes over the task of the system management. Hence development could be concentrated on actual functionality of the system instead of internal system management work (e.g. memory management). A PowerPC version of the Linux kernel is available, as it is a common processor architecture. The version chosen for the project is Linux kernel version 3.2.1 from the [60] repository. A custom kernel was generated by cross-compilation, this is the process of compiling code which was written for a specific architecture for the required systems architecture, in this case PowerPC. The compilation includes an ethernet driver for the Xilinx ethernet IP core and a compact flash driver for the internal compact flash card.
These integrations have multiple advantages. The ethernet access permits a remote login to the unit, which is a necessary criterion for operation in remote locations of the accelerator. Due to the structure of Linux, it allows a very flexible software design. Part of this design is the storage of the FPGA image on the internal compact flash card on the one hand, and a server based Root File System (RFS) on the other.
The actual FPGA image, including the bootloader code and Linux kernel, is stored on the internal compact flash card of each device. At system start-up,

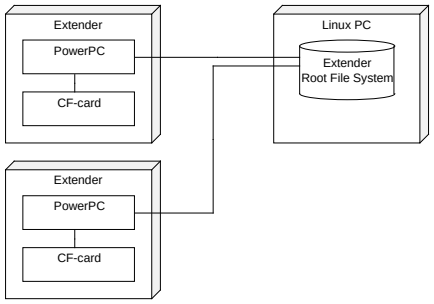

Figure 4.12: System layout showing two Extender stations and the central linux based server. At startup, the FPGA image for each Extender station is loaded from the respective CF-card. The root file system is then loaded via NFS from the server. This allows station specific FPGA hardware designs to be loaded as well as having the advantage of having only one (common) data base for the software processing tasks.

at first the FPGAs logic cells are configured, as such preparing the hardware. The bootloader code is then executed and loads the kernel, which can access the ethernet connection. The RFS is then loaded from a remote server. For multiple units this design has the advantage of having to do changes to the operating system only in the server's directory in contrast to a change on each single device. Figure 4.12 graphically illustrates the server based RFS.
In case of the compact flash integration, accessing the stored FPGA image at runtime is possible. As this makes the compact flash card also accessible from Linux, a new FPGA image can be written to the internal compact flash card. Both changes, FPGA image and RFS are activated at the next reboot of the BPM-Extender devices.

BPM-Extender Linux device file Hardware in Linux is made accessible through so called device files. These are files and folders in the `/dev` folder of the file system. Device files can be read and written like ordinary files.
Controlling the BPM-Extender IP core in Linux is achieved by mounting a special BPM-Extender device as a kernel module. A new device folder in the `/dev` folder is created and linked to the BPM-Extender IP core driver. The kernel module serves two tasks: First, it allows the access to the BPM-Extender configuration. Second, it installs the required interrupt handler.
The BPM-Extender IP core is controlled through its configuration memory. This is made available by mapping it into the address space of the processor. The core can then be configured from the so called user space by reading and writing to the device.
Whenever important events occur, an interrupt is raised and a predefined pro-

gram, the so called interrupt handler, is executed. The interrupt handler for BPM-Extender IP core interrupt is installed by the device file driver. In most modes of operation, it is used for the the DMA operation.

Linux memory The board's memory as well as the FPGA internal memory is combined into one continuous memory space. The total available memory is the 256 MB external memory plus 256 kB FPGA internal memory. The internal memory contains the configuration and status information for the different IP cores. The BPM-Extender IP core configuration memory is also mapped into this region.

The external memory is used by the Linux kernel for program execution. The

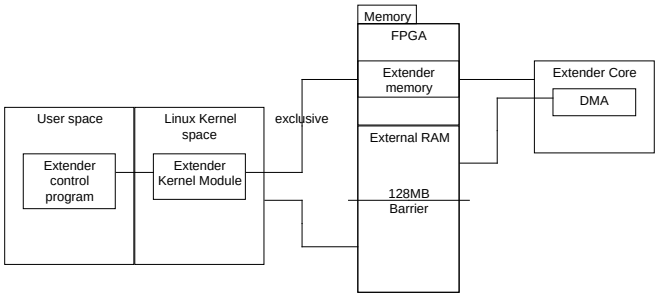

Figure 4.13: Linux system memory access. The joint memory space is accessed from user space through a kernel module for configuration and status data. The orbit data is written by the DMA core into the upper 128 MB of memory, which is not directly used by the kernel, but is accessible through the BPM-Extender kernel module.

kernel is restricted to use only the lower 128 MB for operation by kernel command line. The upper 128 MB of the external memory is not utilized by the Linux kernel, but it remains accessible by kernel functions. Thereby an exclusive memory region, which is used by the BPM-Extender DMA IP core, is created.

To ensure safe operation the Linux operating system splits code execution into to environments: kernel space and user space.
Access to the low level functions (e.g. direct access to the system's memory) is only possible from kernel space.
High level programs are run in user space, accessing the kernel's function through the device files. This allows a safe usage of the low level functions as illegal instructions are intercepted by the device file drivers.
In case of the BPM-Extender, the corresponding kernel module allows exclusive access to the BPM-Extender memory space inside the global memory space. Figure 4.13 shows the memory layout and access to this memory from Linux.

Linux BPM-Extender Interrupt The BPM-Extender core contains an interrupt core, outputting an interrupt line to the PowerPC interrupts. This interrupt line is exclusive to the BPM-Extender IP core, this is called a non-shared interrupt. It enables the BPM-Extender IP core to interrupt the processor and run a custom interrupt handler code.

The BPM-Extender IP core supports different interrupt modes. In general the interrupt is connected to the DMA IP core. An interrupt is raised when the core has finished writing the orbit data to memory. This is possible for continuous operation, resulting in one interrupt each 100 ms, as well as for a set number of samples, resulting in one interrupt at the end of operation.

The interrupt handler gathers the data from the memory and processes it further. Depending on the mode of operation, the data is processed, saved or both. A possible option for this is averaging of the data to a rate of 10 Hz, suitable for the DELTA control system. If set by configuration, the data is saved to a file in the mounted Network File System (NFS). This is possible in all modes of operation.

Linux BPM-Extender user space program To ease the access to the BPM-Extender IP core, which is accessible by using a raw-byte interface of a Linux device, a Linux user space program was programmed. It is cross compiled for the PowerPC architecture and takes over the task of accessing the BPM-Extender IP core. It offers the functionality of reading and writing the complete BPM-Extender IP core memory configuration. It is controlled via command line switches, making automated access possible.

4.2 I-Tech Libera Hadron FPGA design

Inside a hadron machine feedback loop, the BPMs data is read out by the I-Tech Libera Hadron. The beam position is calculated and then distributed trough the fast data network to the corrector stations, which are BPM-Extender devices. Figure 4.14 illustrates the I-Tech Libera Hadron inside the hadron feedback control loop.

The internal FPGA structure of the I-Tech Libera Hadron, due to the resemblance in tasks, is similar to the structure of the BPM-Extender. Figure 4.15 is a graphical representation of the system's layout. The four analog position signals coming from the BPMs plates are converted by 14 bit ADCs with a frequency of 125 MHz into digital values. These are transferred to the GSI FPGA IP core, where signal conditioning and position calculation, as well as additional calculations (e.g. intensity), takes place. This position information is then passed

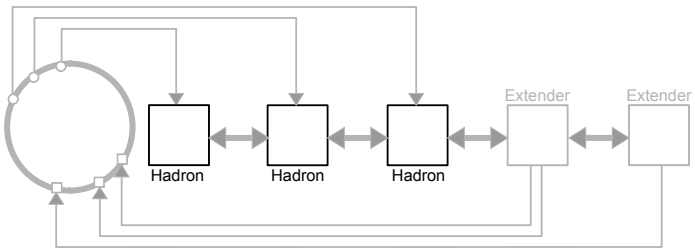

Figure 4.14: Depicted hadron feedback control loop containing I-Tech Libera Hadron as used for BPM readout and data distribution.

on to the BPM-Extender IP core which is modified for the hadron data input. The data is then distributed around the orbit data network.

In addition to the FPGA, a Single Board Computer (SBC) is installed inside the I-Tech Libera Hadron providing a Linux front-end for control and status information.

The BPM-Extender IP core was reduced to the components which are utilized in the hadron design. A new data front-end, the hadron data collector IP core, was implemented. The clocking core and the DCC core are taken from the BPM-Extender design. Figure 4.16 shows the structure in detail.

Position data arrives with bunch frequency at the input port of the Hadron data collector. As the DCC data exchange rate is 10 kHz, the data has to be averaged. All samples arriving during one 10 kHz period are added up, the number of added samples is stored. The sum and the number of samples are then transferred via DCC. The actual position is re-obtained by division on the processor level, saving the necessity of division implementation on the FPGA level. Additionally the number of samples shows a good overview of the number of recognized bunches, a valuable tool for debugging.

Setting and readout of configuration and status values is accomplished by an extension to the hadron register receiver IP core. The memory is directly integrated into the SBC memory map, thus making it available for access via Linux.

4.3 I-Tech Libera Hadron measurement system

To conduct proof of concept measurements a mobile measurement system for hadron machines was built based on the distributed feedback design. It consists of a small 19 inch rack which contains all the electronics, power and network distribution, an accompanying control PC and optionally a function generator as clocking/trigger source. Figure 4.17 shows the component layout of the system.

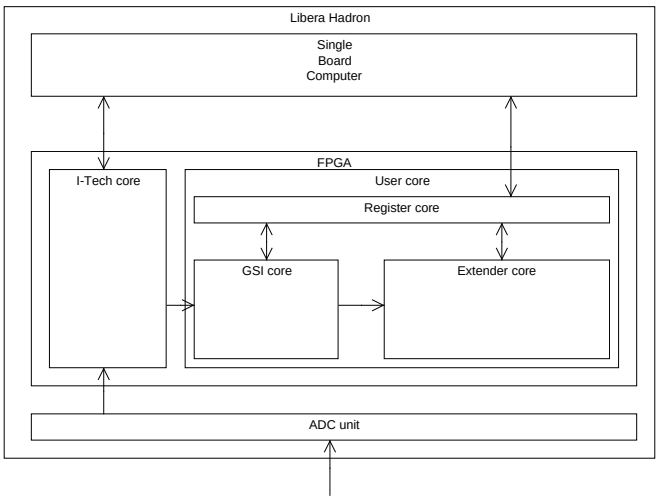

Figure 4.15: Internal I-Tech Libera Hadron structure. The orbit data (blue arrows) flows trough the ADCs which are controlled by the manufacturer's core (I-tech). The beam position is then calculated from the digitized values (GSI-core). This position data is transferred to the BPM-Extender IP-core which distributes it over the orbit data network. The whole system is controlled (black arrows) by an in-built SBC running Linux trough access to the configuration memory. This memory is contained by the user core inside the register core.

The main components of the rack are four I-Tech Libera Hadron, connected to the BPMs and one BPM-Extender device, which build the orbit data network by sequential connection via DCC over SFP optical cable. The measurement data is distributed among the I-Tech Libera Hadron as well as send to the BPM-Extender, which acts as a so called sniffer in this design. This means, it participates in the data transfer, but does not inject own position data into the network.

DELTA Trigger Splitters (see appendix B.1.5) are used to split up the trigger and clocking for the rack's components. Electric or optic input signals can be used, enabling easy adaptation to different accelerators trigger and clocking signals. The clocking signal is used to establish a common time base between the devices, the trigger signal has multiple uses. On the one hand it synchronizes the orbit data network, on the other hand measurement can be started by trigger. For independent use and testing, an ethernet controlled function generator is utilized as a possible trigger and clocking source.

Each of the devices is connected to the rack's internal standard ethernet network. The network is a local network, accessible from the outside over the

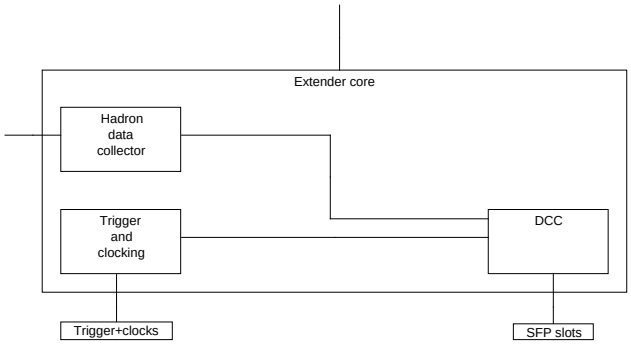

Figure 4.16: Extender core inside the I-Tech Libera Hadron. Triggering and clocking, configuration memory interface and DCC interface are reused from the electron design (see section 4.1. The hadron data interface is integrated additionally.

attached control PC. It serves as Dynamic Host Configuration Protocol (DHCP) server for the measurement system IP-subnet, as front-end to the outside and as Linux RFS server for the BPM-Extender.

An ethernet switch-able power socket was installed to remotely reboot the I-Tech Libera Hadron, the BPM-Extender device or the function generator if necessary.

Installation and migration of the measurement system was simplified by integrating all necessary components into one rack. The connections to the outside are power, ethernet and the BPM input signals for the I-Tech Libera Hadron.

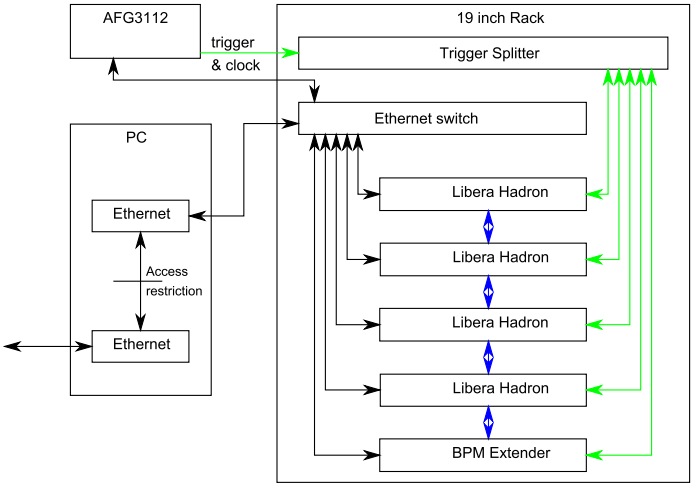

Figure 4.17: Simplified view of the I-Tech Libera Hadron measurement system. Ethernet(black) connects all devices, trigger and clock(green) is internally distributed, the DCC fast data network(blue) connects the libera hadron and the BPM-Extender, which acts as a sniffer. External access is possible via restricted ethernet connection.

4.4 DELTA installation

The complete installation of a fast orbit feedback system at DELTAs storage ring is divided into two steps. At first the DAQ (including the orbit data network) is installed, in a second step the actual feedback calculation as well as corrector power supplies and corrector magnets are added. The first being one of the tasks of this thesis, the second task is covered in [95].

The DAQ installation consists of the BPM-Extender device installation, Bergoz BPMs connection, trigger and clocking network installation, orbit data network installation and ethernet network installation. Figure 4.18 shows an overview of the different BPMs installed at the DELTA storage ring.

Extender installation Fourteen BPM-Extender devices were installed at the DELTA storage ring to access all Bergoz MX-BPMs. The BPM-Extender device chassis, as well as the Bergoz MX-BPMs, fit to standard 19 inch racks. By mounting both devices stacked, cable length is kept to a minimum. Due to the tight space constraints under the storage ring magnet structure, standard racks did not fit. Instead a new support was designed. It allows the stacking of one MX-BPM, one BPM-Extender and optionally one Trigger splitter.

Bergoz connection Each Bergoz MX-BPM is connected to the corresponding BPM-Extender device in the same rack with a standard 15 pin SUB-D one-to-

one cable. To minimize cable length, these cables were custom made by the electronics department.

Trigger and machine clock distribution The distribution of clock and trigger signals is achieved by using the so called DELTA Trigger Splitter (see appendix B.1.5). Each of these device is capable of serving up to four receiving units. To serve all BPM-Extender devices, four Trigger splitters were installed around the storage ring. Three of these devices feed four BPM-Extender devices, while one device feeds is attached to two BPM-Extender devices. All trigger splitters were installed inside the new support racks.

To distribute the trigger and clock signals to the Trigger splitters, a multi-core optical cable was used. It contains 12 optical cables and has a total length of 100 m. Four of these cables, one to each trigger splitter were installed. The cables join up in the control room, where the Master Trigger splitter is situated. Currently one trigger signal and the machine clock signal is transmitted. Optical cables were chosen on the one hand because of the pre-existing infrastructure (of Trigger splitters and optical cable to the I-Tech Libera devices), on the other hand because they are not liable to electromagnetic interference.
Each trigger splitter is connected to the corresponding BPM-Extender units by using two 20 m signal cable equipped with a 2-pin connector. One cable transmits the trigger, the other cable transmits the machine clock. The signal is transmitted differentially to increase external noise tolerance.

Fast orbit data network installation Even though the topology for the orbit data network can be freely chosen, due to the comparably short circumference and therefore comparably short transmission delay, a ring topology was installed. This means each BPM-Extender unit has two connections, one to each neighbor. The connections in total consist of 13 cables, each 20 m long, containing two optical fibers, one for each direction. For later experiments the I-Tech Libera devices were added to this structure by integrating them into the loop. To and from the I-Tech Libera racks the 20 m cable was used, between each I-Tech Libera a 50 cm cable was sufficient.

Ethernet network installation Each BPM-Extender unit was connected to the nearest ethernet switch. These were already installed. The cable length differs for nearly every device, this is of no consequence as the data transmission time is not important in this case.

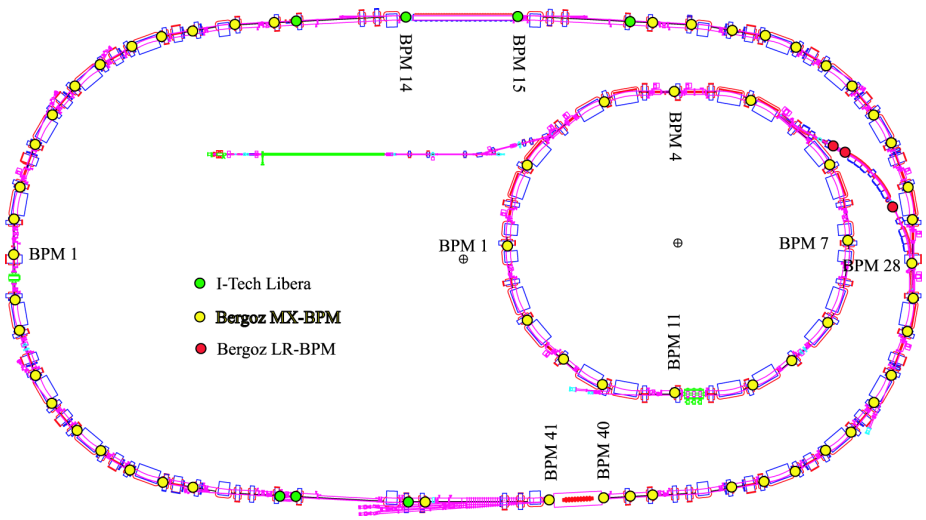

Figure 4.18: Distribution of BPMs around the DELTA storage ring. The standard BPM type are the Bergoz BPMs while locations around the insertion devices are equipped with I-Tech Libera devices. Special BPMs are also used for the transfer structures.

4.5 COSY installation

Prior to installation at COSY, a Matlab [92] accelerator toolbox [56] model of the basic COSY lattice was created by converting the existing MAD-X [10] lattice file (see fig. 4.19). This was used by P. Towalski to study the effects of the current corrector magnets as well as a possible local orbit feedback system for the electron cooler [95, 96].

To gain position information about the beam at the COSY accelerator, the measuring system (see section 4.3) was installed at the storage ring. It is connected to COSY-BPM 19 and COSY-BPM 20. These BPMs surround the COSY electron cooler (see fig. 2.3).

In this case the horizontal position signal is used. It is split into a direct and and amplified connection for calibration purposes. Each BPM is attached to one I-Tech Libera Hadron. The data is then made available by utilizing the BPM-Extender device. Figure 4.20 shows a structural view of the installation. The reference clock for the DCC was generated by the internal function generator. A timing variable trigger signal was externally supplied by the COSY timing system. Both signals were distributed to the devices using the internal clock and trigger splitter. Remote access to the system was available through the ethernet connection of the accompanying PC.

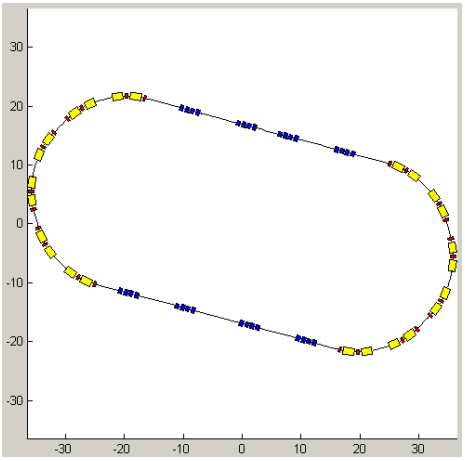

Figure 4.19: Rendered image of the basic COSY lattice, modeled for the first time using the Matlab Accelerator Toolbox.

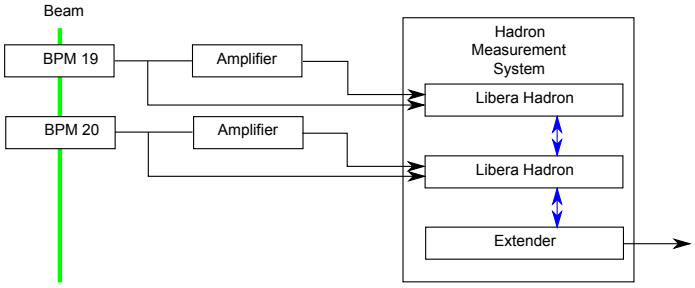

Figure 4.20: Simplified view of the I-Tech Libera Hadron measurement system at COSY, showing the path of the data. The DCC fast data network is illustrated in blue. Clocking and trigger signals are not shown.

4.6 GSI installation

The measuring system described in section 4.3 was also used for measurements at the SIS18 in the end of 2012. The system was installed in the electronic's room of the SIS18. The four I-Tech Libera Hadron were connected to the corresponding BPM plates of SIS18 BPM 9 to 12. The internal function generator was used to generate a common clock. The trigger signal, generated at the start of each ramping, was taken from the GSI timing system. To do reference measurements the inputs were split utilizing power-splitters between the native SIS18 I-Tech Libera Hadron and the measurement system. Figure 4.21 illustrates the setup.

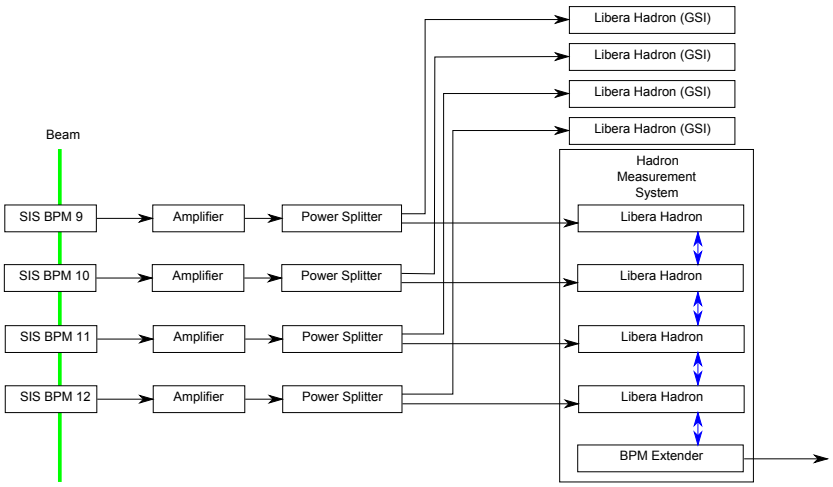

Figure 4.21: Simplified view of the I-Tech Libera Hadron measurement system setup at GSI. The BPM signal is split for reference tests. The data is transferred using the DCC fast data structure(blue) and is then available at the BPM-Extender. Clocking and trigger are not shown. The data from the GSI I-Tech Libera Hadron is stored centrally on a data server (see [47])

.

4.7 Testing

Testing in general is conducted to determine functionality and behavior according to design specification. This is also the case for the all hardware and software developed during this thesis. This section describes the strategies taken for the intensive testing which was conducted during the DAQ system development. It is divided into two categories: First, hardware testing, which regards all hardware developed and used for the system as well as externally acquired devices. Second, software testing, which presents an overview of the strategies used to ensure proper functionality of the developed software structure.

Hardware testing

The task of testing a hardware device is dependent on the nature of the device. The complexity of a single test usually scales with the complexity of the device to be tested.

The tested developed devices are the DELTA-clock-splitter and the BPM-Extender device, both developed by the physic's electronics development department. The clock-splitter does not contain software, therefore an electrical test, e.g. correct physical layout and conductivity as well as correct signal shape, was conducted by the department.
The BPM-Extender device consists of single PCBs connected by the FPGA on

the FPGA-board (see section 4.1). The internal hardware testing was split into two levels: the electrical test and test as integrated component. A simple example for the electrical test is the internal board housing the external ethernet connector, a simple male to female ethernet connector on a PCB. Each of the single electrical connections has to be conducting between the corresponding pins with no connection to others or ground.
Testing as integrated component was conducted in nearly all cases by black-box tests using a specially developed FPGA suite. The software tests all in and outputs, the ADCs and the XUP on-board components. Black-box tests expect a corresponding output after a specified input, without any regard of how it is produced. A simple example is a front-end switch, its electrical conductance state, as received by the FPGA has to change value when being pressed. A more complex example, including a set of well defined in and outputs, would be the ADC chips. These were tested for general functionality as well as properties like calibration and time stability. Therefore, after completing these tests an Extender device is regarded as being ready to use for programming.

The externally acquired hardware was tested by the corresponding manufacturer.

Software testing

Overall, the software development consisted of the developed for two systems: The BPM-Extender and the I-Tech Libera Hadron.
The BPM-Extender software is a complex system, divided in a FPGA part, a PowerPC drivers and PowerPC Linux part. The test strategy applied, to reduce the complexity of the test while maintaining assurance of functionality, was a bottom up strategy. The basic units and components are tested first, then the superordinated components and finally the system as a whole. In case of changes during the development phase, these tests were repeated for the components involved, again from the corresponding lowest units and components to the top.
The I-Tech Libera Hadron software is pure VHSIC Hardware Description Language (VHDL) code, the testing strategies applied are the same as for the BPM-Extender systems FPGA layer.

FPGA testing As the FPGA design is divided into components, having a clear hierarchy, each component was tested separately. For most of the components suitable VHDL test benches, these are surrounding VHDL structures supplying set input signals and expecting corresponding output signals, and test cases were developed to conduct black-box tests. Test cases are input/output combinations which show the significant functionality of the component, for most of the components a complete test of all possible input signals/states and

corresponding output signals/states is not possible due to the large configuration space. An example would be a simple clock frequency divider, after application of an enable signal and a base-clock, an output of a divided-clock signal is expected.
The functionality of the whole FPGA design was verified by a time behavioral analysis, this process was partly automated, partly manual.

PowerPC testing After integrating the PowerPC into the design, a test program was designed to ensure full functionality of the added FPGA components. The most important of these being the RAM and the PLB. In case of the RAM the functionality consists of storing data at internal addresses. An example for a simple test is to write predefined sequences of data, covering all possible addresses during the process. This data is then read in a second step from RAM and compared for consistency with the known written value.

Linux testing The Linux software is consisting of two parts: The kernel module and the user side program. The kernel module creates a linux device file, therefore the tests were run as black-box tests using the device. The user side program, which writes to this devices was tested with the device programmed to loop-back (each input is output again). This ensured correct writing and reading of the data.

After passing these tests, the BPM-Extender system was ready to be integrated into the measurement network.

4.8 Implementation summary

During development and testing the BPM-Extender hardware platform proved to be reliable and to meet the specifications. This includes the integration of the modified XUP-board into the surrounding hardware. All non-XUP-board integrated features, from simple LEDs to the more complex ADC-board, are utilized. The visual aids strongly enhance the practicality during development as well as in every-day use.
The high complexity of the software reflects the complexity of the task. The breakdown into different layers (see section 4.1.3) is a necessity to break-down this complexity. Even though each parallel process on the lowest level is contained in different software units, the collective functionality had to be ensured. Especially the integration of the DCC-IP core, including the required data-transfer, data-processing and debugging, required intensive modifications. The middle layer lacks extensive debugging capabilities as it is only functional in correspondence with the top and bottom layer. This resulted in a successful

example driven development. The top layer was prepared using the supplied software framework. The integration of the custom DAQ IP core was straightforward. The time required for system synthesis is about 45 minutes on a current PC system, due to the integration of the PowerPC processor, PLB and memory-cores. Hence a well tested and debugged low and middle layer is a synthesis-requirement. The full system is too complex to be simulated, it is tested and debugged by using PowerPC software. The latest available Linux kernel was compiled for the device. Establishing and accessing a linux device is well documented in general and completes the system's development.

Chapter 5

Measurements

An universal approach to a measurement task always brings up the question of representative measurement cases. As the developed system is targeted to hadron and electron storage rings, the DELTA electron storage ring and the COSY- and SIS18 hadron storage ring are ideal showcase candidates. The main part of the developed system is the BPM-Extender. Its main capability is the data acquisition process of measuring, processing and distributing the beam position data. The availability of global beam position data at a constant rate of 10 kHz, at nearly arbitrary locations at a storage ring, opens up a number of possibilities for beam diagnosis and orbit controls. The measurements at the SIS18 and COSY are a result of the versatility of this approach.
Potential also lies in the further processing of the fast beam motion data. The developed system features two possible processing points. On one hand the locally measured data can be processed directly on the respective BPM-Extender (in case of electron accelerators) or I-Tech Libera Hadron (for hadron accelerators). This allows fast data processing directly on the FPGA, which is well suited for complex and calculation intensive tasks. In case of the I-Tech Libera Hadron this feature is utilized for position pre-processing. On the other hand the distributed global data can be received from the data distribution network at any place and subsequently processed. The processing capabilities then depend on the connected device. Currently two options are available. The first is a system based on the BPM-Extender platform. This approach has been taken for the DELTA measurements. It allows to record the fast 10 kHz data, as well as the averaged the beam position data at a data rate of 1 Hz. This data is then utilized as basis for the existing slow orbit feedback. The second option of access is an FPGA based PCI card for off-the-shelf PC systems. It is utilized in the design at the Diamond light source described in [97].

5.1 DELTA

DELTAs beam orbit is, due to the existing slow orbit feedback [110] and local measurements with 10 kHz [94], well known. Nevertheless, the global beam motion in the higher frequency range has, to date, not been subject to research. This gap is closed by the developed system. Still, these measurements can only be a first analysis of the beam motion; the determination of the source of observed effects is out of the scope of this work.
This section presents the results of the global beam position measurements at DELTA. The primary goal was the characterization of global beam motion up to the system's nominal data rate of 10 kHz. For the first time at DELTA the required measurements are possible by the use of the newly developed system.

The secondary goal was to increase the accuracy of the slow orbit position from 10 µm(rms) to below 5 µm(rms). This is achieved by averaging the fast orbit data from a 10 kHz data rate down to 1 Hz.

All measurements were conducted using the permanently installed DELTA data acquisition and data distribution system (see section 4.4).
The measurement uncertainty is examined in section 5.2.

5.1.1 Fast global beam motion

To verify correct operation of the installed system a number of preparatory measurements have been made. These provided the data-basis for the follow up measurements of the fast global beam motion.

Preparatory measurements

To certify the operation of the system, a number of measurements were made while exciting the beam using dedicated prototype corrector magnets (see [95]). Due to the deflection of the beam to amplitudes well above the noise floor, the recorded beam position mainly follows the excitation frequency.
An example is shown in fig. 5.1 where a sinusoidal voltage with a frequency of 100 Hz was applied to a corrector. The sinusoidal motion is non-linear in this case. This is due to the use of a single corrector magnet for deflection of the beam. The deflection is then transformed by the magnetic accelerator optics structure, resulting in a non-linear offset. Fast beam motion of this frequency is not observable using the DELTA slow orbit feedback system due to the continuous sampling rate of the control system software of 1 Hz.

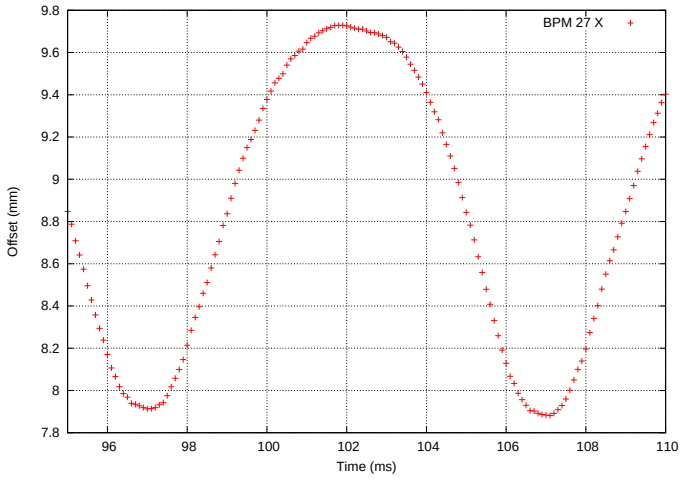

Figure 5.1: Horizontal beam position at DELTA BPM 27 during beam excitation using a 100 Hz sinusoidal voltage excitation on one dedicated horizontal corrector magnet. The measurement shows the successful operation of the installed DAQ system, from sampling of the pick-up signal, transfer of the data using the fast data network, to saving the data on the DELTA control system data server.

Fast global orbit motion

The global fast orbit data is a synchronous recording of the beam position of all available BPMs. The measured position data from each BPM was processed by a Fast Fourier Transform (FFT) to obtain the spectral distribution of the global beam motion. This distribution allows a detailed look at the frequency components of particle beams movement, thus helping to identify the sources of this unwanted motion. Figures 5.2 and 5.3 show the combined spectrum of the observed global DELTA electron transverse beam motion for a single-bunch beam. The maximum observable orbit motion frequency for the system is limited by the utilized Bergoz electronics. These have a 3 dB bandwidth of less than 1 kHz [52]. Therefore the maximum frequency for this analysis was set to 2 kHz, which is also the range of interest for a possible feedback. As the source for beam motion is either an electrical or a mechanical distortion, the beam motion for synchrotron light sources are mainly accelerator structure specific. Therefore the multi-bunch spectrum is comparable, which allows to identify distortion frequencies either in single or in multi-bunch mode.
As mentioned earlier in single BPM measurements (see [83, 94]), the characteristic DELTA transverse beam movement frequencies contained in this frequency band were now observed at all included DELTA-BPMs. These are the low frequency components in the range of <20 Hz caused by ground and girder motion.

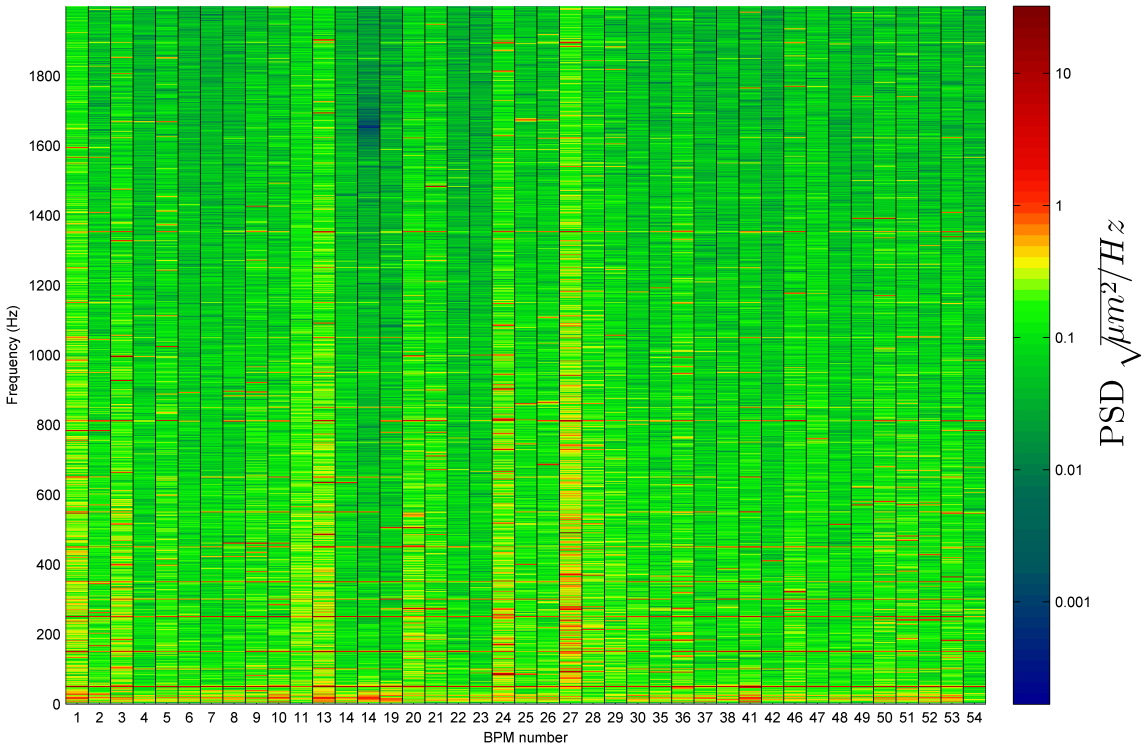

Figure 5.2: Waterfall beam spectrum of all available BPMs at 1.5 GeV, 4.5 mA single bunch, horizontal direction.
The signal was high-pass filtered at 16 Hz in this case to exclude the comparably strong ground and girder movement in this frequency area. Due to the broad signal range, a logarithmic scale was chosen.
Generally the integrated strength of distortions varies from BPM to BPM. There are multiple possible causes for this. On one hand, the deviation of the beam's movement is roughly scaled by the β function, but in this case it is plotted in absolute numbers. On the other hand the measurements mark the first time, that the BPMs are compared to each other since they were installed. A decay of in the performance is possible. The main distortion of the beam position is caused by the 50 Hz and harmonics. It is found to be present at all BPMs in varying strength. Clearly this is the influence of the supply voltage. In relative comparison, the frequency is not as strong in the vertical spectra (see fig. 5.3). This allows the conclusion that it is caused by the main dipole magnets and the respective power supplies. A number of higher frequencies are also present, their origin has not been subject to research yet.

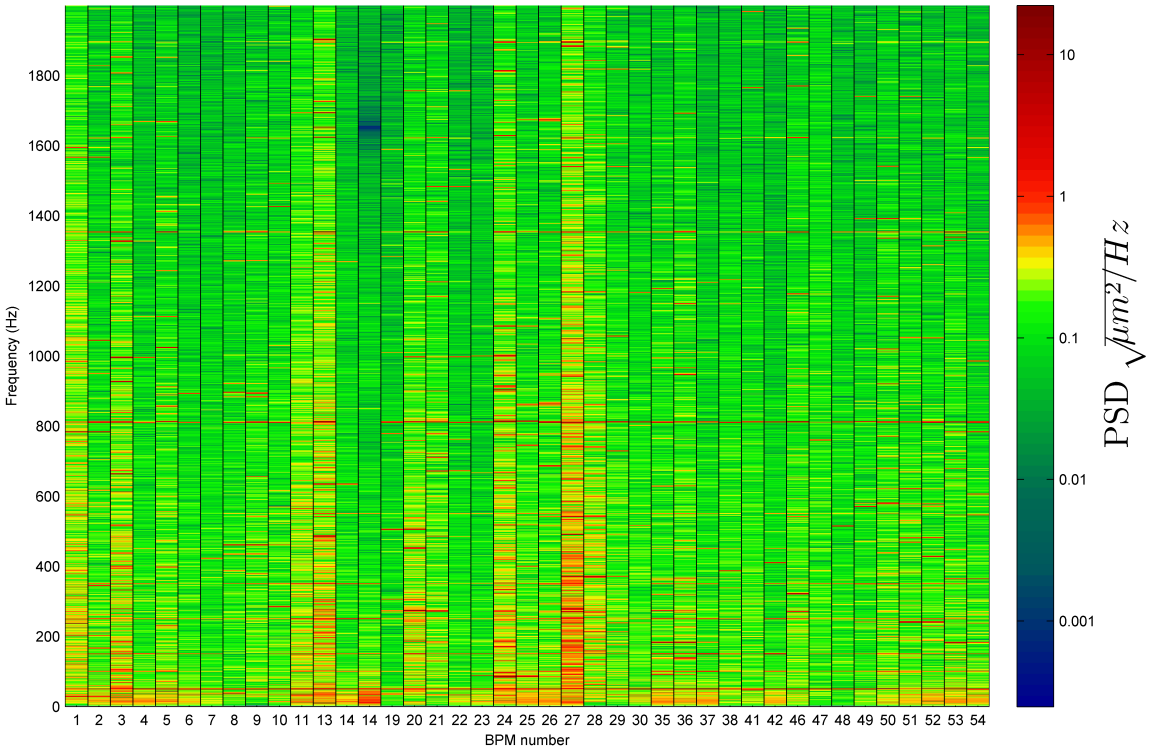

Figure 5.3: Waterfall beam spectrum of all available BPMs at 1.5 GeV, 4.5 mA single bunch, vertical direction.
The signal was high-pass filtered at 16 Hz in this case to exclude the comparably strong ground and girder movement in this frequency area. Due to the broad signal range, a logarithmic scale was chosen.
In comparison to the horizontal spectrum, the ratio of the integrated power of each BPM is very similar. This is not surprising, as the vertical position is calculated from the same signals, running through the same Bergoz electronic as in the horizontal case. The 50 Hz and harmonics signal is much weaker in comparison to the horizontal spectra. Instead a major contribution to the integrated PSD is caused by a 812 Hz component and a 1350 Hz component in some cases.

Most prominent is the 50 Hz and harmonics, caused by the supply voltage.The figure also contains a comparative measurement of BPM 14, which appears twice for this reason. It is equipped with a power-splitter for the pick-up signal. The first displayed column is the BPM-Extender readout, the second column is the I-Tech Libera data of this pick-up. The influence of the internal I-Tech Libera input filter is clearly visible at about 1600 Hz, greatly reducing the signal strength in the frequency range.

The measurement at full data rate shows the ability of the system to continuously and reliably deliver fast orbit data over the data distribution network. The availability of the fast orbit data, at any physical location of this network, allows further utilization of the data. One option is a possible fast orbit feedback. A second option are advanced global beam diagnostics in the frequency range up to 5 kHz.

5.1.2 Slow global beam motion

The analog position signal from the Bergoz electronics at DELTA is currently sampled simultaneously by the BPM-Extender and the control system (see fig. 3.4). A comparative measurement between the two systems was made to verify the received data and to prove the BPM-Extender systems ability to function as a slow orbit feedback data source. The beam position was compared exemplary for the horizontal direction of DELTA BPM35.
The path of data, from the analog Bergoz position signal to the sampled digital value, differ for both systems. The BPM-Extender filters the data in an analog low-pass filter with a cut-off frequency of 40 kHz to reduce artefacts. The analog signal is then directly sampled by the ADC. The nominal ADC sampling precision is 16 Bit. A five times oversampling for each single position value is done for noise suppression. The resulting continuous data rate is 10 kHz (for details see [83]). The required continuous data rate of 1 Hz is obtained by calculating the arithmetic average: As it is recorded, the sampled position data is cut into non-overlapping blocks of 10×10^3 samples. The arithmetic average of this position data is then calculated for this 1 s time period. This is a continuous process, resulting in the position data output rate of 1 Hz. Due to the technology used, the averaging starts immediately after reception of the last sample of each block. The averaged result is then available in less then 500 ns, a delay not notable by the DELTA slow orbit feedback system.
The data path of the currently operating control system is different: The analog position data from the Bergoz electronics is passed through an analog low-pass filter with a cut-off frequency of about 1 Hz. This reduces any high frequency artifacts but also limits the observable frequencies and introduces a time delay.

It is then oversampled by an ADC with 12 Bit precision at a rate of 250 Hz. The obtained values are averaged 32 times. This results in a nominal data rate of 7.8125 Hz for the beam position [110].

For comparison the measurement error of the Bergoz electronic is assumed to be zero. Hence measurement error in this case regards to the statistic error of the sampled position in respect to the position output by the Bergoz electronic. For the control system data-path this error is dominated by the influence of the analog low-pass filter. It induces a delay on the output data, acting as a moving-average filter. Generally the time domain of this delay is in the domain of the filter's time constant, in this case 1 s. For this time domain the theoretical sampling error is 5 µm [110]. Due to the 32 times averaging this value is reduced to 1 µm. In case of higher frequencies the error scales with the filter characteristics.

Even though the BPM-Extender system does feature an analog input filter, the goal is different. The filter was chosen only to remove high-frequency noise and sampling artefacts. The main error contribution is the sampling error of the ADC. A conservative assumption for the ADC is a true resolution of 14 Bits. Including oversampling, this results in a sub-µm statistical sampling error at a constant data rate of 10 kHz (see also section 5.2.3).

Figure 5.4 shows a simultaneous recording of one BPM with both systems. In this case the control system data was extracted from the EPICS logifle, which contains a lower data rate then stated above. The nominal data rate for the BPM-Extender for this measurement was 0.88 Hz, due to required debugging outputs which paused the data readout for ≈0.1 s every second. The start of the measurement was recorded manually for the BPM-Extender with a precision below the measurement interval. The BPM-Extender measurement curve was hence fitted manually to the control systems curve by shifting the starting point. The absolute position difference when averaging both positions over the measurement duration was found to be 3.8 µm. The reason for this is most likely a difference in zero point calibration of the ADCs, as an offset of 1 Bit in case of the control systems ADC shifts the result by 5 µm. This does not limit the functionality as the position utilized for accelerator operation is calibrated relative.

The plot visualizes the effect of the filter induced delay in the control system data path. During measurement the orbit was corrected by the slow orbit correction, resulting in orbit steps. These steps are in a frequency domain above 1 Hz, resulting in a bad resolution of the step itself and a delay in the following orbit position. The BPM-Extender system is not affected, clearly resolving the steps without delay.

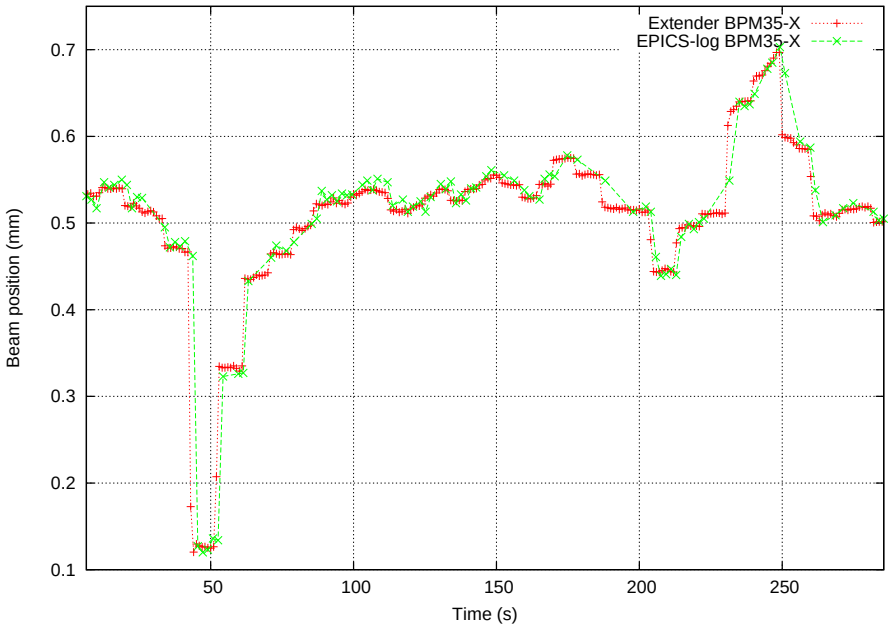

Figure 5.4: Comparison plot for simultaneously recorded horizontal DELTA-BPM 35 data, fitted manually. The deliberately offset orbit position was corrected by the DELTA Slow Orbit Feedback, which results in a clear stepwise change of the beam position, observable in the BPM-Extender data. The change is too rapid for the existing feedback, therefore it is not resolved clearly.

5.2 Error estimation for the BPM-Extender at DELTA

Every measurement is prone to errors. This section characterizes the main error sources for the BPM-Extender system to identify their influence on the measurement results and gives an estimation for the expectable uncertainty of the observed beam position. Therefore a detailed look at the signal processing chain, which is composed of the pick-up buttons, analog Bergoz electronic, sampling and digitally processing, is taken.

5.2.1 BPM

Manufacturing of the pick-up buttons, as well as the process of welding them in to the manufactured vacuum chamber are all mechanical processes. These are prone to size and positioning uncertainties which influence the electric properties of each button and thereby the readout position. The general tolerances for this mechanical processes is about 10µm [54].
In case of round pick-up buttons, the induced complex voltage U_{im} at the input of the BPM electronics is [18]

$$U_{im} = \frac{1}{\beta c}\frac{1}{C}\frac{A}{2\pi a}\frac{i\omega RC}{1+i\omega RC}\cdot I_{beam}$$

where β is the passing beam particles speed in fractions of c. C is the capacitance of the button and the attached cable. A is the distance between the beam's center of mass and the button, having a diameter of a. ω is the angular frequency and R the input impedance of the readout electronics.
The exact electrical and mechanical properties of each individual button, the attached cable and the attached BPM electronics are unknown. The same applies to the particles' frequency and speed, even though the uncertainty in this case is less and easier to determine, as these are well determined properties of the accelerator.
In case of DELTA all of theses errors are systematic and methods for calibration are available [34].

The resulting position error of the Bergoz MX-BPMs electronics is described in great detail in [52, pp. 113] which is summarized in the following. The MX-BPM electronics position error is mainly dependent on the input signal strength, respectable beam current, input signal phase difference (eg. different cable length from pickup button to MX-BPM electronics) and the beam position itself. Apart from the mechanical properties of the BPM knob, the biggest influence on the phase difference are the four cables from the pick-up buttons

to the BPM-electronics at DELTA. These are specified to a length difference of $\pm 2.5\,\mathrm{mm}$ [7]. For the same signal applied to the cables, this corresponds to a phase shift of $\pm 1.5°$ between different cables. This corresponds to a calculated systematic position difference of $\pm 0.66\,\mu\mathrm{m}$ per channel as the signal amplitude is used for the position calculation.
The noise levels for relative position information was observed to be $\pm 11\,\mu\mathrm{m}$ [52]. At low beam currents and therefore low input power to the electronics, this value increases to a position measurement uncertainty of $\pm 1\,\mathrm{mm}$.

5.2.2 ADC-Error

The conversion process is affected by multiple error sources resulting in systematic and random errors. The AD974-ADCs performance can be derived from a number of figures in the data sheet, see [13]. Each of these errors describes a feature of the characteristic quantization curve of the ADC. Ideally this curve is linear with fixed start- and endpoints.
To reduce the systematic error in case of the utilized BPM-Extender devices a calibration of the input was conducted in the electronics department after manufacturing. The random error was measured in a test bench, the procedure is described in [83, ch.6.1.2]. The observed ADCs performance was found to be consistent with the specification in all cases.

The following paragraphs summarize the relevant uncertainties for the different measurement cases.
The AD974 is characterized by the following random errors:

- The biggest uncertainty is given by the integral linearity error σ_{INL}. It combines quantization error and bit-errors (due to manufacturing) by stating the maximum distance between the actual and the ideal characteristic quantization curve with the same endpoints.

- σ_{TN}, the transition noise, characterizes the noise in the conversion process under worst case transitions and temperatures.

- The AD974 features 4 inputs which are multiplexed, crosstalk from channel to channel is possible. This uncertainty is included in σ_{C2C}.

The systematic errors are:

- The full scale error δ_{FS}, and its temperature dependent part δ_{FSD}. They describe the slope of the characteristic quantization curve.

- The bipolar zero error δ_{BZ} and the temperature dependent δ_{BZD}, which describe the offset of the characteristic quantization curve.

Absolute Error for DC measurement

An upper boundary for the measurement error can be obtained when assuming that all errors influence the measurement result to the biggest possible extend. Due to the implementation of the conversion process from analog to digital domain, this is represented by calculating the sum of errors:

$$\sigma_{max} = \sigma_{INL} + \sigma_{TN} + \delta_{FS} + \delta_{FSD}(\Delta t) + \delta_{BZ} + \delta_{BZD}(\Delta t) + \sigma_{C2C}$$

The maximum error for σ_{INL} is ± 3 Least Significant Bits (LSBs) of the conversion process. The noise σ_{TN} is stated to be typically 1.0 LSB. The maximum of σ_{FS} is 0.5% for an external reference. The typical thermal dependency combined in σ_{FSD} is ± 2 ppm/°C. The offset error σ_{BZ} is at maximum of $\pm 10\,\mathrm{mV}$ with a typical temperature dependency σ_{BZD} of ± 2 ppm/°C. The maximum cross talk σ_{C2C}, which is stated to be $-100\,\mathrm{dB}$ for the input range up to 100 kHz, results in deviation of $\pm\ 0.14\,\mu\mathrm{V}$(see eq. (5.4)).
In case of the DELTA measurement the set conversion range is $\pm\ 10\,\mathrm{V}$. The maximum temperature difference was set to an estimated 20 °C. For this case the sum computes to a total uncertainty of $\pm 0.11\,\mathrm{V}$, which would correspond to $\pm 110\,\mu\mathrm{m}$ beam position for a non-calibrated, absolute measurement. The systematic portion of this error can be obtained by a standard bench calibration for the ADCs. Thus the actual position error for such a calibrated system can be expected to be very close to the random error part of this uncertainty, which is small in comparison.

RMS AC Error

The conversion performance of ADCs can be different for DC and AC measurements. This is due to the internal analog characteristics of the ADC, resulting in a degenerated performance in case of AC tasks. Even though, in case of the Bergoz electronics at DELTA, the output signal is held stable for $25\,\mu\mathrm{s}$ (one cycle of the electronic's sample frequency), an upper boundary for the measurement error is derived from these figures. It is again obtained by summing up the relevant errors. The signal to noise and distortion error is the distance of the desired signal to the noise floor inside the signal's spectrum after conversion. The channel to channel crosstalk error is the crosstalk between different input channels:

$$\sigma_{RMS,AC,max} = \sigma_{SINAD,RMS} + \sigma_{C2C,RMS} \tag{5.1}$$

According to [44] the errors can be determined by

$$\sigma_{SINAD,RMS} = \frac{V_{FS}}{2^N} \tag{5.2}$$

where V_{FS} is the full scale ADC voltage and N the Effective Number Of Bits. The Effective Number Of Bits is determined by the conversion from dB to the power of two:

$$N = \frac{\sigma_{SINAD}(f) - 1,76}{6,02}. \tag{5.3}$$

The crosstalk error is calculated by converting from dB back to V, using

$$\sigma_{C2C,RMS} = 10^{\frac{\sigma_{C2C}}{20}} \cdot V_{FS}. \tag{5.4}$$

The AD974 datasheet [13] yields a signal to noise and distortion figure of 83 dB for frequencies up to 50 kHz. In case of the BPM-Extender system, the 40 kHz signal is oversampled 5 times. This reduces the signal to noise and distortion to a theoretical value of $83 + 5 \cdot \frac{3}{2}$ =90.5 dB, which results in an Effective Number Of Bits of N = 14.7. The resulting $\sigma_{SINAD,RMS}$ for a full scale Voltage of 20 V then is 0.75 mV. Entering this figure $\sigma_{C2C,RMS}$ calculates to an maximum RMS crosstalk of 0.2 mV. Hence $\sigma_{RMS,AC,max}$ is equal to 0.95 mV or 0.95 µm of beam position for the BPM-Extender Bergoz position measurement.

5.2.3 BPM measurement error

BPM measurements for feedback applications are usually relative measurements. Determination of the systematic errors is achieved by calibration. This applies to the digital as well as the analog part of the data acquisition chain. In case of the DELTA storage ring the BPMs are calibrated relative to the absolute quadrupole centres (see [46, 111]).

The position-measurement error, as already stated for the design in [52], is dominated by the intrinsic BPM noise of the Bergoz electronics. This is also true for the developed system. In comparison to this noise, an improvement is achieved by averaging of the position values. The statistic uncertainty of the mean measured value $\Delta\overline{z}$ is reduced by n repeated measurements with the same error margin Δz, to

$$\Delta\overline{z} = \frac{1}{\sqrt{n}}\Delta z. \tag{5.5}$$

Assuming that the BPM position output is stable during the measurement phase, which is 25µs long, the ADC-measurement can be regarded as a DC

measurement. The statistic uncertainty of this measurement is reduced by the oversampling ($n = 5$, for details of the sampling process see [83, ch. 5.3.1]) to

$$\Delta\overline{x_5} = \frac{1}{\sqrt{5}} 0.95\,\mu\text{m} = 0.42\,\mu\text{m}. \tag{5.6}$$

The best case Bergoz electronics measurement uncertainty Δx_B is 11 µm [52]. Combining the two yields

$$\Delta x_{B5} = \Delta\overline{x_5} + \Delta x_B = 0.42\,\mu\text{m} + 11\,\mu\text{m} \approx 11.5\,\mu\text{m} \tag{5.7}$$

as statistic error for the single measurement. This value was experimentally confirmed in [83, ch. 6.2.3].

The magnitude between the sampling error and the Bergoz error is a factor of 1 to 20. Depending on the external conditions, e.g. the beam current, this factor quickly gets worse to 1 to 100, or even larger.

The same method of sampling is applied to the measurement for the slow orbit feedback beam position. At DELTA the typical set-up features an 10 kHz data-rate which is then down-sampled to 1 Hz. As this is a pure digital processing, no additional error is added to the result. Under the assumption that the average beam position does not change during the measurement time span, it is valid to apply above calculation. In practice the beam performs betatron oscillations around the average beam position which are of high frequency nature. At a revolution frequency of 2.4 MHz and a 1 s measurement time span, the statistic error of this process is negligible.
The statistic uncertainty for the mean value of the beam position (slow orbit feedback beam position) hence computes to

$$\Delta\overline{x_{B5}} = \frac{1}{\sqrt{10 \cdot 10^3}} \Delta x_{B5} = 0.12\,\mu\text{m}. \tag{5.8}$$

The examination of the relevant errors for the measurement task shows, that the Bergoz electronics to contribute the largest portion to measurement uncertainty. Still the developed system fully exhausts the digital options of further signal processing, reducing this uncertainty to the maximum extent possible. Thereby an overall gain is achieved, specifically when averaging the beam position for a reduced data rate.

5.3 DELTA Summary

The qualities of the developed BPM-Extender system were demonstrated by the conducted fast and slow global orbit measurements. On one hand, the system allows to directly measure the Bergoz electronics generated beam position with a constant data rate of 10 kHz. This is four times higher than the previous data rate. Therefore, for the first time, a global beam motion spectrum of the DELTA electron beam was recorded and evaluated using the Bergoz electronics at their maximum recording frequency. The observed spectra show valuable information about the DELTA beam, pointing to a number of starting points for future research.

Furthermore, the arbitrary processing of the fast orbit data is possible by attaching to the data distribution network at any point. One application of further processing has been implemented, a digitally averaging of the beam's position as data source for the current slow orbit feedback. The digitally processing of the data is advantageous over the existing, partly analog, processing chain in regards to resolution, delay and data rate. It has been demonstrated, that the achievable measurement uncertainty is lower by a factor of 10 in comparison to the existing system.

The system thereby achieves the set goals for DELTA, namely to function as an universal data acquisition system for fast orbit feed-backs as well as to be a research tool for orbit-based diagnostic beam studies.

5.4 GSI

Even though the general principles of position measurement are shared by electron bunches and hadron bunches, in comparison the measurement of hadron bunches is a more complex task. The complexity lies in the physical characteristics of the hadron bunches. In case of the SIS18 the distribution of particles inside each bunch can be arbitrary, resulting in arbitrary signals to the BPMs. In case of electron bunches the distribution is mostly Gaussian. During measurement the particles undergo acceleration, making their velocity v a function of time t, whereas electron bunches reach a velocity of close to c already at comparably low kinetic energies. This results in a changing bunch signal length and a changing bunch revolution frequency which is also dependent on t.
The developed system approaches the task of different beam characteristics by using a different hardware, namely the I-Tech Libera Hadron for the hadron BPMs. In addition to this, the SIS18 I-Tech Libera Hadron approach the challenge of correct bunch recognition by an advanced bunch recognition algorithm, which was also developed at the GSI [76].
The planned feedback system will operate at a fixed frequency, therefore a constant data rate of 10 kHz is required as input. In case of the conducted measurements, the position is generated with bunch revolution frequency, which is higher than the required frequency. Therefore the received bunch positions are averaged during fixed time-intervals to receive a beam position, hence obtaining the constant data rate. The result of these measurements under challenging conditions is a first analysis of the beam position during the ramping phase of the SIS18, giving valuable hints on the design of a future fast orbit feedback for the accelerator.

The SIS18 I-Tech Libera Hadron measurement system (see sections 4.3 and 4.6 and fig. 5.5) was utilized for beam position measurements at the GSIs SIS18 accelerator during a beam diagnostic session. The first goal was the observation of orbit effects during a complete acceleration cycle at different particle energies in prospect of a fast orbit feedback system. Regarding the frequency distribution of the beam motion, repeatability of position and absolute beam offset are of special interest. The secondary goal was the verification of the system's output using the existing GSI system. For both cases position data of an Uranium 238 (73+) ion beam along with the associated bunch frequency was recorded.

The position data was recorded in two sets of measurements. The first set contains accelerator ramps from the injection energy of 11.4 MeV/u to a final particle energy of 300 MeV/u. The phase of acceleration to this energy takes about 3 s.

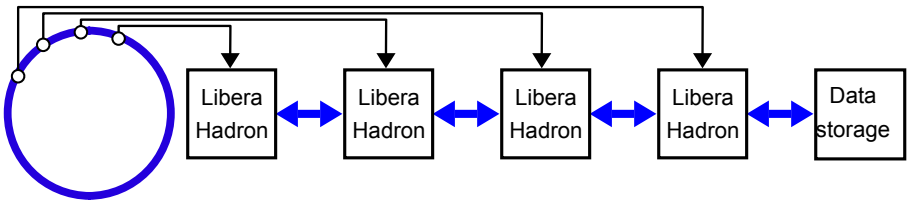

Figure 5.5: Depicted SIS18 measurement scheme. The position data from the BPMs is digitized and processed on the I-Tech Libera Hadron by the developed software. It is then transferred via the distributed DCC-bus to a data storage. For details please see sections 4.3 and 4.6

.

The second set contains accelerator ramps to final energies in the range of 50 MeV/u to 900 MeV/u. As the rate of acceleration, in terms of $\mathrm{eV\,s^{-1}}$, is nearly uniform for the SIS18, the time required for the complete ramping scales linear to the final energy (e.g. 9 s to reach 900 MeV.
The bunch revolution frequency during acceleration is energy dependent, ranging from 850 kHz at injection energy up to a maximum of 6.02 MHz.

5.4.1 SIS18 beam position data analysis

To characterize the applicability of a FOFB system, a number of investigations were conducted:
The successful operation of a fast orbit feedback system at an accelerator depends heavily on the frequency distribution of the beam movement. Therefore a detailed frequency analysis of the measured orbit data was conducted. After computation of the beam-orbit-deviation frequency spectrum, it is examined to identify any dominant frequencies. The region of interest for the design of the feedback algorithms in this case, due to the technical constraints, is in the range of 0 Hz to 500 Hz.
Beam losses are also caused by momentary position-offsets of the beam. To characterize the magnitude of the off-center beam, the average and momentary maxima of the beam position were calculated. The influence of a feedback on the beam is simulated and the obtained values, with and without feedback, are compared.
A possible application for a FOFB at SIS18 is the correction of hysteresis-induced deviations between consecutive ramps in relation to a calculated average ramp. The influence of a feedback on the beam's position is simulated and compared to the recorded position data.
The basis of the analysis is the recorded position data during ramping. Each single measurement includes the position data of one ramping and, depending on the accelerator parameters, up to 5 seconds of revolving beam. In total 168 ramps were analysed.
The measurements were grouped by the final beam energy. Depending on the analysis, each group was split into the ramping part and the flat top section (see section 2.5). To verify correct bunch recognition and thereby the validity of the measurements, the number of bunches per 100 µs measurement frame was also recorded. The conducted analysis is identical for each group and both measurement sets. An example of the data received is illustrated in figs. 5.6 and 5.7.
The measurement uncertainty of the recorded SIS18 orbit data is composed by the combined errors of the BPM system [17]:

- The BPMs calibration factor (see section 2.4.1) is frequency dependent [55].
- The signal to noise ratio of the utilised amplifiers is signal level dependent.
- The so called Effective Number Of Bits of the 14-Bit I-Tech Libera Hadron ADC.
- The position calculation algorithm (e.g. averaging, integration) method and error.

The theoretical position resolution for the orbit measurement of the I-Tech Libera Hadron system can be obtained by dividing the BPM diameter by the theoretical number of ADC steps. The shoebox type BPMs have an aperture of 200 mm horizontally and 70 mm in the vertical plane [55]. Dividing this by the ADC steps, which are $2^{14} = 16384$, yields a theoretical sampling resolution of approximately 12.5 µm (horizontal) and 4.5 µm (vertical). This theoretical resolution is by far not reached in practice. In case of the position measurement, the difference of the signal intensity, which is induced on the BPM plates, is measured. For every particle type accelerated, the ADCs input range has to be adjusted to the signal intensity. This adjustment is usually not perfect, reducing the actual number of possible ADC steps. Precision of the input signal is also lost due to mechanical tolerances, signal transmission, and a loss of precision in the follow up calculations. In case of a 10 kHz data rate, the measurement duration allows an averaging of about 100 turns of the SIS18 beam. Including the improvement of the measurement uncertainty by averaging, under the assumption that the beam motion during this period is small in comparison to the measurement uncertainty, the relative position measurement resolution is in the domain of 100 µm.

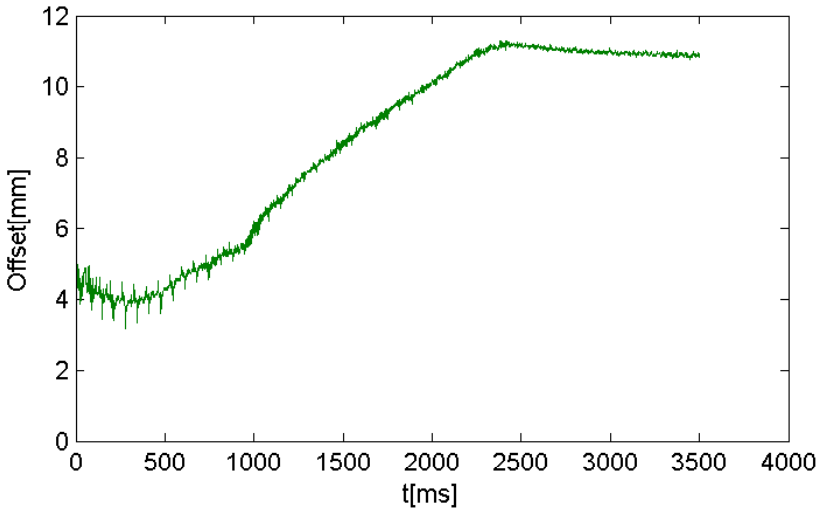

Figure 5.6: Measured SIS18 BPM12 horizontal position during a 300 MeV/u acceleration cycle. The vertical position was omitted for simplicity. The ramping starts at 0 ms, the flat top is reached at 2500 ms. In this case a drift during ramping and a slightly opposite drift during the flat top section is observed. This drift occurs during multiple rampings, hence it could be corrected by a feed-forward system. Nevertheless a feedback system can directly improve the beam's positional stability in such cases. During the first 1000 ms a number of higher frequency and larger amplitude position-deviations are visible. In these cases a feedback system is the only option to reduce these perturbations.

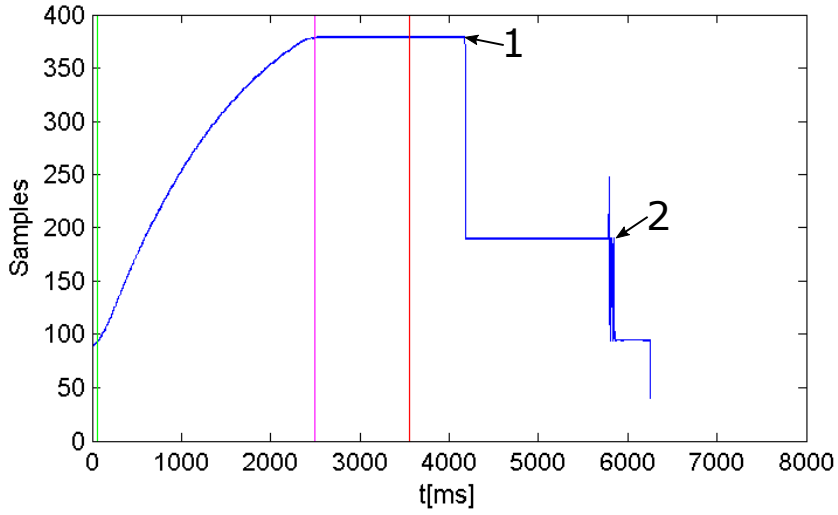

Figure 5.7: Number of samples per measurement time-frame, for the measurement shown in fig. 5.6, actually the number of recognized bunches, which passed the BPM plates during one 100 µs) measurement time frame. During the ramping (0 ms-2500 ms) the velocity of the particles is increased with their energy. This results in more bunches passing the BPM in a fixed time interval. The expected rise of this number was clearly observed. During the flat top (2500 ms-4000 ms) the energy and revolution frequency stays constant resulting in an observed constant number of samples during this period. The procedure to extract the beam from the SIS18 accelerator for this ramp utilizes a bunch-elongation process, during which the number of bunches is halved twice by the means of the radio frequency system combining two adjacent bunches (at 4100 ms (1) and 5800 ms (2)). The jitter of the bunch count at 5800 ms is the result of the change in bunch structure during this process. For the further analysis the recorded position data was divided into the ramping and the flat top part. The used intervals are indicated by the vertical bars in green (50 ms), violet (2500 ms) and red (3500 ms).

SIS18 beam orbit frequency spectrum

Figure 5.8 shows the combination of the computed average beam spectra for each BPM and for different ramping energies. For clarity the frequency range of the figure is limited to dominating frequencies up to 250 Hz. Figure 5.9 shows the corresponding integrated Root Mean Square (RMS) beam motion, the numerical results are found in table A.1. The integrated motion at 250 Hz is already a benchmark for the beam motion in the complete frequency range. The data is obtained by first performing a fast fourier transformation for each ramp in the region of 0 Hz to 5 kHz over the whole ramping period. These spectra were then averaged for each measurement set (i.e. final particle energy) and combined for each BPM. The fast fourier transformation underlies a number of constraints in this case. The number of data points for analysis is limited by the 10 kHz data rate and ramping times between 0.5 s and 3 s, resulting in 500 to 30000 samples per spectrum. As a result the frequency and time resolution is comparably low. Also, due to the non-periodic nature of the signal, the leakage-effect on the computed spectrum can be observed. The application of a moving Hanning-window function, a common method which addresses this matter, yields no significant improvement as the frequency resolution is reduced even further. Nevertheless in case of 300 MeV measurement data of 137 different ramps was averaged, reducing the measurement uncertainty.
The single measurement spectra, as well as the shown averaged spectra, are all quite similar. In general a $1/f$ (pink noise) structure is observed with no common dominant frequency. This characteristic directly influences the possibility of a fast feedback system. According to the obtained data, an ideal feedback with a comparably low cut-off frequency (e.g. 50 Hz), would on average, improve the RMS beam noise by 90 percent. The underlying reason is the low frequency nature of the main distortions, of which the absolute beam amplitude is also well above the BPM noise floor.
A common distortion frequency, which could be counter-measured by a fast feed-forward system, is not present in the observed data. Only part of the datasets show a 50 Hz and harmonics frequency component, even though this was not analysed in detail, it is most likely to be the interference of the power supply network.

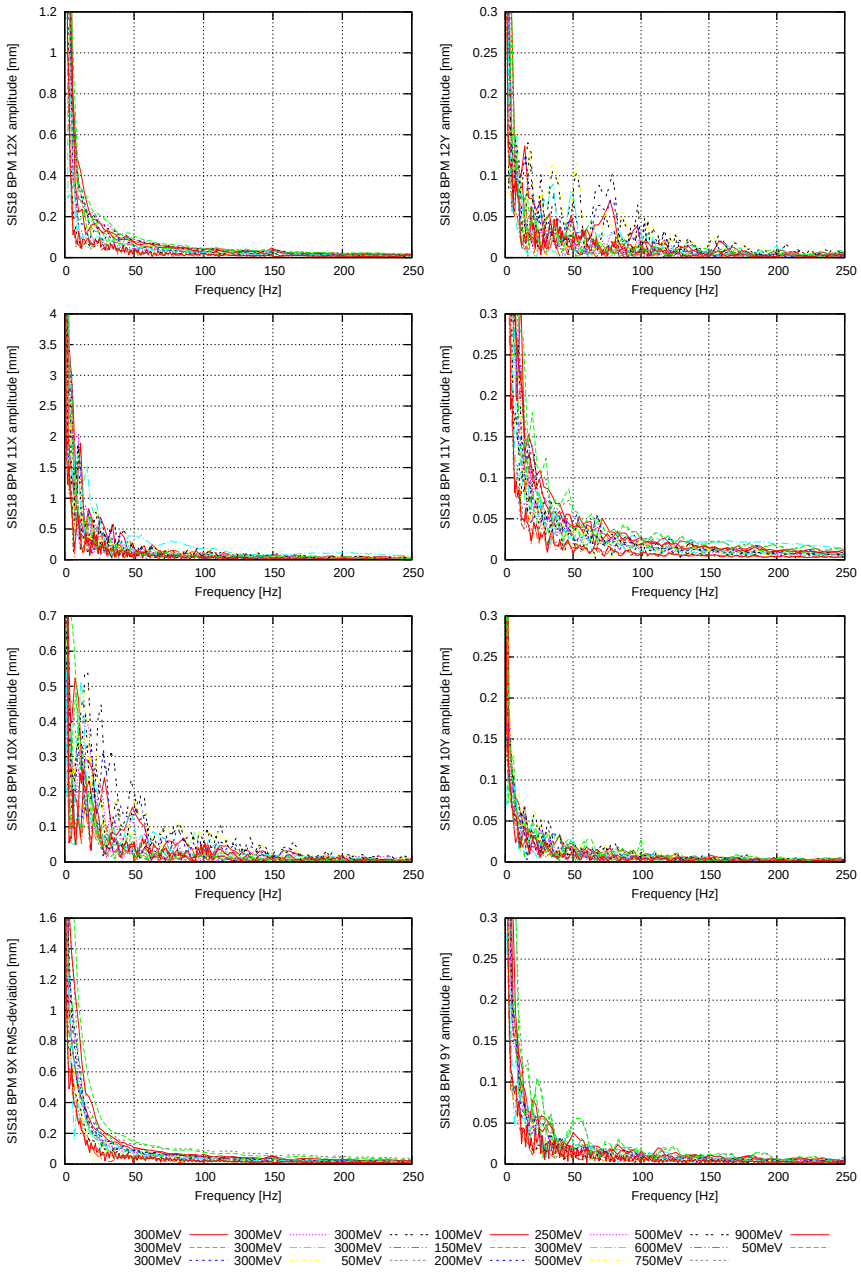

Figure 5.8: Horizontal and vertical spectrum of each BPM for different final energies (per nucleon), averaged over the complete time of ramping, plotted against respective frequency intervals.

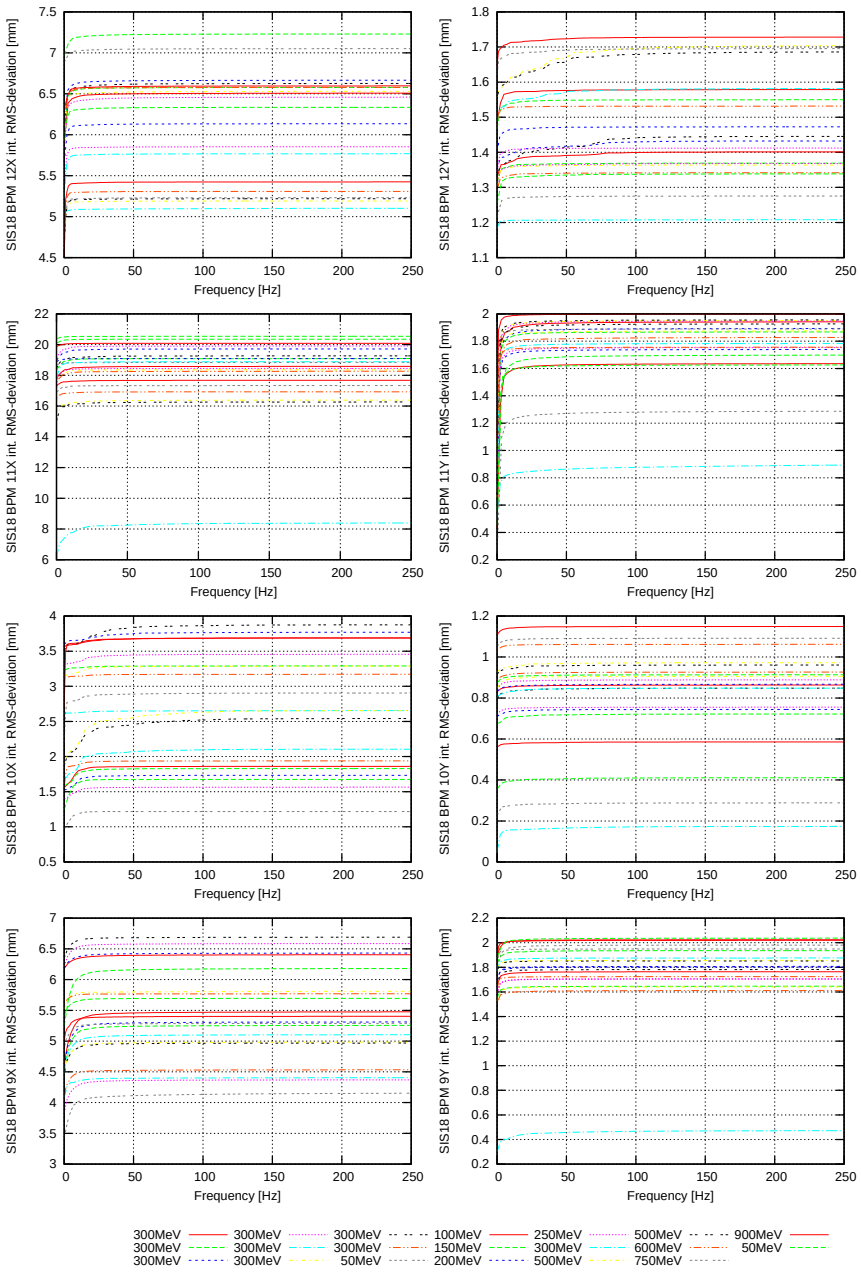

Figure 5.9: Horizontal and vertical integrated RMS-beam motion of each BPM for different final energies (per nucleon), averaged over the complete time of ramping, plotted against respective frequency intervals.

SIS18 beam offset performance

The frequency spectrum analysis of the preceding chapter shows the RMS beam motion averaged over the duration of complete ramps. In terms of beam position related beam loss, the RMS-motion is representative for the long term stability (minutes to hours) of the revolving beam. In case of ramping, momentary position deviations of the beam are important factors causing possible partial or complete beam loss.
To obtain further information about the frequency range of the observed beam behavior, a simulated fast feedback correction was applied to the measured beam position. In this case the correction characteristic of the FOFB was assumed to be a sixth order butterworth low-pass filter with a cut-off frequency of 250 Hz. To simulate the effect of the feedback, the data path of an ideal feedback was simulated. At first the filter was applied to the position data of each ramp. After filtering only the content of the orbit deviation, which could be corrected by this feedback remained. This correction is then applied to the beam's position by subtracting this orbit content from the measured orbit. As this does not take into account the characteristics of a real feedback loop, it is an ideal correction. After the subtraction the corrected orbit is obtained. This allows a more sophisticated look at the effects on the beam as well as a rough estimate of the effectiveness of a FOFB for the observed ramps.
The combined results of the numerical analysis of the measurement data for the vertical and horizontal direction are shown in table A.1.
The obtained figures for horizontal and vertical direction are similar in relative numbers, while the absolute numbers for the horizontal direction are larger. The reason for this is the combined influence of the large ramped dipole magnet-fields and the fields of the accelerating radio frequency-cavities on the beam. Even minor deviations of the ideal values of one component immediately results in a beam offset.
The maximum offset is the key figure for orbit related beam loss. It is calculated by choosing the absolute maximum beam offset of all ramps of the respective BPM. Hence it is the figure of merit for a worst-case scenario. The comparison of the uncorrected and corrected values show only a minor reduction of these values. This is due to the fact, that the values are caused by momentary, high frequency, large amplitude position deviations. Due to their high frequency they are not corrected, even of the assumed ideal feedback. In some cases the value was increased. The cause for this is the internal delay of the feedback loop, in this case expressed by the phase shift of the utilized filter, causing an additional offset (see section 2.4.1).

The average offset is obtained by averaging the beam offset in relation to the

BPM defined center of all measured ramps of the respective BPM over time. A correction of this offset would typically be done by correcting the predefined ramping curve of the magnetic lattice. These distortions are typically of a low frequency nature. A correction using a feedback is possible, resulting in calculated average value for the corrected case below 1 mm (horizontal) and 0.1 mm (vertical) beam offset.

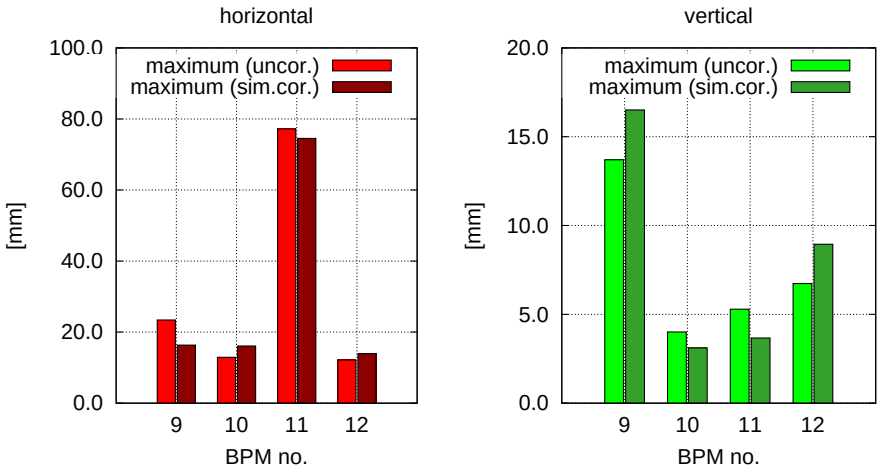

Figure 5.10: Comparison of the maximum peak height for recorded data (uncor.) and a simulated correction (sim. cor.) on this data, for horizontal and vertical direction of SIS18 BPMs 9-12. In this case the magnitude of the maxima is not changed. This is due to the frequency distribution of theses maxima, which are typically single, high frequency events. As such they are not significantly affected by the simulated correction, having a cutoff frequency of 250 Hz. Please note the different scales. The numerical data is found in table A.1.

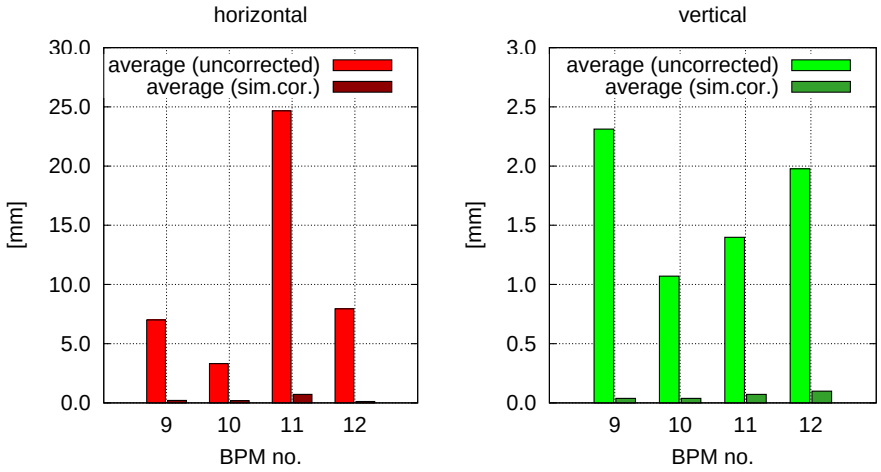

Figure 5.11: Comparison of the average beam offset position for recorded data (uncor.) and a simulated correction (sim. cor.) on this data, for horizontal and vertical direction of SIS18 BPMs 9-12. The average offset is typically a low frequency drift away fro the ideal orbit. As such it is well in the simulated feedbacks correction frequency range (up to 250 Hz) and is effectively reduced. Please note the different scales. The numerical data is found in table A.1.

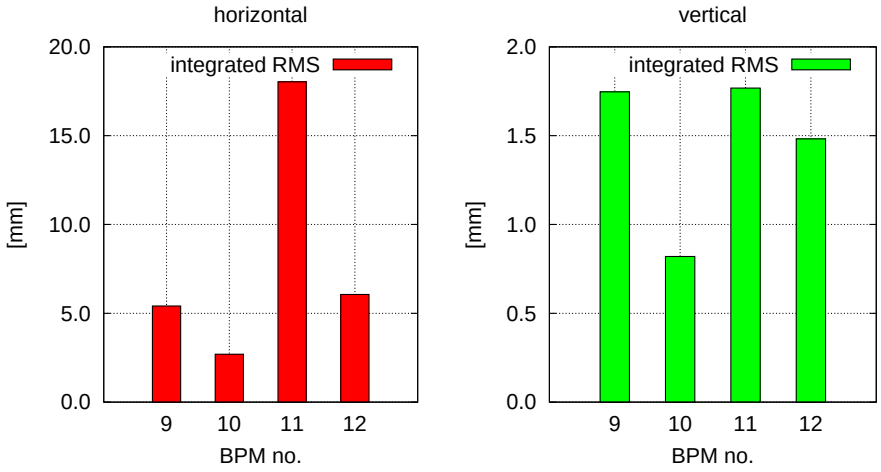

Figure 5.12: Visualization of the integrated RMS beam offset position for horizontal and vertical direction of SIS18 BPMs 9-12. In this case BPM 11 shows a much higher beam deviation as the other recorded BPMs. Please note the different scales. The numerical data is found in table A.1.

SIS18 ramp to ramp beam orbit performance

A key figure for reliable accelerator operation is the reproducibility of given reference orbit. During the period of ramping and the following flat top a difference of the orbit to the preceding ramp can be caused by the hysteresis effect (see section 2.5.1) in the accelerator magnets. A position deviation would be most likely caused by the main dipoles due to their strong influence on the beam position. Therefore the horizontal orbit deviation for each group of measurements, recorded with the same accelerator parameters, was analyzed.
As a benchmark figure the statistical variance was chosen. The analysis contains two steps: First the measurements were grouped by final kinetic energy. Then the mean position and the variance over time for each group and BPM was calculated. The numerical analysis was conducted for the period of ramping and the flat top phase. In a second step the maximum, as well as the average variance of all group results were computed.
The values for the mean variance are a benchmark for the reproducibility of the beam position of consecutive ramps. The maximum variance can be regarded as a worst-case benchmark figure.
As in section 5.4.1 the analysis was repeated for an assumed FOFB with a correction rate of 250 Hz. This allows to inspect frequency distribution of the values in combination with the phase delay caused by the filter, which is also the case for an actual feedback.

Table A.2 gives a summary of the obtained values. The numbers show the average variance during ramping and the flat top phase to be in the magnitude of 10^{-2} mm^2 for the observed ramps. This means the calculated underlying beam motion is within measurement uncertainty.
It is apparent from this table that, in comparison to the other BPMs, the variance of SIS18 BPM11 is up to two magnitudes larger. This is due to the comparably larger amplitudes of the signal (see fig. 5.8 for comparison).

In comparison to the average variance, the maxima of the variances are four magnitudes larger. This means that the maxima are dominated by seldom peak values of the signal. During ramping the cause of the overall maxima are spikes in the original signal with comparably large amplitude and slightly deviating phase. During flat top this number is reduced to a maximum absolute value of below 1 mm^2 (except for SIS18 BPM11) also caused by slightly phase shifted components in the signal.

The frequency nature of the distortions is obtained by comparison to the filtered values: The average variance is roughly halved by the filtering while the variance maxima are reduced, even in the worst case (BPM10 for ramping), by roughly 1/5th (34.345 mm→6.860 mm).

Overall the obtained values show a very good reproducibility of the beam position on average during ramping as well as during flat top. The average beam deviation is inside the range of the measurement uncertainty of 100 µm (see section 5.4.1). The absolute maximum of the position deviation was observed to be four orders of magnitude larger than the average variance.

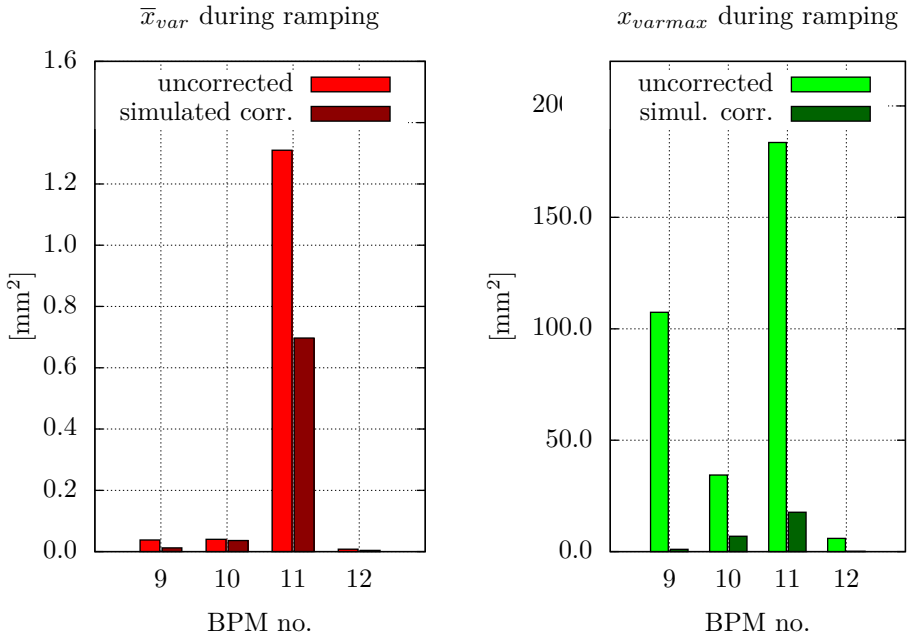

Figure 5.13: Comparison of two different figures of merit for horizontal ramp-to-ramp position reproducibility for the SIS18 BPMs 9 to 12 during ramping. The left side shows the average variance computed over all recorded ramps, for the uncorrected case and after a simulated correction was applied. Due to the very small deviation the effect of the simulated feedback is limited. As a result, the reproducibility of the beam position can be regarded as very good. The figure on the right shows the absolute maximums of the deviation, computed for the uncorrected and simulated correction case respectively. The maximums are caused by momentary spikes in the beam's position. Still these are effectively corrected by the simulated feedback. Therefore a feedback system would be beneficial to reduce momentary beam deviations during ramping. Please note the different scale The numerical data is found in table A.2.

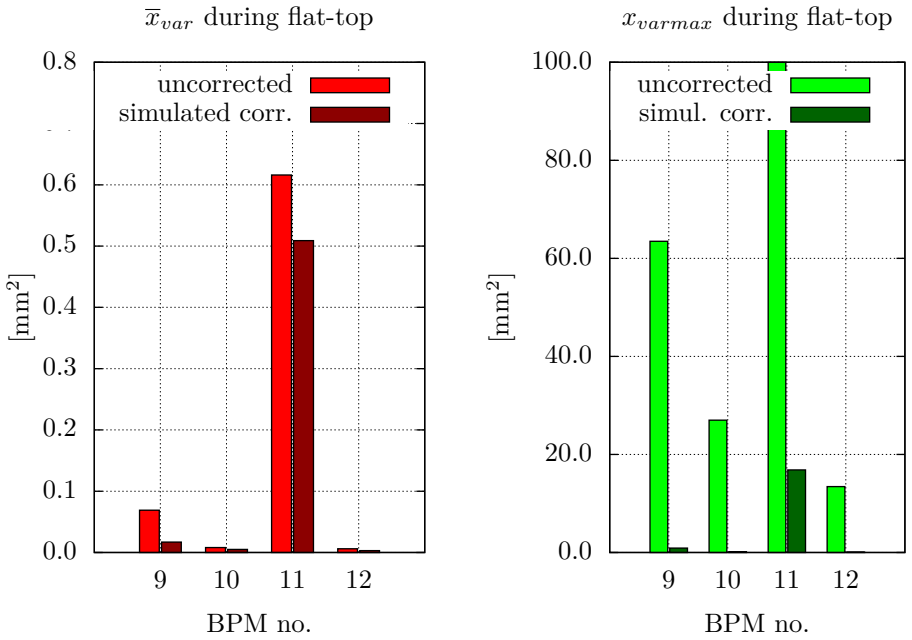

Figure 5.14: Comparison of two different figures of merit for the horizontal ramp-to-ramp position reproducibility. The data was recorded for the SIS18 BPMs 9 to 12 during the flat-top phase of the ramping. The left side shows the average variance computed over all recorded ramps, for the uncorrected case and after a simulated correction was applied. Similar to the situation during the actual ramping (see fig. 5.13), due to the very small deviation the effect of the simulated feedback is limited. On the right side are the maximums of the variances. Again the data suggests these to be caused by momentary spikes in the beam's position, in a frequency range which is effectively corrected by the simulated feedback. Please note the different scale. The value of BPM 11 is cut away for a better overview. The numerical data is found in table A.2.

5.4.2 SIS18 data acquisition system comparison

To validate the correctness of the averaged data, position data were recorded simultaneously by the GSI DAQ system and the BPM-Extender system. It has to be noted, that this is a comparison of two I-Tech Libera Hadron measurements, fed by the same input signals divided by power-splitters (see section 4.6). The difference is the processing of the data. The BPM-Extender system processes the data in real time during measurement resulting in a data rate of 10 kHz. The recorded GSI data is processed off-line after measurement, the data rate is equal to the bunch frequency corresponds to the bunch frequency (850 kHz to 6 MHz). Both systems operated independent from one another, apart from the BPM connection and a common trigger to start the measurement. As a result the exact sampling frequency and point in time of the GSIs- and the

measurement systems I-Tech Libera Hadron is different. In this case the sampling is not affected, as each bunch position is oversampled by the I-Tech Libera Hadron. Also the format in which the data (position and time) is saved in the GSI system differs from the BPM-Extender system format. This results in a loss of precision as the conversion from one format to another has to be fitted in its parameters. Figures 5.15 and 5.16 show the comparison of the recognized number of bunches passing the BPM plates during each 100 µs measurement time-frame. Due to the calculations required, this is a good figure of merit if the algorithm is working correctly. The clearly visible zig-zag of counts is a result of the fixed time-frame, native to the measurement system and calculated from the GSI data.
The calculated position is averaged in each time-frame by the number of bunches recorded for this time-frame, thereby only the measurement uncertainty of the averaged value is influenced by the different number of bunches. For the SIS18 bunch counts, this accounts for a difference in measurement uncertainty of roughly 1/80th to 1/300th (beginning of ramping to flat top). This applies to I-Tech Libera Hadron measurement system, as well as to the calculated GSI data.
A comparison of both measured positions is shown in figs. 5.17 and 5.18. The measurements differ for two major reasons: On the one hand, the four BPM signals are split by four power splitters before being read out by each I-Tech Libera Hadron. The exact characteristics of each power-splitter which was utilized is unknown. On the other hand, having a larger influence on the measured position, the GSI I-Tech Libera Hadron were already equipped with an improved bunch-recognition and position-calculating algorithm.
A combination of these influences lead to an observed systematic error in the horizontal position of +3.55 mm. It was corrected by calculation of the average position and subtraction of the difference. Also the deviation in position, especially between 80 ms and 100 ms can be explained due to this differences. Figures 5.19 and 5.20 show a comparison of the spectra for both measurements. The systematic frequency deviation in this case is due to the fitting of both measurements sample-frequency for maximum overlap.

The measurement confirms the correctness of the averaging algorithm and the functionality of the I-Tech Libera Hadron hadron internal connection between the GSIIP core and the developed hadron IP core. Even though the calculated position is not identical due to measurement constraints, it shows a good agreement. The same applies to the calculated spectra, even under the constraint that the number of data-points is comparably small for such calculation.

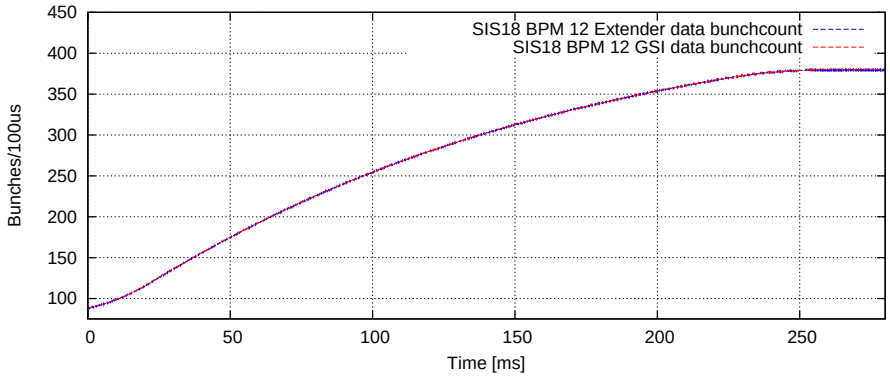

Figure 5.15: Comparison of the number of recognized bunches at BMP12 during each 100 µs measurement time-frame for one ramp of GSI SIS18. The I-Tech Libera Hadron/BPM-Extender system bunch-count is recorded during measurement, the GSI data bunch-count is calculated using recorded data. A correct identification of the bunches is observed, both measurements clearly represent the ramping process (see section 2.5). The acceleration phase is clearly visible in the rising bunch-count at the beginning. The same applies for the flat-top section, identified by the constant bunch-count. All bunch-positions recorded during one time-frame are averaged to obtain the beam position (see fig. 5.17).

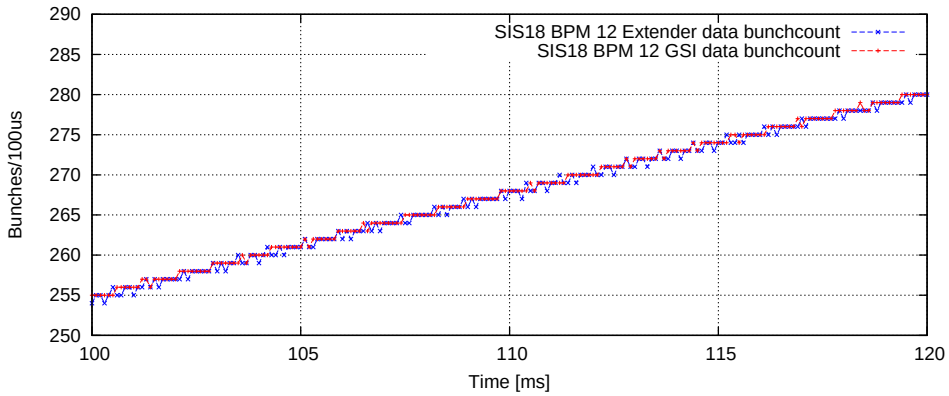

Figure 5.16: Magnification of fig. 5.15, showing a close-up of the zig-zagging data which is caused by the fixed-interval averaging-calculation (see text). As this is a comparison measurement of two separate systems, nevertheless the datasets agree very well.

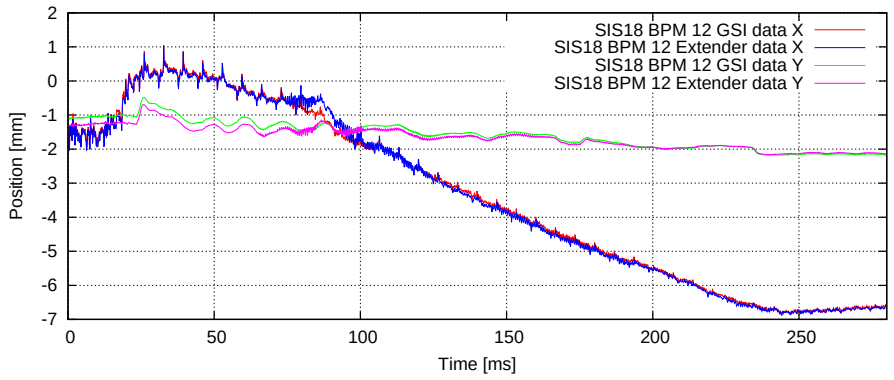

Figure 5.17: Comparison of the measured horizontal and vertical position of GSI SIS18 BPM 12 during one ramping. Because of non-ideal accelerator settings, the horizontal position is prone to a clear drift during the ramping. Due to measurement constraints and manual fitting the position is not identical. Still the agreement of the observed data is impressive, especially in the small high frequency spikes of the horizontal data (see fig. 5.18 for a more detailed view).

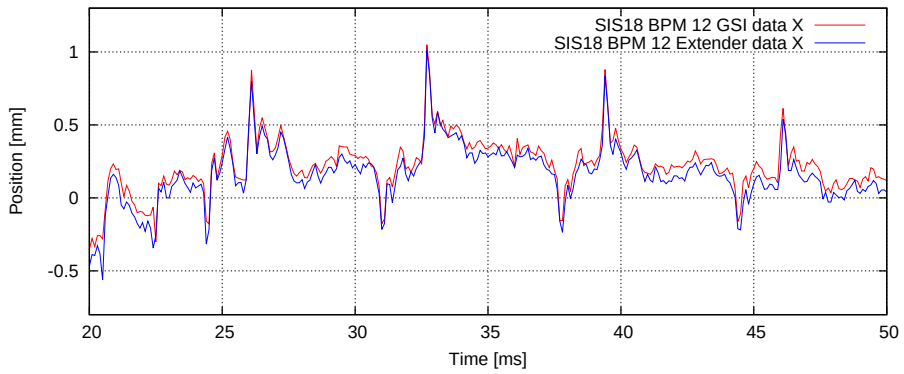

Figure 5.18: Close up of the compared horizontal position of fig. 5.17. Differences in the measurement would be most prominent in case of rapid beam movement with a big offset, as shown. Both measurements show a good agreement in the limits of measurement uncertainty, even though the underlying original BPM signal was split into two data paths.

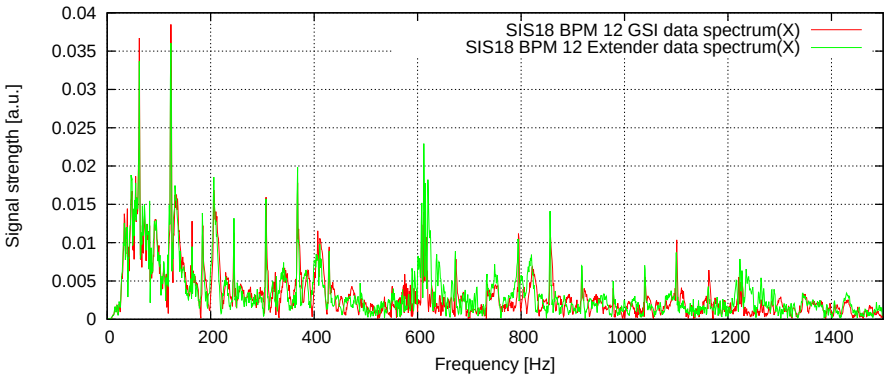

Figure 5.19: Comparison of the beam motion spectra of fig. 5.17. For clarity only the horizontal spectra are shown. The spectrum shows even clearer the agreement of both measurements, as the distribution in the frequency domain is nearly identical. The origin of the dominating disturbances was not subject to research in this case.

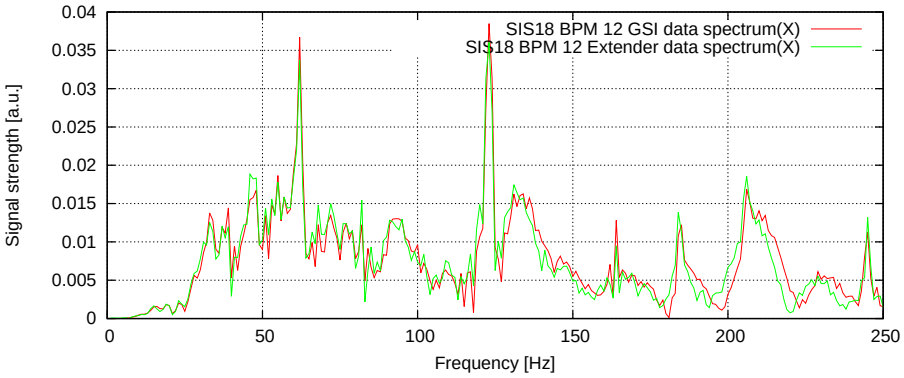

Figure 5.20: Close-up view of fig. 5.19, showing the first two major disturbances of the beam's position. A slight difference in the frequency is present, which is due to required manual fitting of the underlying sampling-frequency.

5.4.3 SIS18 measurement summary

The feasibility of a feedback was examined by different criteria applied to the beam position during the recorded ramps. The first being the analysis of the averaged beam motion spectra. It showed the majority of motion to be contained in the low frequencies below 50 Hz. In case of a feedback, the low frequency content is technically good to correct.
The beam position versus time during the ramping period was recorded, it showed large momentary peaks of the beam motion which are not easily correctable due to the high frequency and amplitude involved. Nevertheless, the simulated influence of an ideal feedback was able to reduce the beam offset below 1 mm (horizontal) and 0.1 mm (vertical).
The conducted characterization of the magnetic hysteresis during consecutive ramps showed an excellent repeatability of the beam position. The deviation between consecutive ramps was found to be within the limits of measurement uncertainty. A deviation of the beam position due to the effect of magnetic hysteresis was not observed in the recorded data. The parallel measurements of the GSI and the developed I-Tech Libera Hadron system have shown a reliable and correct operation of the DAQ-system.
Therefore the set goals, namely the development and testing of a universal data acquisition system for a fast orbit feedback, have been achieved with the concluded measurements at the SIS18 accelerator facility.

5.5 COSY

Further measurements, in preparation of a hadron feedback system, were conducted at COSY accelerator facility (see section 2.2). The hadron measurement system (see section 4.3) was utilized, using the setup described in section 4.5. The goal of these measurements was the evaluation of the ion-beams bunch position signal. This especially regards the bunch-recognition for the different accelerator modes. The set-up also allowed testing of the system's remote access capabilities as well as practical tests of the DCC network in combination with the I-Tech Libera Hadron.
In this respect the COSY accelerator is the ideal facility for such measurements. The installed hadron measurement system was tested with various measurement schemes at different beam energies, particles, intensities and bunch patterns, as well as using the amplified and non-amplified BPM knob signals. These features in combination with remote access capabilities and easy physical access to the measurement system outside of the accelerator tunnel allowed to gain valuable information of the measurement system.
The conducted tests are the first measurements of a COSY hadron beam utilizing I-Tech Libera Hadron. During these tests successful recognition of the bunches was possible in about 25% of the cases studied. This was expected as the component responsible for bunch-recognition utilized inside the I-Tech Libera Hadron was designed for the SIS18 accelerator (see fig. 4.15). A bunch position is calculated from the integrated single channel bunch signal. An integration window is created by the bunch recognition using a double threshold discriminator. The developed algorithm is described in detail by U. Rauch [76]. A number of parameters are available for tuning the recognition, e.g. the thresholds used internally for the calculation.
To aid the process in the future, the directly sampled BPM-plate signal is available for readout on the I-Tech Libera Hadron.
Figure 5.21 shows an example of this data. The base-line of the signals was aligned by calculating the average signal value in between the bunches and offsetting one signal by the difference. The orbit position data, averaged to a data rate of 10 kHz, was transferred from the I-Tech Libera Hadron to the BPM-Extender. The integration of the DCC and averaging of the data on the I-Tech Libera Hadron operated as expected. After reception of the data by the BPM-Extender, it was stored directly on the measurement system integrated PC via ethernet connection. This then allowed further analysis of the data. The remote access capabilities of the system were intensively tested by accessing it from outside the accelerator facility using a secured connection. This showed starting points for further improvements to increase the usability of the system.

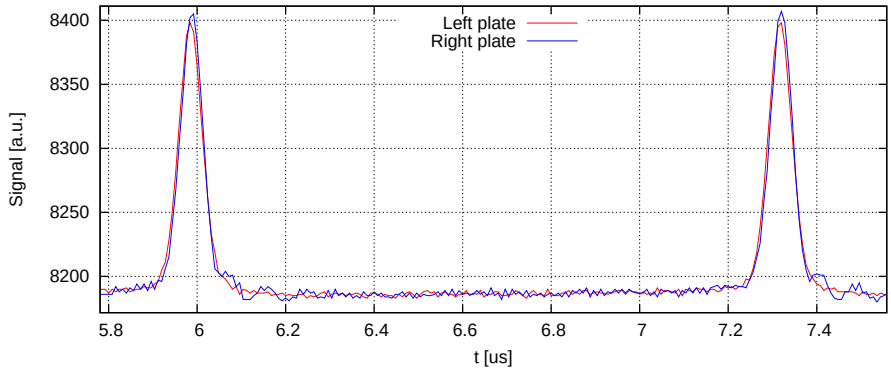

Figure 5.21: COSY BPM 20 horizontal-plate bunch-signal at 970 MeV acceleration scheme from I-Tech Libera Hadron input. The base line (offset) of the signals was aligned for overlapping by calculating the average signal hight and subtraction of the difference. In the presented case the beam was horizontally slightly off-centre, resulting in a slightly higher amplitude on the right BPM plate during the time of the bunch signal.

In case of the successful recognition, a frequency spectrum analysis of the beam position in the full frequency range of 0 to 5 kHz was conducted. The fast Fourier transformation over the period of one ramping each showed a 1/f pink noise structure. In case of the amplified signal also traces of 50 Hz and harmonics were observed.
As this was a proof-of-principal measurement, using a I-Tech Libera Hadron for the first time to measure the beam position of the COSY beam, the low recognition rate is not surprising. Even though a full analysis of the COSY beam movement was not possible as not enough data from complete ramps could be collected, the measurement clearly shows the possibility of using the I-Tech Libera Hadron as BPMs at the COSY facility. Therefore the set goals, namely the development of a ready universal data acquisition system for a local fast orbit feedback at COSY, have not been reached to the full extent. Nevertheless the development of the system itself would not have been possible without the experience and improvements made during the measurements at the COSY accelerator facility.

Chapter 6

Summary

This thesis set out with the aim of developing a versatile distributed data acquisition system for fast feedback applications and to study the suitability of the system at the electron accelerator DELTA and the hadron accelerators COSY and SIS18. This aim has been reached.
Feedback applications by now are common in the accelerator field, the potential of a FPGA based approach to accelerator feedback applications at DELTA was already shown by a preceding prototype fast local orbit feedback system [83,94]. Nevertheless, an universal orbit feedback DAQ approach, as presented, has not been implemented beforehand. This approach requires an adaptation of the system to the different accelerator facilities. The adaption regards beam- (e.g bunch structure and timing) as well as technical properties (e.g. control system connection, signal amplification). These requirements are addressed in two ways: On the one hand, all systems are based on the developed common hardware platform BPM-Extender, allowing adaptations to be made in software and a quick adjustments to different conditions. On the other hand it is reached by integrating I-Tech Libera Hadron electronics, allowing to directly connect to hadron BPMs. In this context, the ability to create nearly arbitrary bus configurations which is the key property of the utilized bus system, was demonstrated to be of great use. This applies especially to the DELTA data acquisition system due to the mixture of different BPM devices and changes in configuration due to ongoing research.
The prospects of the system were shown by measurements at DELTA , the SIS18 and the COSY facility. A reliable operation as data source for a fast-, as well as the existing slow-orbit-feedback at DELTA has been demonstrated. Even though the system is currently not integrated into the control system by EPICS, the required underlying software structure has been prepared for this task.

The conducted studies at COSY were proof-of-concept measurements, by which a thorough debugging of the hadron system was possible. The potential of the remote access, which greatly eased this process, has been demonstrated. The measurements at COSY suggest, that after tuning of bunch recognition and input signal amplifier levels, a reliable 10 kHz position data source will be available.
The successful SIS18 studies are a direct result of the experience gained during the COSY measurements. Even though only a limited number of accelerator ramps at four of the twelve BPMs was analyzed, the recorded position data allows an evaluation of the SIS18 beam motion during ramping. The majority of beam motion was observed to be in the frequency range below 50 Hz. Even though high frequency position deviation was present, a simulation of an ideal feedback showed promising results. The repeatability of the position during consecutive ramps was observed to be excellent. An influence of magnetic hysteresis was not confirmed.

6.1 Conclusion and outlook

The main issue to this thesis was the development and technical realization of the universal data acquisition approach, followed by the measurement analysis of selected orbit-perturbation criteria.

It has been shown, that a universal approach to a beam position feedback is feasible. Even though accelerator specific adaptation is always required, the options given by FPGAs and micro-controller software are able to reduce, if not minimize this drawback. It is these options which make a combined effort to develop a universal system worthwhile.

For DELTA two key aspect are gained. First the the improved statistic position uncertainty for the slow-orbit-feedback data from 5 µm to 0.12 µm. Once fully integrated into the control system, it will influence all slow-position related measurements in the current control system.
Second is the possibility of a fast orbit feedback, improving the beam's orbit and thereby the synchrotron light quality. Currently the development of this system is ongoing [95].

In case of COSY the immediate results might seem limited at first. But, even though no detailed analysis of the beam motion could be conducted, the approach of using a universal beam-position data-acquisition was shown to be successful. Only by exchanging the BPMs electronics, the developed system was directly adopted to the hadron environment. At the time of writing the system is expected to be fully functional after suitable parameter-tweaking, delivering hadron position data from the COSY accelerator with a constant data rate of

10 kHz. Also all further measurements would have not been possible without the preparatory aspects of the system's deployment at the accelerator. One example are the remote access capabilities, which were intensively used.

The SIS18 studies were able to contribute to the planned feedback design of the new FAIR facility storage rings. To improve the beam quality in terms of the beam position, the measurement data suggests a two-fold approach: The repeated deviation from the ideal orbit during the ramping period could be countered by the use of a feed-forward system. This system would utilize the data from the preceding ramps to correct the position on the following. The system could then be further improved by the integration of a feedback system, further reducing unexpected beam motion.
Such an approach is expected to reduce the beam motion of the SIS18 beam during acceleration to below 1 mm RMS.

Appendix A

Tables

		Uncorrected			Simulated correction	
	BPM number	max. [mm]	average [mm]	int. RMS [mm]	max. [mm]	average [mm]
horizontal	9	23,428	7,008	5,410	16,336	0,212
	10	12,915	3,312	2,699	16,086	0,187
	11	77,193	24,662	18,034	74,518	0,722
	12	12,175	7,940	6,063	13,902	0,116
vertical	9	13,704	2,312	1,747	16,510	0,038
	10	4,009	1,070	0,820	3,107	0,038
	11	5,287	1,398	1,768	3,668	0,072
	12	6,736	1,977	1,482	8,949	0,099

Table A.1: Summary of the horizontal and vertical beam position signal for SIS18 BPMs 9 to 12. The numerical analysis was conducted for all observed ramps. A simulated correction (cutoff-frequency 250 Hz) was applied for further distinguish the effects on the beam's position. Average denotes the average beam position. The RMS values show the integrated RMS deviation of the position.

		Uncorrected		Simulated correction	
	Name	$\overline{x}_{var}$ $[mm^2]$	x_{varmax} $[mm^2]$	$\overline{x}_{var}$ $[mm^2]$	x_{varmax} $[mm^2]$
During ramping	BPM X9	0,038	107,416	0,012	1,031
	BPM X10	0,040	34,345	0,036	6,860
	BPM X11	1,310	183,610	0,697	17,677
	BPM X12	0,008	5,913	0,004	0,136
During flattop	BPM X9	0,069	63,485	0,017	0,91
	BPM X10	0,008	26,988	0,005	0,153
	BPM X11	0,616	674,956	0,509	16,837
	BPM X12	0,006	13,452	0,003	0,092

Table A.2: Statistic analysis results summary of horizontal ramp-to-ramp position reproducibility for SIS18 BPMs 9 to 12. The analysis is split into the ramping and the flat top section of the ramping. x_{varmax} is the absolute maximum of the observed variance.

Appendix B

Tools

During the course of this thesis, a number of tools, hardware as well as software, were utilized. This chapter provides an overview of these tools.

B.1 Hardware

B.1.1 Tektronix AFG3102

A Tektronix AFG3102 signal generator, capable of supplying two arbitrary waveforms, was used for all signal generation. During testing the main clock was generated (square wave) as well as trigger (peak) signals. The ADCs were tested with arbitrary generated waveforms. The generator also features remote control via Ethernet. This feature is utilized by the hadron measurement system (see section 4.3).

B.1.2 HP 54699A

A number of analogue (e.g. beam position signals) as well as digital signals (e.g. status signals) had to be monitored and/or examined externally, especially during the design and debugging stage. The HP 54699A oscilloscope was used for this task. It features two signal channels for signals up to one hundred MHz.

B.1.3 I-Tech Libera Electron, Brilliance

The I-Tech Libera Electron is a commercially available, FPGA based, beam diagnostic system from Instrumentation Technologies [91]. Currently 12 I-Tech Libera Electron and 5 I-Tech Libera Brilliance BPMs are being used for beam diagnostics at DELTA. Part of this diagnostics is the utilization as BPMs for the DELTA SOFB and the upcoming FOFB.

B.1.4 I-Tech Libera Hadron

Another product from Instrumentation Technologies aimed towards hadron accelerators is the I-Tech Libera Hadron. The product version used features the same FPGA as the I-Tech Libera Electron/Brilliance, an ADC suited for hadron BPMs and a reduced filtering logic (in comparison to the I-Tech Libera Electron/Brilliance). Due to this properties it is utilised as data source for the hadron FOFB.

B.1.5 DELTA Trigger Splitter

A dedicated electronic device, the so called "DELTA trigger splitter", is utilized for clock and trigger signal distribution around the DELTA storage ring. It features four signal inputs, either copper or glass fibre based. Each input is distributed to four outputs on a differential LEMO-connector. This results in a hierarchical, tree like structure of the signal distribution network. This network is the foundation for the synchronous operation of the FOFB stations.

B.1.6 Bergoz Instrumentation BPMs

The Bergoz Instrumentation MX-BPM (or Bergoz MX-BPM) is an analog electronic used to calculate the beam position from BPM knob signals. This signal is then processed further for the FOFB system. Details of these BPMs are presented in [83, ch. 3.1.1].

B.2 Software

B.2.1 Sigasi HDT

The Sigasi Hardware Development Toolkit (HDT) is an Eclipse [19] based Integrated Development Environment (IDE) for the VHDL. It currently features VHDL error reporting while typing, smart content assistance and VHDL code inspection and navigation [67]. Most of the VHDL development during this thesis was done on basis of the Sigasi HDT.

B.2.2 Xilinx ISE and XPS

The Xilinx Integrated Software Environment (ISE) is an IDE for Xilinx FPGAs, which concentrates on the development of VHDL code, synthesis for the Xilinx FPGA product range and integrated FPGA programming capabilities. The internal simulator was intensively used to verify the different design components,

while the programming capabilities were used for the actual implementation of components, like hardware test routines.

The Xilinx Platform Studio (XPS) is an IDE which allows to combine so called IP cores (see section 2.7.2) to complete designs. After synthesis these designs are programmed to the FPGA. The developed FOFB FPGA design was created using the XPS IDE. The ISE and XPS are described in greater detail in [83, Ch. 3.2]. The version used in both cases was 10.3, which is the last version to support the Xilinx Virtex 2 Pro, the FPGA used in all devices.

B.2.3 Xilinx SDK

Xilinx offers the Xilinx Software Development Kit (SDK), an eclipse [19] based IDE, adopted for software development in the "C" language for the FPGAs PowerPC processor. It was mainly used to write small communication programs to test the hardware/software interaction on the FPGA.

B.2.4 Matlab

MATLAB is a programming IDE by Mathworks [92]. The main focus is data analysis, for which the data is represented using matrices. It includes many pre-defined functions as well as extendibility by so called toolboxes. The data analysis of the BPM data was written in MATLAB. For the COSY lattice analysis the so called "accelerator" toolbox [56] was used.

Appendix C

Acronyms

ADC Analog-Digital-Converter . . . 43
ASIC application specific integrated circuit . . . 33
BMBF Bundesministerium für Bildung und Forschung . . . 4
BNC Bayonet Neill–Concelman . . . 56
BPM knob Beam Position Monitor pickup button . . . 8
BPM Beam Position Monitor . . . iv
BoDo Booster Dortmund . . . 5
CAN Controller Area Network . . . 9
CF Compact Flash . . . 53
CHG-FEL Coherent Harmonic Generation Free Electron Laser . . . 3
COSY Cooler Synchrotron . . . 5
CPLD Complex Programmable Logic Device . . . 33
DAQ data acquisition . . . 6
DCC Diamond Communication Controller . . . 41
DC Directed Current . . . 57
DELTA Dortmunder Elektronen Speicherring Anlage . . . 4
DIMM Dual In-line Memory Module . . . 53
DHCP Dynamic Host Configuration Protocol . . . 69
DMA Direct Memory Access . . . 60
EPICS Experimental Physics and Industrial Controls System . . . 9
ESR Experimentierspeicherring . . . 13
FAIR Facility for Antiproton and Ion Research . . . 3
FESA Front End Software Architecture . . . 46
FFT Fast Fourier Transform . . . 81
FIFO First In First Out . . . 59
FIFO First In First Out . . . 59
FOFB Fast Orbit Feedback . . . 4
FPGA Field Programmable Gate Array . . . 4
FZJ Forschungszentrum Jülich . . . 3
GAL Generic Array Logic . . . 33
GPIB General Purpose Interface Bus . . . 9
GSI GSI Helmholtzzentrum für Schwerionenforschung GmbH . . . 3
HDL Hardware Description Language . . . 34
HDT Hardware Development Toolkit . . . 122
HESR High Energy Storage Ring . . . 3
IDE Integrated Development Environment . . . 122

IOC Input Output Computer . . . 9
IP core Intellectual Property Core . . . 34
ISE Integrated Software Environment . . . 122
LCD Liquid Crystal Display . . . 56
LED Light Emitting Diode . . . 51
LHC Large Hadron Collider . . . 5
LSB Least Significant Bit . . . 89
LTI Linear Time Invariant . . . 38
LINAC Linear Accelerator of DELTA . . . 8
NFS Network File System . . . 66
PBPM Photon Beam Position Monitor . . . 16
PC Personal Computer . . . 9
PCB Printed Circuit Board . . . 51
PLA Programmable Logic Array . . . 33
PLB Processor Local Bus . . . 61
PSD Power Spectral Density . . . 19
PSI Paul Scherrer Institute . . . 5
RAM Random Access Memory . . . 53
RMS Root Mean Square . . . 99
RFS Root File System . . . 63
RHIC Relativistic Heavy Ion Collider . . . 6
RTL Register Transfer Level . . . 34
SATA Serial Advanced Technology Attachment . . . 54
SBC Single Board Computer . . . 67
SDK Software Development Kit . . . 123
SFP Small form-factor pluggable . . . 50
SIS18 Schwer-Ionen-Synchrotron . . . 3
SIS100 Schwer-Ionen-Synchrotron . . . 13
SIS300 Schwer-Ionen-Synchrotron . . . 45
SMA Sub-Miniature-A . . . 52
SOFB Slow Orbit Feedback . . . 23
SSH Secure Shell, see also [106] . . . 45
SVD Singular Value Decomposition . . . 17
T1 Transferkanal 1 . . . 8
T2 Transferkanal 2 . . . 8
Tcl Tool Command Language . . . 9
TU Technische Universität . . . 7
VHDL VHSIC Hardware Description Language . . . 75
XPS Xilinx Platform Studio . . . 123
XUP Xilinx University Program . . . 51

Appendix D

Glossary

channel to channel crosstalk The AD974 is able to multiplex four input channels onto one ADC. As a result the values of the channels influence each other. The Channel to Channel crosstalk is a figure of how strong this influence actually is. It is typically expressed in Volts. 89

characteristic quantization curve ADCs convert a continuous analog voltage into discrete (quantized) digital values. The mapping between the domains is expressed by the characteristic quantization curve. It contains all quantization errors. 88

control system Machinery consisting of multiple components has to be controlled. A control system is a set of additional devices taking over the part of commanding, regulating, directing or managing this task. 8–10

Direct Memory Access Is the technique of reading and writing the system's memory directly, that is without having to pass the processor of the system first. This enables higher data throughput and reduces the processor load. The so called scatter gather DMA is a technique where the data is written into non-consecutive memory regions (scattered). To read this data, an index (or an information where the last write was) has to be created. The data is then read from the different addresses and combined again (gather). This technique is required because modern operating systems fragment the memory space, so big chunks of continuous memory is often not available.. 60, 61

Effective Number Of Bits is a benchmark figure for ADCs for quick performance evaluation. A n-bit ADC has 2^n signal levels. For some ADCs the resolution is high enough to always contain a noise floor, which reduces

the effective resolution. The ENOB represents the number of bits above the noise floor e.g. 15Bits ENOB for a 16Bit ADC. 90, 95

golden orbit is a predefined, reference orbit. It is calculated as the path of the "'Sollteilchen"' traveling through the accelerator's magnetic structure. Usually a center of quadrupole and sextupole orbit is chosen to minimize optics distortion, but may vary in case of insertion devices.. 17, 128

ideal orbit is a predefined, accelerator specific orbit. It is the orbit going through all the magnetic centers of the accelerator's quadrupoles.. 128

insertion device is a magnetic field structure in synchrotron light sources to explicitly create synchrotron light. Dipole magnets, Wigglers and Undulators are examples of insertion devices.. 128

interrupt in the processor domain is a signal which interrupts the normal operation. Important events in the system may require immediate processor time. The in built mechanism of interrupts ensures this functionality. When an interrupt is raised, the normal operation of the processor is halted, a predefined interrupt handler code is executed and afterwards the processor resumes its normal operation.. 61

magnetic structure is the composition of all magnets influencing the particle beam at an accelerator.. 128

Multiple Input and Multiple Output in system theory refers to feedback systems which are, in contrast to Single Input and Single Output systems, more complex by featuring more than one input and output. 37

orbit is the position of the particle beam inside the vacuum chamber. The measured orbit is composed from all BPM readouts and corresponds to the barycenter of the electrons passing by the cutting plane of the respective BPM. It is usually expressed as deviation from the golden orbit or ideal orbit.. 14, 17, 19, 26, 128

pick up button is a button or plate, electrically isolated and integrated into the vacuum chamber, which couples electromagnetically to the charged beam particles. 15

PowerPC is a microprocessor architecture originally created by the AIM alliance, nowadays often utilized in embedded systems. Two PPC405A type processors are embedded onto the FPGA fabric of the Xilinx Virtex2Pro FPGA.. 59–63, 66, 123

Processor Local Bus is a computer bus architecture, developed by IBM. As such it connects the different hardware in an embedded design.. 59, 60

RocketIO is a Multi-Gigabit Transceiver implementation by Xilinx. It is used for fast data transfer with guaranteed performance e.g. for fast communication networks. 52

signal to noise and distortion Used to rate an ADC. It is a measure for the difference of level of a desired signal to the level of background noise and distortion from the ADC process. 89, 90

Single Input and Single Output in system theory, refers to feedback systems with one in and output. 37, 128

Bibliography

[1] Michael Abbott et al. Performance and future development of the diamond fast orbit feedback system. In *Proceedings of EPAC08, Genoa, Italy*, 2008. THPC118.

[2] A.Streun. Practical guidelines for lattice design, internal report sls-tme-ta-1999-0014. `http://ados.web.psi.ch/slsnotes/tmeta9914.pdf`, 1999. [Online, accessed 09.04.2013].

[3] Riccardo Bartolini. S19 accelerator physics option, lecture 10: Real life in an accelerator. `http://www-pnp.physics.ox.ac.uk/~delerue/accelerator_option/Oxford_undergraduates_2010.pdf`, 2012. [Online, accessed 23.04.2013].

[4] Michael Böge. Achieving sub-micron stability in light sources. In *9th European Particle Accelerator Conference, Lucerne, Switzerland, 5 - 9 Jul 2004*, 2004. pp.211, THXCH01.

[5] O. Biebel. Physik der Teilchenbeschleuniger. `http://homepages.physik.uni-muenchen.de/~Otmar.Biebel/beschleuniger/beschleuniger_05.pdf`, 2003/2004. Lecture, [Online, accessed 04.02.2013].

[6] J. Biri et al. Beam position monitor electronics at the cooler synchrotron cosy-jülich, 1993/1994. RealTime '93 Conference, Vancouver, 1993 and IEEE Trans. Nucl. Sci. 41 (1994) p. 221.

[7] Wolfgang Brembt. Private communications, 2012.

[8] G. I. Budker. An effective method of damping particle oscillations in proton and antiproton storage rings. *Atomic Energy*, 22(5):438–440, 1967.

[9] CERN. Lhc general parameters (protons). `https://edms.cern.ch/lhc_proj/plsql/lhcp.page?p_number=1000&p_banner=0`, 2013. [Online, accessed 23.04.2013].

[10] CERN. Mad - methodical accelerator design. http://mad.web.cern.ch/mad/, 2013. [Online; accessed 09.04.2013].

[11] SOLEIL Company. Diagnostics group. http://www.synchrotron-soleil.fr/portal/page/portal/Soleil/Organisation/OrganisationSources/GroupeDiagnostic, 2015. [Online; accessed 02.12.2015].

[12] Seiko Epson Corporation. Eg-2102ca product page. http://www5.epsondevice.com/en/quartz/product/osc/low_jitter_saw/eg2102ca.html, 2013. [Online, accessed 09.04.2013].

[13] Analog Devices. Ad974 4-channel, 16-bit, 200ksps data acquisition system data sheet rev. a. http://www.analog.com/static/imported-files/data_sheets/AD974.pdf, 05/1999. [Online; accessed 14.09.2012].

[14] J. Dietrich et al. Simulation and correction of the closed orbit in the cooler synchrotron cosy-jülich. In *Proc. EPAC 1992*, 1992.

[15] FAIR. Accelerators. http://www.gsi.de/en/start/fair/aufbau_der_fair_beschleunigeranlage.htm, 2012. Accessed 23.07.2012.

[16] FAIR. Fair home. http://www.fair-center.de, 2012. Accessed 23.07.2012.

[17] P. Forck. Private communications, 2013.

[18] P. Forck et al. Beam position monitors. http://www-bd.gsi.de/index.php?cmd=staff&id=108, 2005. [Online, accessed 11.12.2012].

[19] Eclipse Foundation. Eclipse - the eclipse foundation open source community website. http://www.eclipse.org/, 2012. [Online, accessed 25.07.2012].

[20] GSI Helmholtzzentrum für Schwerionenforschung GmbH. Fair baseline technical report. https://www-alt.gsi.de/documents/DOC-2006-Jul-40-1.pdf, 2006. [Online, accessed 15.01.2013].

[21] GSI Helmholtzzentrum für Schwerionenforschung GmbH. GSI Beschleunigeranlage. http://www.gsi.de/portrait/beschleunigeranlage.html, 2011. [Online; accessed 19.08.2011].

[22] GSI Helmholtzzentrum für Schwerionenforschung GmbH. Gsi setup of the proposed accelerator facility fair. http://www.fair-center.eu/public/what-is-fair/accelerators.html, 2012. fair-topologie_e.jpg, accessed 23.07.2012.

[23] GSI Helmholtzzentrum für Schwerionenforschung GmbH. Sis18 sections. http://www.gsi.de/en/start/beschleuniger/beschleunigeranlage/sis18/sis18_sections.htm, 2012. [Online, accessed 25.07.2012].

[24] GSI Helmholtzzentrum für Schwerionenforschung GmbH. Beam properties. https://www.gsi.de/en/work/fairgsi/primary_beams/projekte/sis18_upgrade/sis18/beam_properties.htm, 2013. [Online, accessed 19.04.2013].

[25] GSI Helmholtzzentrum für Schwerionenforschung GmbH. Sis18 - injection. http://www.gsi.de/start/beschleuniger/fachabteilungen/linac/unilac/machine_description/sis_18_injection.htm, 2013. [Online, accessed 23.04.2013].

[26] GSI Helmholtzzentrum für Schwerionenforschung GmbH. Study of strongly interacting matter (hadronphysics3). http://www.gsi.de/en/user/funding/hadronphysics3.htm, 2013. [Online, accessed 19.04.2013].

[27] Andreas A. Galatis et al. First tests with the sis18 digital bpm system. In *Proceedings of DIPAC 2007, Venice, Italy*, page 66f. CERN, 2007. CERN-85-19-V-1.pdf, accessed 10.1.2013.

[28] ELECTRONIC ASSEMBLY GmbH. Displays mit RS-232. http://www.lcd-module.de/produkte/rs232.html, 2012. [Online, accessed 09.04.2013].

[29] Forschungszentrum Jülich GmbH. Experiments, ANKE, TOF, WASA & Co. http://www.fz-juelich.de/ikp/EN/Forschung/Experimente/Experimente_node.html, 2013. [Online, accessed 23.04.2013].

[30] Forschungszentrum Jülich GmbH. Forschungszentrum Jülich - Beschleuniger - HESR. http://www.fz-juelich.de/ikp/DE/Forschung/Beschleuniger/_doc/HESR.html, 2013. [Online, accessed 30.10.2013].

[31] Forschungszentrum Jülich GmbH. Summary of cosy data and beam parameters. http://apps.fz-juelich.de/pax/paxwiki/images/4/42/COSY_data.pdf, 2013. [Online, accessed 23.04.2013].

[32] Marc Grewe. *SVD-basierte Orbitkorrektur am Speicherring Delta*. PhD thesis, Universität Dortmund, 2005.

[33] K. Hacker, R. Molo, S. Khan, L. L. Lazzarino, C. Lechner, Th. Maltezopoulos, T. Plath, J. Rossbach, S. Ackermann, J. Bödewadt, M. Dohlus,

N. Ekanayake, T. Laarmann, and H. Schlarb. Measurements and simulations of seeded electron microbunches with collective effects. *Phys. Rev. ST Accel. Beams*, 18:090704, Sep 2015.

[34] Peter Hartmann. Private communications, 2008, 2012.

[35] Peter Hartmann et al. Experience with libera beam position monitors at delta. In *Proceedings of DIPAC, Venice, Italy*, 2007. TUPB21.

[36] R.O. Hettel. Beam stability issues at light sources. `http://www-ssrl.slac.stanford.edu/spear3/stability_ssils01.pdf`, 2002. 25th ICFA Advanced Beam Dynamics Workshop SSILS,SSRC, Shanghai.

[37] N. Hubert et al. The soleil bpm and orbit feedback systems. `https://accelconf.web.cern.ch/accelconf/d07/papers/tupc20.pdf`, 2007. Proceedings of DIPAC 2007, Venice, TUPC20, [Online, Accessed 02.12.2015].

[38] H. Huck et al. Coherent harmonic genereration at the delta storage ring. In *Proc. FEL2011, Shanghai, China*, 2011. MOOA5.

[39] Xilinx Inc. Xilinx university program virtex-II pro development system hardware reference manual. `http://www.xilinx.com/univ/XUPV2P/Documentation/ug069.pdf`, 04/2008. v1.1.

[40] Xilinx Inc. Logicore ip processor local bus (plb) v4.6 (v1.05a). `http://www.xilinx.com/support/documentation/ip_documentation/plb_v46.pdf`, 2010. [Accessed 01/08/2012].

[41] Xilinx Inc. Logicore ip interrupt control (v2.01a). `http://www.xilinx.com/support/documentation/ip_documentation/interrupt_control.pdf`, 2012. [Online; accessed 01/08/2012].

[42] Xilinx Inc. Xilinx inc. http://www.xilinx.com/, 2013. [Online, accessed 04/04/2013].

[43] Bergoz Instrumentation. Mx-bpm product page. `http://www.bergoz.com/products/MX-BPM/MX-BPM.html`, 07/07/2008. [Online; accessed 02.07.2008].

[44] Maxim Integrated. The abcs of adcs: Understanding how adc errors affect system performance. `http://www.maximintegrated.com/app-notes/index.mvp/id/748`, 2002. [Online, accessed 14.09.2012].

[45] Andreas Jankowiak. *Strahldiagnose und Closed-Orbit-Charakterisierung mit HF-Strahllagemonitoren am Beispiel the Synchrotronstrahlungsquelle DELTA*. PhD thesis, Universität Dortmund, 1999.

[46] Andreas Jankowiak et al. The delta beam based bpm calibration system, 1998. Proc. BIW, SLAC-SSRL, USA.

[47] G. Jansa et al. A new daq installation for the sis18 beam position monitoring system at gsi. In *ICALEPCS, Kobe, Japan*, 2009. THP047.

[48] Forschungszentrum Jülich. COSY - Der Beschleuniger. `http://www2.fz-juelich.de/ikp/cosy/de/index.shtml`, 2011. [Online, accessed 19.08.2011].

[49] Forschungszentrum Jülich. COSY - Der Beschleuniger. `http://www2.fz-juelich.de/ikp/cosy/de/index.shtml`, 2012. cosy.floorplan.gif, [Online, accessed 23.07.2012].

[50] Vsevolod Kamerdzhiev. Transverse feedback system for the cooler synchrotron cosy-jÜlich -first results. In *DIPAC Proceedings*, 2003. MOPD23.

[51] Vsevolod Kamerdzhiev. Private communications, 2013.

[52] Boris Keil. *A Unified Distributed DSP-Based Beam Diagnostics and Global Feedback System for Ramped Electron Storage Rings: Development, Construction and Applications.* PhD thesis, Universität Dortmund, 2003.

[53] Olaf Kopitetzki. *Iterativer Algorithmus zur strahlbasierten Vermessung und Korrektur von Magnetfehlaufstellungen am Speicherring Delta.* PhD thesis, Universität Dortmund, 2009.

[54] Peter Kortmann. Private communications, 2012.

[55] P. Kowina et al. Optimisation of "'shoe-box type"' beam position monitors using the finite element methods, 2005. DIPAC 2005.

[56] SLAC NATIONAL ACCELERATOR LABORATORY. New accelerator toolbox homepage. `http://www.slac.stanford.edu/grp/ssrl/spear/at/`, 2013. [Online; accessed 09.04.2013].

[57] Kevin Lang. Private communications, 2009,2013.

[58] L.H.A. Leunissen. *Non-linear transverse dynamics at the Cooler Synchrotron COSY.* PhD thesis, Technische Universiteit Eindhoven, 1997. ISBN 90-386-0617-6.

[59] B. Lorentz et al. Status of the cooler synchrotron cosy-jülich. In *Proc. of EPAC 2004, Lucerne, Switzerland*, 2004. TULPT043.

[60] Secret Lab Technologies Ltd. Git source tree linux-2.6.git. `http://git.secretlab.ca/`, 2012. [Online, accessed 7.08.2012].

[61] R. Maier et al. Electron cooling in cosy-jülich. In *Proc. of EPAC 1990*, 1990. p.1580 ff.

[62] R. Maier et al. Non-beam disturbing diagnostics at cosy-jülich. In *EPAC 1990*, 1990.

[63] Dieter Möhl. Transverse dynamics ii: emittance. `http://cas.web.cern.ch/cas/Holland/PDF-lectures/Moehl/Moehl-final.pdf` and `CAS05-20may.pdf`, 2005. [Online, accessed 16.01.2013].

[64] L.S. Nadolski et al. Orbit stability status and improvement at soleil. In *Proceedings EPAC 2008*, 2008. THPC065.

[65] N.Bongers et al. Expertsystem for COSY-Control. In *Proc. of the first EUROPEAN PARTICLE ACCELERATOR CONFERENCE*, page 1126f. CERN, 1988.

[66] N.Bongers et al. The cosy control system. In *Proceedings of the third EUROPEAN PARTICLE ACCELERATOR CONFERENCE Volume 2*, page 1149ff. CERN, 1992.

[67] Sigasi nv. Sigasi the future of vhdl design. `http://www.sigasi.com/`, 2012. [Online, accessed 25.07.2012].

[68] David Ondreka. Sis18 closed orbit feedback project: Ion optical aspects. `http://www-bd.gsi.de/dokuwiki/lib/exe/fetch.php?media=collaborations:orbitfeedback:sis18_orbit_feedback_optics_20091127.pdf`, 2009. [Onlin, accessed 04.06.2013].

[69] PAC09. *Magnetic Field Control in Synchrotrons*, 2009. Joint Accelerator Conferences Website (JACoW), accessed 29.1.2013.

[70] A. Parfenova. *Linear and nonlinear Response Matrix and its application to the SIS18 synchrotron*. PhD thesis, Universität Frankfurt, 2008.

[71] A. Parfenova et al. Improving the sis18 performance by the use of the orbit response method. In *PAC07 Proceedings*, 2007. THPAN016.

[72] PCaPAC08. *FESA - The front-end software architecture at FAIR*, 2008.

[73] P.C.Chiu et al. Photon bpm electronics development at taiwan light source. In *DIPAC 2011 Proceedings*, 2011. MOPD23.

[74] B.N. Taylor P.J. Mohr. Codata internationally recommended values of the fundamental physical constants. `http://physics.nist.gov/cuu/Constants/index.html`, 2012. [Online, accessed 06.02.2013].

[75] V. Ptitsyn et al. Slow orbit feedback at rhic. In *BIW10, Santa Fe, New Mexico, US*, 2010. TUPSM108.

[76] U. Rauch et al. Investigations on baseband tune measurements using direct digitzed bpm signals. In *Proceedings of 5th CARE-HHH-ABI Workshop, p. 58*, 2007.

[77] Günther Rehm. Xbpm experience and plans at diamond light source. `http://www.bnl.gov/nsls2/workshops/docs/X-rayBeamPositionMonitors_Feb2009/03_Rehm_XBPMExperienceandPlansatDiamondLIghtSource.pdf`, 26.02.2009. [Online, Accessed 22.04.2013].

[78] Martin Reiser. *Theory and Design of Charged Particle Beams*. Number 9 in Wiley Series in Beam Physics and Accelerator Technology. John Wiley and Sons, 2 edition, 2008.

[79] Thomas Schilcher. Psi diagnostic publications. `https://diagnostics.web.psi.ch/publications/`, 2015. [Online; accessed 02.12.2015].

[80] Detlev Schirmer. Entwicklung von Strahloptiken für den Testspeicherring DELTA auf Basis der Triplett-Struktur, 1989. Diploma Thesis.

[81] V. Schlott. Global position feedback in sr sources. `http://ados.web.psi.ch/slsnotes/tmeta020212.pdf`, 2002. EPAC'02, Paris, France.

[82] V. Schlott et al. Fast orbit feedback and beam stability at the swiss light source. `https://diagnostics.web.psi.ch/publications/BIW04_FOFB.pdf`, 2004. BIW 2004, Knoxville, USA, [Online, Accessed 02.12.2015].

[83] Gerrit Schünemann. Fpga based data acquisition system for fast orbit feedback at the electron storage ring delta, 2008. Diploma Thesis.

[84] Deming Shu. Development of synthetic-diamond-based front end xbpm at the advanced photon source. `http://www.bnl.gov/nsls2/workshops/docs/X-rayBeamPositionMonitors_Feb2009/09_Shu_DevelopmentofSynthetic-Diamond-BasedFrontEndXBPMattheAdvancedPhotonSource.pdf`, 26.02.2009. [Online, Accessed 22.04.2013].

[85] A. Smolyakov et al. Comparison of the present and planned operation of the sis18 and the ags booster with intermediate charge state heavy ions. `http://public.bnl.gov/docs/cad/Documents/Comparison%20of%20the%20present%20and%20planned%20operation%20of%20the%`

20SIS18%20and%20the%20AGS%20Booster%20with%20intermediate%20c.pdf, 2005. [Online, accessed 24.04.2013].

[86] K. Steffen. Basic course on accelerator optics. In *Cern Accelerator School General Accelerator Physics*, page 25ff. CERN, 1984. CERN-85-19-V-1.pdf, accessed 10.1.2013.

[87] Ralph J. Steinhagen. Large scale orbit correction for the lhc. http://iwbs2004.web.psi.ch/documents/program/Steinhagen.Ralph/1.pdf, 2004. 3rd Int. Workshop on Beam Orbit Stabilization 2004, [Online, accessed 19.02.2013].

[88] Ralph J. Steinhagen. Real-time beam control at the lhc. http://accelconf.web.cern.ch/accelconf/pac2011/talks/weobn2_talk.pdf, 2011. PAC'11 talk, [Online, accessed 06.02.2013].

[89] A. Streun. Lattices and emittance. http://cas.web.cern.ch/cas/BRUNNEN/Presentations/PDF/brsl1.pdf, 2003. [Online, accessed 22.01.2013].

[90] Avago Technologies. Afbr-57r5apz product page. http://www.avagotech.com/pages/en/fiber_optics/storage/4g_fibre_channel/afbr-57r5apz/, 2013. [Online, accessed 08.04.2013].

[91] Instrumentation Technologies. Accelerator. http://www.i-tech.si/accelerators-instrumentation, 2012. [Online; accessed 25.07.2012].

[92] Inc. The MathWorks. Matlab, the language of technical computing. http://www.mathworks.com/products/matlab/index.html, 2013. [Online; accessed 27.02.2013].

[93] Uppsala University The Svedberg Laboratory. Hesr electron cooler design study. https://www-alt.gsi.de/documents/DOC-2009-Mar-172-1.pdf, 2009. [Online, accessed 1.1.2016].

[94] Patryk Towalski. Implementierung einer schnellen lokalen Orbitkorrektur für den Speicherring Delta, 2008. Diploma Thesis.

[95] Patryk Towalski. *PhD Thesis (in preparation)*. PhD thesis, TU Dortmund University, 2013.

[96] Patryk Towalski. Private communication, 2013.

[97] I.S. Uzun. Inital design of the fast orbit feedback system for diamond light source. http://http://www.i-tech.si/docs/papers/icalepcs05_initial_design_of_the_fast_orbit_feedback_system_for_DIAMOND_light_source.pdf, 2008. [Online, Accessed 06/07/2008].

[98] I.S. Uzun. Diamond Light Source Fast Orbit Feedback Communication Controller Specification and Design. http://controls.diamond.ac.uk/downloads/other/fofb_cc/doc/CTRL-FOFB-CC-0001.pdf, 2009. [Online, Accessed 07.03.2016].

[99] J. Wenninger. Orbit stabilization at the large hadron collider (lhc), 2004. Presentation, IWBS04, 07.12.2004.

[100] Helmut Wiedemann. *Particle Accelerator Physics*. Springer, 3rd ed. 2007 edition, 5 2007.

[101] Wikipedia. Field-programmable gate array — wikipedia, the free encyclopedia. http://en.wikipedia.org/w/index.php?title=Field-programmable_gate_array&oldid=442996964, 2011. [Online; accessed 19.08.2011].

[102] Wikipedia. Negative feedback — wikipedia, the free encyclopedia. http://en.wikipedia.org/w/index.php?title=Negative_feedback&oldid=502423421, 2012. [Online, accessed 26.06.2012].

[103] Wikipedia. File:hysteresiskurve.svg. http://upload.wikimedia.org/wikipedia/commons/c/c9/Hysteresiskurve.svg, 2013. [Online, accessed 29.01.2013].

[104] Wikipedia. Hysterese — wikipedia, die freie enzyklopädie. http://de.wikipedia.org/w/index.php?title=Hysterese&oldid=113375709, 2013. [Online, accessed 29.01.2013].

[105] Wikipedia. Hysteresis — wikipedia, the free encyclopedia. http://en.wikipedia.org/w/index.php?title=Hysteresis&oldid=535392850, 2013. [Online, accessed 29.01.2013].

[106] Wikipedia. Secure shell — wikipedia, the free encyclopedia. http://en.wikipedia.org/w/index.php?title=Secure_Shell&oldid=540622828, 2013. [Online, accessed 27.02.2013].

[107] Wikipedia. File:bode-pt1.svg. https://upload.wikimedia.org/wikipedia/commons/a/a8/Bode-PT1.svg, 2014. [Online, accessed 9.02.2016].

[108] Prof. Dr. K. Wille. *The Physics of Particle Accelerators: An Introduction*. Oxford University Press, 2001.

[109] F. Zimmermann. Luminosity limitations at hadron colliders. http://snowmassserver.snowmass2001.org/Working_Group_M5/

www/PAPERS/pplumi.pdf. CERN, Geneva, Switzerland [Online, Accessed 24.04.2013].

[110] Dirk Zimoch. *Implementierung eines Orbitkorrektursystems an der Synchrotronstrahlungsquelle DELTA*. PhD thesis, Universität Dortmund, 2002.

[111] Dirk Zimoch et al. Beam based machine modelling for orbit control and feedback at delta. In *Proceedings EPAC, Paris, France*, 2002. WEPLE025.

Acknowledgments

I would like to express my very great appreciation to the people who made this dissertation possible. First of all Professor T. Weis, my research supervisor, for his encouragement and useful critiques of this research work, Professor J. Dietrich, head of the COSY accelerator facility and Dr. M. Schwickert, department leader of the GSI beam instrumentation group, as well as Professor H. Klingbeil for being my second supervisor. I would also like to thank Dr. P. Hartmann, for his advice and assistance during the progression of the work. My grateful thanks are also extended to P. Towalski, my co-worker, for the great time and the multitude of discussions we had. It was a blast.
My special thanks are extended to all my co-workers, scientific and technical, at DELTA. It is fair to say, that everyone made a contribution in one way or the other. My thanks also go out to N. Koch and his team from the physics' electronics development facility for his help with the electronic- and electromechanical design.
I would also like to thank the staff from COSY for their assistance, especially Dr. V. Kamerdzhiev for all his support. The same applies to the GSI staff, most notably to Dr. P. Forck for all his help.
I also wish to acknowledge the help and information provided by the beam diagnostics groups from the Diamond Light Source and Synchrotron SOLEIL, as well as the PSI.

Finally, I wish to thank my parents for all their support and I would like to express my deep gratitude to my wife Ina, for her willingness to support me and her encouragement, which allowed me to realize this dissertation.